Spring 2020

Factors impacting the transport and enhanced oil recovery potential of polymeric nanogel in sandstone

Haifeng Ding

Department: Geosciences and Geological and Petroleum Engineering

FACTORS IMPACTING THE TRANSPORT AND ENHANCED OIL RECOVERY POTENTIAL OF POLYMERIC NANOGEL IN SANDSTONE

by

HAIFENG DING

A DISSERTATION

Presented to the Graduate Faculty of the

MISSOURI UNIVERSITY OF SCIENCE AND TECHNOLOGY

In Partial Fulfillment of the Requirements for the Degree

DOCTOR OF PHILOSOPHY

in

PETROLEUM ENGINEERING

2020

Approved by:

Dr. Baojun Bai, Advisor
Dr. Mingzhen Wei
Dr. Shari Dunn-Norman
Dr. David Wronkiewicz
Dr. Wen Deng

PUBLICATION DISSERTATION OPTION

This dissertation consists of the following four articles, formatted in the style used by the Missouri University of Science and Technology:

Paper I, which can be found on pages 20 to 56, has been published in *Industrial & Engineering Chemistry Research Journal*.

Paper II, which can be found on pages 57 to 80, is intended for *SPE International Petroleum Technology Conference (IPTC).*

Paper III, which can be found on pages 81 to 106, is intended for submission to *Energy & Fuels.*

Paper IV, which can be found on pages 107 to 137, has been published in *Journal Fuel*.

ABSTRACT

Enhanced oil recovery (EOR) using nanometer-sized particles has drawn great attention in the oil industry because of their various advantages brought by size. However, their applications on a field scale are very limited, especially for deformable nanoparticles. The objective of this research is to explore the transport behavior of deformable polymeric nanoparticles (nanogel), the factors impacting these behavior, and their EOR potentials. First, 240 published nanoparticle core flooding experiment data were collected and analyzed about the extent to what the nanoparticles can improve oil recovery. Results show that on the laboratory scale the incremental oil recovery could be as high as 30% of the original oil in place while most studies reported increments around 5%. Secondly, constant pressure-driven filtration tests were conducted to study how different factors would affect the near-wellbore transport of nanogel. It is found that nanogel in lower salinity environment or high concentration results in higher resistance factors. The nanogel injectivity increases with the permeability but has no noticeable impact by the driven pressure. Third, the impacts of nanogel injection velocity on nanogel transport and oil recovery improvement have been investigated. Due to the shear-thinning behavior of nanogel, resistance factors are higher with lower nanogel injection rates regardless of whether the oil is presented in the porous media or not. Nanogel flooding velocity impacts residual resistance factors in an oil-and-water two-phase condition but not in a water-only one-phase condition. Finally, the effect of the crosslinker concentration on the physicochemical properties of nanogel, adsorbing behaviors, and the oil recovery improvement were investigated. Results show that the nanogel with a higher crosslinker concentration and a lower swelling ratio has lower dispersion viscosity, less adsorption, and less oil recovery improvement.

ACKNOWLEDGMENTS

First of all, I would like to thank my supervisor, advisor, Dr. Baojun Bai. During my time in the research group, he supported me both academically and financially. He taught me how to design a study, how to conduct an experiment, how to write a paper, and most importantly, how to be a researcher.

I would like to sincerely appreciate my committee members: Dr. Mingzhen Wei, Dr. Shari Dunn-Norman, Dr. Wen Deng, and Dr. David Wronkiewicz. They are always willing to help and motivate me with their expertise and insightful comments. I also sincerely appreciate my colleagues and friends. They help me in both research and my daily life. I would express my special appreciation to Dr. Jiaming Geng, Dr. Ayman Almohsin, and Dr. Xindi Sun.

I want to thank my family, especially my late maternal grandparents. No words can express how much I love them and how much I cherish every moment with them after living in a foreign land for six years.

Last but not the least, as the coronavirus is wreaking havoc around the world, I want to pay tribute to the health care workers and other people who are fighting this disease. They are making contributions for a better world, and I wish I will make my own contribution with the knowledge I have learned.

TABLE OF CONTENTS

Page

PUBLICATION DISSERTATION OPTION iii

ABSTRACT iv

ACKNOWLEDGMENTS v

LIST OF ILLUSTRATIONS xi

LIST OF TABLES xv

SECTION

1. INTRODUCTION 1

1.1. BACKGROUND OF THE PROBLEM 1

1.2. RESEARCH SCOPE 4

1.2.1. Research Objectives 4

1.2.2. Papers in This Dissertation. 5

2. LITERATURE REVIEW 7

2.1. AN INTRODUCTION OF ENHANCED OIL RECOVERY (EOR) 7

2.1.1. Thermal EOR Methods. 7

2.1.2. Miscible or Solvent Injection EOR Methods. 8

2.1.3. Chemical EOR Methods. 8

2.2. GEL TREATMENT 9

2.2.1. Solution to Excessive Water Production Problem. 9

2.2.2. In-Situ Gel System. 10

2.2.3. Preformed Gel System. 11

2.3. NANOGEL (POLYMERIC NANOPARTICLES) IN EOR 12

2.3.1. Application of Nanomaterials in EOR 13

2.3.2. Nanoscale and Microscale Polymeric Particles..... 16

PAPER

I. EXPERIMENTAL DATA ANALYSIS OF NANOPARTICLES FOR ENHANCED OIL RECOVERY 20

ABSTRACT..... 20

1. INTRODUCTION 21

2. DESCRIPTION OF THE DATASET 24

3. DATA VISUALIZATION METHODS 25

4. RESULTS AND DISCUSSIONS..... 27

4.1. NANOPARTICLE PROPERTIES 27

4.2. DISPERSION PROPERTIES..... 29

4.3. MATERIALS PROPERTIES..... 30

4.4. EXPERIMENT APPROACH..... 34

4.5. OIL RECOVERY IMPROVEMENT..... 37

4.6. EOR MECHANISMS STUDIES 37

4.7. FACTORS THAT AFFECT THE EOR OF NANOPARTICLES 42

5. UNDER-RESEARCHED TOPICS 46

6. CONCLUSIONS..... 49

REFERENCES 49

II. AN INVESTIGATION OF FACTORS INFLUENCING THE NEAR-WELLBORE TRANSPORT OF NANOGEL..... 57

ABSTRACT..... 57

1. INTRODUCTION 58

2. STUDY DESCRIPTION 60

2.1. MATERIAL 60

2.2. FILTRATION EXPERIMENTS 60

2.3. NANOGEL CHARACTERIZATION 62

3. RESULTS AND DISCUSSIONS 63

3.1. NANOGEL CHARACTERISTICS 63

3.2. FILTRATION EXPERIMENTS 67

3.2.1. Filtration of Nanogel in Different Salinity 67

3.2.2. Filtration of Nanogel at Different Dispersion Concentration. 70

3.2.3. Filtration of Nanogel in Porous Media with Different Permeability 73

3.2.4. Filtration of Nanogel at Different Driven Pressure. 74

4. CONCLUSIONS 75

REFERENCES 77

III. A LABORATORY STUDY OF IMPACTS OF FLOW RATE ON NANOGEL TRANSPORT AND OIL RECOVERY IMPROVEMENT 81

ABSTRACT 81

1. INTRODUCTION 82

2. EXPERIMENTAL MATERIALS 84

2.1. MATERIALS 84

2.2. NANOGEL CHARACTERIZATION 85

3. EXPERIMENTAL METHOD 88

3.1. EXPERIMENTAL SETUP 88

3.2. EXPERIMENTAL PROCEDURES 89

3.2.1. Nanogel Injection in One Phase Condition. 89

3.2.2. Improving Oil Recovery with Different Nanogel Injection Rates. 90

4. RESULTS AND DISCUSSIONS 91

4.1. NANOGEL INJECTION IN ONE PHASE CONDITION 91

4.2. IMPROVING OIL RECOVERY IN POROUS MEDIA 98

5. CONCLUSIONS 103

REFERENCES 103

IV. IMPACTS OF CROSSLINKER CONCENTRATION ON NANOGEL PROPERTIES AND ENHANCED OIL RECOVERY CAPABILITY 107

ABSTRACT 107

1. INTRODUCTION 108

2. EXPERIMENTAL MATERIALS AND METHODS 110

2.1. MATERIALS 110

2.2. NANOGEL CHARACTERIZATION 111

2.3. ADSORPTION BETWEEN NANOGELS AND ROCK SURFACES 112

2.4. OIL RECOVERY IMPROVEMENT BY NANOGELS 114

3. RESULTS AND DISCUSSIONS 116

3.1. NANOGEL CHARACTERIZATION 116

3.2. ADSORPTION OF NANOGELS ON ROCK SURFACES 121

3.3. IMPROVING OIL RECOVERY IN POROUS MEDIA 128

4. CONCLUSIONS 133

REFERENCES 134

SECTION

3. CONCLUSIONS AND RECOMMENDATIONS 138

3.1. CONCLUSIONS 138

3.2. RECOMMENDATIONS 140

BIBLIOGRAPHY 142

VITA 150

LIST OF ILLUSTRATIONS

SECTION Page

Figure 2.1. The mechanism of in-situ gel system 10

Figure 2.2. Comparison of millimeter PPG before and after swelling 12

Figure 2.3. Silicon dioxide nanoparticles captured by a scanning electron microscope (SEM) 14

Figure 2.4. Contact angle measurement of crude oil/nanofluid system on a water-wet quartz plate 15

Figure 2.5. Mechanism of conformance control using Brightwater® 18

Figure 2.6. SEM micrographs of polymeric nanoparticle (nanogel) before (left) and after (right) fulling swelling 19

PAPER I

Figure 1. Distribution of the Numbers of Collected Tests from Each Publication..... 25

Figure 2. Schematic of a Combination Plot of Box Plot and Violin Plot. 26

Figure 3. Distributions of Important Nanoparticle Properties 28

Figure 4. Summary of Nanoparticle Dispersion Properties 30

Figure 5. Distribution (and Relationships) of Various Core Properties..... 32

Figure 6. Distribution and Relationships of Parameters Regarding Oil Properties 33

Figure 7. Parameters Regarding Core Flooding Approach..... 36

Figure 8. Distribution of (a) Initial Oil Recovery and Final Oil Recovery; and (b) Incremental Oil Recovery. 38

Figure 9. Distribution of IFT Tests Results and the Relationship to Other Parameters ... 40

Figure 10. Distribution of Wettability Tests Results and the Relationship to Other Parameters 41

Figure 11. Resistance Factor and Residual Resistance Factor Distributions..... 44

Figure 12. Effect of Injection Scenario on (a) Incremental Oil Recovery and (b) Nanoparticle Dispersion Injection Volume 45

Figure 13. Impacts of (a) Particle Type and (b) Particle Polarity on Incremental Oil Recovery. 46

Figure 14. Impacts of Nanoparticle Concentration on Incremental Oil Recovery. 47

Figure 15. Impacts of Surface Area on Incremental Oil Recovery 48

PAPER II

Figure 1. Schematic Diagram of the experimental setup 61

Figure 2. Hydrodynamic diameter (left) and zeta potential (right) of nanogel at different brine concentration. 64

Figure 3. Viscosity of nanogel dispersions at different NaCl concentration (left) and nanogel concentration (right) 65

Figure 4. Viscosity at 160 1/s (except 5,000 mg/L dispersion) of nanogel dispersion at . different NaCl concentration (left) and nanogel concentration (right) 65

Figure 5. Equivalent flow rates of 100 1/s and 160 1/s shear rates 66

Figure 6. Production rates over time (A) and resistance factor at 70^{th} min (B) at different salinity 68

Figure 7. Filtration results fitted by intermediate blocking model (A) and Standard blocking model (B) at different salinity 70

Figure 8. Production rates over time (A) and resistance factor at 70th min (B) at different nanogel concentration 71

Figure 9. Filtration results fitted by intermediate blocking model (A) and Standard blocking model (B) at different nanogel concentration 72

Figure 10. Production rates over time (A) and resistance factor at 70th min (B) at different permeability 74

Figure 11. Filtration results fitted by intermediate blocking model (A) and Standard blocking model (B) at different permeability 75

Figure 12. Production rates over time (A) and resistance factor at 70th min (B) at different driven pressure 76

Figure 13. Filtration results fitted by intermediate blocking model (A) and Standard blocking model (B) at different driven pressure 77

PAPER III

Figure 1. Dry nanogel captured by SEM 85

Figure 2. (A) Nanogel size measured via DLS; (B) Zeta potential measured via ELS 86

Figure 3. Viscosity of nanogel dispersion at different shear rates and their equivalent flow rates. 87

Figure 4. Schematic Diagram of the experimental setup 88

Figure 5. Injection pressure and cumulative nanogel retention during nanogel flooding and following water injection..... 94

Figure 6. Resistance factors and residual resistance factors when nanogel was injected at different flow rates 95

Figure 7. Adsorption of nanogel fitted by Pseudo-second-order kinetic model 96

Figure 8. The relation between nanogel injection flow rates and adsorption rate constants 97

Figure 9. Injection pressure and oil recovery during nanogel flooding and second water flooding 99

Figure 10. Resistance factors and residual resistance factors at different nanogel flooding flow rates 101

Figure 11. Incremental oil recovery at different flow rates 102

PAPER IV

Figure 1. Schematic diagram of the experimental setup..... 114

Figure 2. SEM images of dry nanogels, with scale bar 100 nm long 117

Figure 3. Hydrodynamic diameters of nanogels in DI water and brine..... 117

Figure 4. Zeta potential of nanogels in DI water and brine 119

Figure 5. Nanogel dispersion at different shear rates 120

Figure 6. Dispersion viscosity at 70 1/s..... 122

Figure 7. Injection pressure and effluent concentration during nanogel injection (adsorption) 124

Figure 8. Pseudo-second order kinetics model for nanogel adsorption..... 126

Figure 9. Impacts of crosslinker concentration on resistance factors, adsorption, desorption, and retention 127

Figure 10. Injection pressure and effluent concentration during and following brine injection (desorption) 129

Figure 11. Interfacial tension reduction by nanogels 130

Figure 12. Injection pressure and oil recovery of each oil displacement test 131

Figure 13. Incremental oil recovery and plugging capability of different nanogels 133

LIST OF TABLES

PAPER I Page

Table 1. Parameters in the Dataset 24

PAPER II

Table 1. Filtration tests to be conducted in this task 62

Table 2. Fitting parameters of blocking models at different salinity 70

Table 3. Fitting parameters of blocking models at different nanogel concentration 72

Table 4. Fitting parameters of blocking models at different permeability 76

Table 5. Fitting parameters of blocking models at different driven pressure 77

PAPER III

Table 1 Components of the HPAM-based nanogel 84

Table 2. Applied nanogel flooding injection flow rates, equivalent velocities, and equivalent shear rates 89

Table 3. Properties of cores for adsorption core flooding study 92

Table 4. Relative parameters of the fitting model 96

Table 5. Weight of nanogel adsorbed, desorbed, and retained inside porous media 97

Table 6. Properties of cores for oil displacement core flooding study 98

PAPER IV

Table 1. Components of HPAM-based nanogels 111

Table 2. Properties of cores for adsorption core flooding study 113

Table 3. Properties of cores for oil displacement core flooding studies 115

Table 4. Parameters for the fitting of the pseudo-second order kinetics model 126

1. INTRODUCTION

1.1. BACKGROUND OF THE PROBLEM

It is estimated that only approximately 30% of the original oil in place (OOIP) can be recovered in the world after primary and secondary recovery processes (1). Subsequently, a large amount of oil resource is left for the enhanced oil recovery (EOR).

Various EOR methods have been studied and applied in the industry, including thermal, miscible or solvent injection, and chemical methods (2). Thermal methods are applied to reduce oil viscosity in heavy oil reservoirs and vaporize oil into the solvent in light oil reservoirs. The miscible or solvent injection is applied for increasing the miscibility or displacement efficiency between oil and injected fluids (3). Chemical methods involve the injection of specific fluids into a reservoir to increase oil recovery by wettability alteration, interfacial tension reduction, mobility control, or conformance control.

In the recent decade, applying nanoparticles as a chemical EOR method has drawn great attention in the academia and industry. Multiple types of nanoparticles have been investigated for EOR purpose. Among all, silica nanoparticle, metallic oxide nanoparticle, and polymeric nanoparticle are being studied most frequently (4).

There are various mechanisms for this EOR method to improve oil displacement efficiency both macroscopically and microscopically.

On the macroscopic scale, reservoir heterogeneity is a major problem to cause low oil recovery. Injected fluids tend to go through higher permeability zones and leave a significant amount of oil in unswept zones. Moreover, such a phenomenon could lead to

excessive water production problems, which raises environmental and economic concerns. World widely, an average of about three barrels of water is produced along with every one barrels of oil (5). Preformed particle gel (PPG) treatment has become a solution to improve the macroscopic displacement efficiency and reduce water production. PPG has varied sizes from nanometer to millimeters, and the size selection for a specific reservoir depends on the permeability of high permeability streaks or channels. It is usually preferred to use submicron and nano-size gel particles if a reservoir has no abnormal super-K channels, such as open fractures, conduits, vugs, and so on.

On a microscopic scale, nanoparticles can improve oil recovery by mechanisms like wettability alteration and interfacial tension (IFT) reduction. Wettability is important to oil displacement efficiency of a waterflooding. Performing waterflooding in a water-wet system is generally more efficient compared to that in an oil-wet system (6). It has been proven that nanoparticle dispersion can change porous media wettability. By controlling the flow and spatial distribution of fluids, the wettability would affect oil recovery during water flooding (6). It was found that liquid containing nanoparticles could change the wettability of a solid surface (7,8). Numerous research further confirmed the ability of nanoparticles to alter porous media into a more water-wet condition (9–12). Reducing interfacial tension is another approach to improve oil recovery. When interfacial tension (IFT) decreases, displacement efficiency is improved remarkably regardless of the porous media wettability (13). Studies have shown that nanoparticles can assist surfactants to achieve a higher IFT reduction. Additionally, nanoparticles alone can reduce IFT, due to the adsorption onto the surface of fluids (14). Greater IFT reduction eventually leads to further incremental oil recovery (15–20).

Despite all the proposed EOR mechanisms, nanoparticles are not widely applied on a field scale currently (21). This suggests that we still need a better understanding of nanoparticles. Experimental core flooding research is one of the best ways to study the mechanisms, effects, and EOR potentials.

Some researchers have reviewed the EOR studies of nanoparticles with a focus on previous core flooding studies. But most of those articles review previous studies case by case. In this dissertation, nanoparticle core flooding researches were investigated from a data statistic perspective. A dataset was constructed by collecting all relevant information available from those publications. Histograms, the combination of box plots and violin plots, bar charts, and scatter plots were utilized for visualization of the statistical analysis.

Since most of the previous nanoparticle research studied silicon and metallic particles. More tasks were conducted in this dissertation to investigate the polymeric nanoparticle, which is also referred as nanogel. It is unique from other nanoparticles as polymeric particles are deformable and swellable when being dispersed in water or brine. Such properties give those particles better in-depth transportation properties and conformance control effect.

Three series of studies using core flooding tests were conducted to understand the injectivity and EOR potential of a nanogel in sandstone reservoirs. Its transport behavior in the porous media, impacts of injection velocity, and impacts of crosslinker concentration would be discussed.

1.2. RESEARCH SCOPE

The ultimate goal of this PhD work is to improve the understanding of the mechanisms, EOR capability, and influencing factors of nanoparticles as an enhanced oil recovery method.

1.2.1. Research Objectives. Four tasks were carried out to achieve this goal and the objectives of these tasks are listed below.

- Objective 1: Despite many researchers have proposed that nanoparticles can be applied as an EOR agent, they are not widely applied on a field scale currently (14). This suggests that we still need a better understanding of nanoparticles. Experimental core flooding research is one of the best ways to study the mechanisms, effects, and EOR potentials. A statistical analysis of previous nanoparticle core flooding studies would be important for a better understanding of this EOR method.
- Objective 2: The transport behavior is crucial for the understanding of polymeric nanoparticles (nanogel). Previously, multiple researchers have studied its transport behavior by running filtration tests with filter membrane(21,22). However, the membrane only represents an ideal scenario. To mimic a more realistic near wellbore condition, using natural cores as porous media is essential to a study. Filtration tests need to be carried out to study different factors that affect the transport of nanogel in near-wellbore conditions.
- Objective 3: During any chemical flooding, the fluid flow velocities change from the wellbore to the in-depth of a reservoir. Velocity is always linked with different viscous forces, injectant retention, degradation, etc. Different velocities also

correlate different equivalent shear rates inside porous media, which makes it more crucial for non-Newtonian injection fluids. For a better understanding of nanogel flooding, the injection velocity is one of the many aspects awaiting further studies.

- Objective 4: Typically, nanogels are polymerized using monomers and crosslinkers, which transform polymers from linear structures to 3D structures (23). Nanogel properties — including its swelling ratio and strength — can be fine-tuned by the crosslinker concentration (24,25). Hence, the effect of the degree of crosslinking on the physicochemical properties of nanogel, the corresponding adsorbing behavior on rock surfaces, and consequently, the oil recovery improvement was necessary to be studied.

1.2.2. Papers in This Dissertation. For the first task, a dataset was constructed by collecting all relevant information available from current publications. Data analysis methods were utilized. For the next three tasks, physical experiments and characterization experiments were conducted. The target nanoparticle was partially hydrolyzed polyacrylamide (HPAM)-based nanogel, which is a type of polymeric nanoparticle. Four papers were completed to address each of the four research objectives:

- Paper I: Many review articles have discussed previous experimental studies on nanoparticles for EOR case by case (14,26–30). Up to now, no studies have been carried out to analyze the subject from a statistic standpoint. Thirty-nine published studies with a total of 240 laboratory core flooding tests using nanoparticles were collected and analyzed for this task. A dataset was constructed by collecting all relevant information available from those publications for analysis.

- Paper II: Filtration tests using Berea sandstone core chip were carried out to investigate the transport of nanogel in near-well bore conditions. Different factors were considered for the constant-pressure filtration experiments, including salinity, injection pressure, nanogel concentration, and permeability.
- Paper III: In this task, core flooding experiments with different nanogel injection flow rates were conducted. Two porous media conditions were applied to study the impacts of flow rate: in the porous media saturated solely by water phase, the injectivity and adsorption behavior of nanogel were investigated; in the porous media containing residual oil, impacts of injection flow rate on nanogel plugging and improving oil recovery were studied.
- Paper IV: This task investigated the impact of crosslinker concentration on nanogel properties, transport, and the improvement of oil recovery. The HPAM-based nanogels with different crosslinker concentration were prepared by suspension polymerization for the work. The impacts of crosslinker concentration on nanogel properties, injectivity, and EOR potential were studied.

2. LITERATURE REVIEW

2.1. AN INTRODUCTION OF ENHANCED OIL RECOVERY (EOR)

Commonly, three oil recovery mechanisms exist during oil production: primary recovery, secondary recovery, and tertiary recovery. During the primary recovery, oil is produced by the natural energy of reservoirs. Such energies include solution-gas drive, gas-cap drive, fluid/rock expansion, gravity drainage, and natural water drive. During the second recovery, when the initial energy of a reservoir has depleted, fluids such as water and gas would be injected into the reservoir to maintain reservoir pressure and replace oil. However, there are various issues like residual oil, vicious finger, reservoir heterogeneity, and fracturing existing during this stage. Consequently, only 35%-50% of the original oil in place can be recovered after the first and secondary recovery worldwide (3). Hence, a large amount of oil resource is left for the tertiary recovery.

It is worth noting that many production operations are not followed this chronological order because of the nature of respective reservoirs (3). For example, the primary recovery is often skipped when operating in a heavy oil reservoir. At this circumstance, the tertiary oil recovery is often known as enhanced oil recovery (EOR) in the industry and academia. Numerous EOR methods have been studied and applied in the industry, includes thermal, miscible or solvent injection, and chemical methods (2).

2.1.1. Thermal EOR Methods. Thermal methods are applied to reduce oil viscosity in heavy oil reservoirs and vaporize oil into the solvent in light oil reservoirs. Huff-and-puff is one of the most common thermal methods. In a huff-and-puff project, steam is injected into a well for some time between 2 to 4 weeks. The well would be shut

in for days to let the formation be “soaked”. The resulting high temperature will increase the oil rate by reducing oil viscosity and increasing reservoir pressure. This process could be repeated after the oil production rate returning to the predetermined level. The other thermal methods include steam flooding, combustion, and hot water flooding.

2.1.2. Miscible or Solvent Injection EOR Methods. The miscible or solvent injection is applied for increasing the miscibility or displacement efficiency between oil and injected fluids (3). There are two situations: 1) First-contact-miscible. It is a more effective situation, where oil would be miscible and produced along with injection fluid. 2) Multiple-contact-miscible, where the injected gas would be miscible with oil in the in-situ of a reservoir. A dynamic fluid-mixing process in which an injected gas exchanges components with in situ oil until the phases achieve a state of miscibility within the mixing zone of the flood front.However, the injection phase could be miscible with the oil phase under proper pressure, temperature, and composition.

2.1.3. Chemical EOR Methods. Chemical methods involve the injection of specific fluids into a reservoir to increase oil recovery by wettability alteration, interfacial tension reduction, mobility control, or conformance control. Surfactant is often used to reduce the interfacial tension between oil and water phases and modify the wettability of reservoirs to make a favorable condition to produce more oil (31). Polymer flooding is a common method to increase sweep efficiency. It achieves the goal by reducing viscous fingering and improving reservoir homogeneity (32).

In recent years, crosslinked polymer gel treatment for conformance control gains interest in the industry. It can reduce the permeability of water channels/streaks and

divert more injection fluids to unswept zones in order to increase oil recovery and reduce water production (33).

Enhanced oil recovery with nanoparticles is another novel concept to improve oil recovery by utilizing the advantages of the small size of particles. It is proved that most of the nanoparticles for EOR purposes can reduce interfacial tension and alter wettability (7–12,14). Besides, the polymeric nanoparticle is also capable of improving reservoir homogeneity, especially for those with low permeability (34). This Ph.D. work mainly focuses on EOR with the nanoparticles, especially polymeric nanoparticle (nanogel).

2.2. GEL TREATMENT

Gel treatment is considered as an effective solution to improve the injection profile. It is designed to plug higher permeability zones and divert injected fluids to un-swept areas.

2.2.1. Solution to Excessive Water Production Problem. During oil production projects, excessive water production is always a concern from both environmental and economic perspectives. It is a source of pollution and could corrode facilities. At a high water cut, every time a barrel of oil is produced, 4 US dollars need to be spent to combat the problem (5). Eventually, excessive water production leads to early shutting down or abandon of a production well.

The heterogeneity of reservoirs is a major reason responsible for the issue. During oil displacement projects, injected fluids always have a trend to go through higher permeability zones/streaks, which would cause low sweep efficiency and high remaining oil saturation. This often results in poor sweep efficiency and watered-off layers. Gel

treatment is considered as an effective solution to such a problem as it improves the injection profile. It is designed to plug higher permeability zones and divert injected fluids to un-swept areas. Currently, the in-situ gel system and preformed gel system are the two major gel treatment systems.

2.2.2. In-Situ Gel System. As shown in Figure 2.1, This method is often applied by first injecting water-like gelant, which is often composed of polymer, crosslinker, and additives. Because of the permeability difference, more gelant is placed in higher permeability zones. After shutting in the well, gelation would occur in reservoirs and result in permeability reduction in the previous higher permeability zones. more water would go through lower permeability zones and thus sweep efficiency is increased (35).

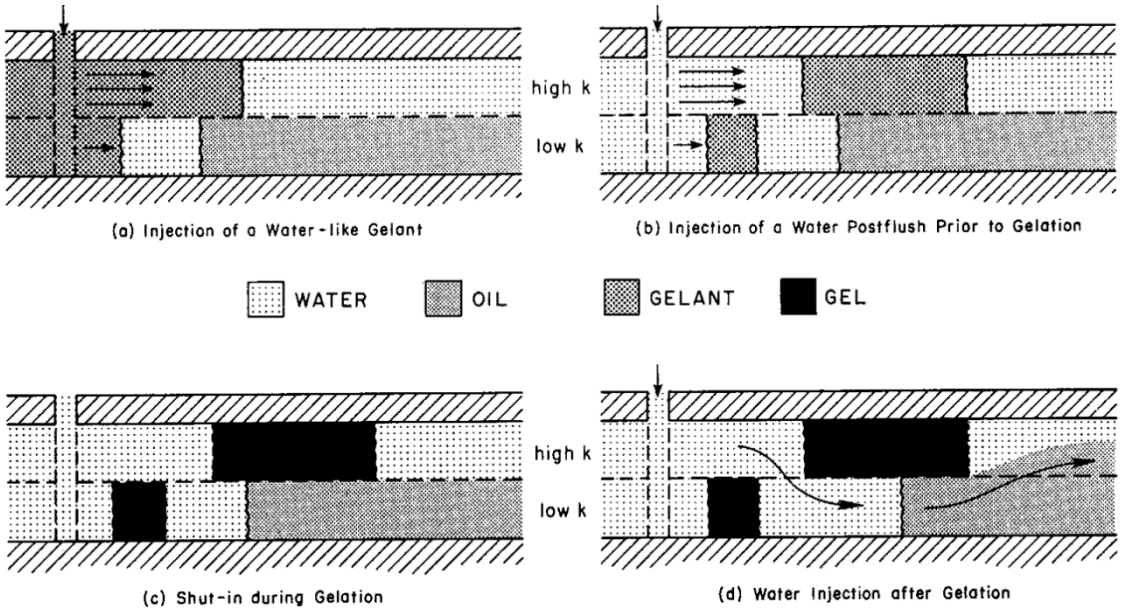

Figure 2.1. The mechanism of in-situ gel system (35)

The in-situ gel system can be classified into monomer gels and polymer gels. The monomer gel consists of the water-like monomer solution, of which gelation occurs via

polymerization (36). Due to the difficulty of gelation control, environmental and health risks caused by monomer's toxic makes this treatment unpopular in the oil industry. On the contrary, polymer gels are widely applied in the industry nowadays since they are more stable, economical and environmentally friendly (37). Normally, polymer gels are formed with particle hydrolyzed polyacrylamides, crosslinkers and some additives (38).

2.2.3. Preformed Gel System. As the name implicates, preformed gels, , are formed and crosslinked at surface facilities rather than in the formation after injection, which makes the gelation process to be better controlled. Considering the pumping and injection issues of bulk preformed gels, particle gels are most applied for this purpose, which is named as also known as preformed particle gel (PPG). The range in particle sizes can be controlled from millimeter-scale to nanometer-scale, depending on the needs of a specific reservoir.

The concept of using millimeter-size PPG to control conformance concept was initiated by the Research Institute of Petroleum Exploration and Development (RIPED), PetroChina. It is an improved super absorbent polymer, also known as SAP. Such materials could absorb water that is over a hundred times as their initial weight and still stay stable under high temperature and pressure (39). The comparison of a PPG sample before and after swelling is shown in Figure 2.2 (40).

The size of this type of PPG usually ranges from 10 micrometers to a few centimeters, depending on the features of target zones. Comparing to in-situ polymer gels, it is capable of resisting higher temperatures (up to 120 degrees centigrade) and different salinities. Besides, it is easy and quick to prepare since it can be mixed in any convenient water and can be well dispersed in a short period. The injection process is also

easy to be monitored. Moreover, due to the deformability, it is easier to transport through throats (33).

Figure 2.2. Comparison of millimeter PPG before and after swelling (40)
Left tube: dried particles; right tube: swelling particles

However, due to their relatively large size, millimeter-sized PPGs can only be used to plug high permeability channels or fractures. PPGs with smaller particle sizes are desired when handling operations in lower permeability reservoirs. Those PPGs would be introduced in the later sections.

2.3. NANOGEL (POLYMERIC NANOPARTICLES) IN EOR

Nanotechnology has been a hot topic since the end of the last century. It is defined by the National Nanotechnology Initiative (NNI) as the understanding and control of matter with a dimension between 1 to 100 nanometers (41). At this size range, materials

have different or enhanced properties (42) such as larger surface area (43) and quantum physics properties (44). Nanotechnology has been studied and applied in many domains such as medical (45), civil engineering (44), food science (46) and the oil and gas industry. The application of nanoparticles in the oil and gas industry addresses challenges from multiple aspects. Due to their small size, they could be used as sensors to detect reservoir properties such as temperature (47) and heterogeneity (48) inside porous media. During drilling, nanoparticles improve operations at extreme reservoir conditions (49), decrease water invasion (50), and reduce fluid loss (51). When performing hydraulic fracturing, they reduce the leak-off rate and stabilize fluid viscosity under high temperature and high pressure conditions (43).

2.3.1. Application of Nanomaterials in EOR. Applying nanoparticles as a chemical EOR method has also drawn great attention in academia and industry. As stated in the previous section, there are various mechanisms for this EOR method to improve oil displacement efficiency both macroscopically and microscopically.

Silica nanoparticle (SiO_2) is the most common type to be studied currently because of the good degree of control and physical-chemistry surface properties. It can be produced to be either hydrophilic, neutral, or lipophilic (52). It is also less non-toxic and less expensive to be produced compared to other types (14). A typical silica nanoparticle under a scanning electron microscope (SEM) is shown in Figure 2.3.

Various researchers have conducted tests to prove its ability to improve oil recovery in porous media. Studies have found that interfacial tension reduction and wettability modification are the main mechanisms of silica nanoparticle (53). Li et al. (2013) measured the IFT was reduced from 19.5 mN/m to 8 mN/m when adding

nanoparticles into the water. (18). Shahrabadi et al. (2012) observed a 32.5 mN/m reduction (from 35.5 to 3 mN/m) with silica nanoparticle (20). Hendraningrat et al. (2013) conducted contact angle tests on water-wet surfaces. The objective hydrophilic silica nanoparticle successfully modify the plate to a more water-wetcondition, as shown in Figure 2.4 (54). However, with the lipophilic nanoparticle, the rock surface could be more oil-wet (55). Both IFT reduction and contact angle modification were found to be higher when the nanoparticle concentration was increased (18,54).

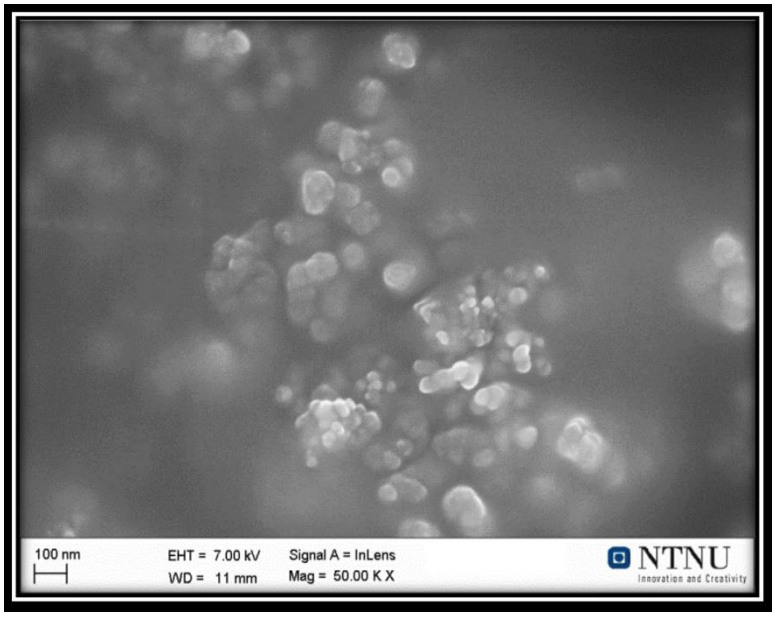

Figure 2.3. Silicon dioxide nanoparticles captured by a scanning electron microscope (SEM) (16)

Numerous core flooding tests were also been carried out to prove the EOR potential of silica nanoparticles. El-Diasty (2015) tested silica nanoparticles with diameters ranging from 5 – 60 nm. Particles with diameters between 15 – 20 nm resulted in the highest oil recovery increment (around 30% of OOIP) (56). Hendraningrat (2013)

conducted core flooding test using nanoparticle dispersions with different concentration. 500 ppm dispersion improve oil recovery the most among all samples (100 – 1,000 ppm) (54). Researchers have also proved that all of hydrophilic, neutral, and lipophilic particles are able to improve oil recovery (57,58).

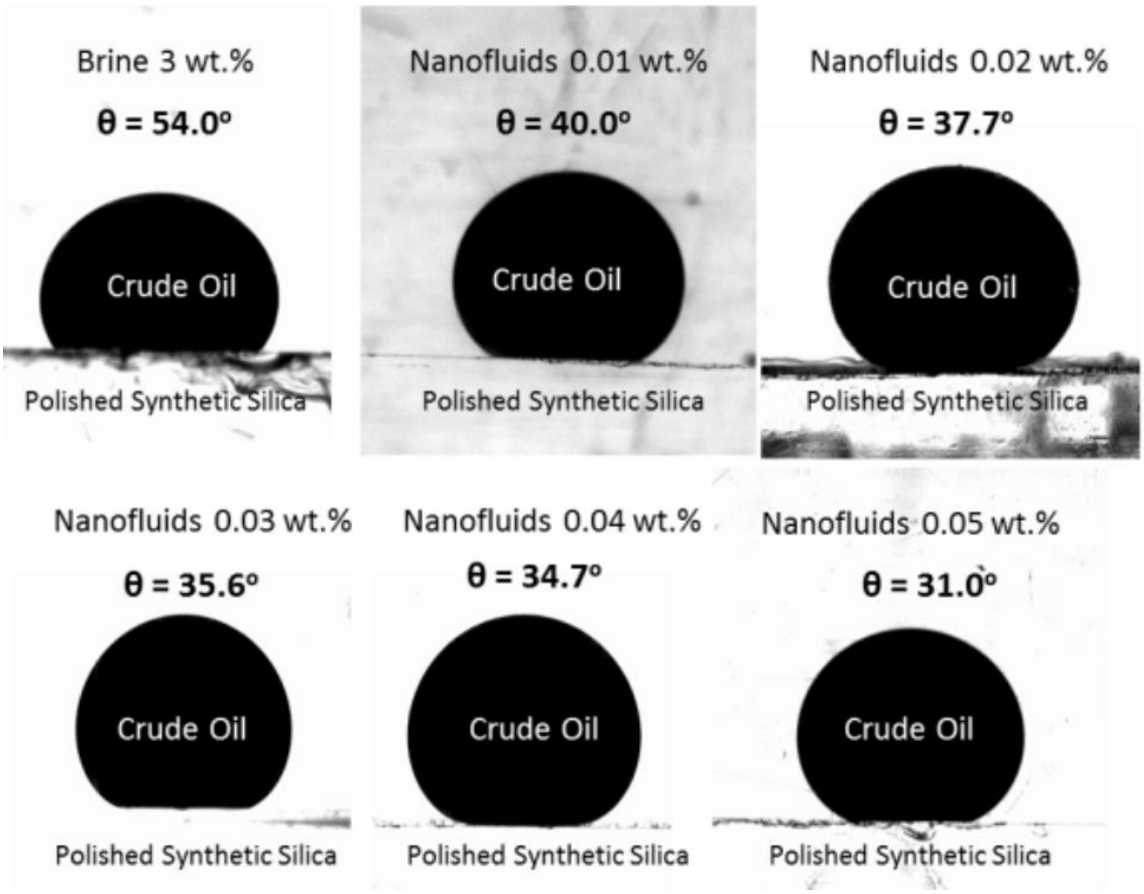

Figure 2.4. Contact angle measurement of crude oil/nanofluid system on a water-wet quartz plate (54)

Metallic oxide nanoparticles include multiple types like Al2O3, Fe2O3, and TiO2 particles (59,60). Like silica nanoparticles, metallic oxide nanoparticles could also reduce IFT and modify wettability (61,62). Tarek (2015) has tested different types of metallic

oxide for EOR. The research concluded that oil recovery could be improved more with a mixture of different metallic oxide (59).

Other than reducing IFT and modifying wettability, polymeric nanoparticle could improve sweep efficiency and injection fluids viscosity (63). The difference between the polymeric particle and silica/metallic particles is notable: unlike the others, polymeric particles are deformable and swellable when being dispersed in water or brine. Such properties give particles better in-depth transportation properties (64). Hence, polymer particles were often proposed for conformance control (65). Nano-meter sized polymer particle would be a good candidate for treatment in low permeability porous media.

2.3.2. Nanoscale and Microscale Polymeric Particles. Institut Français du Pétrole (IFP) has reported several micrometer-sized particle gels (microgel) with size ranging from 0.1 to 10 micrometers (66). They were formed by crosslinking polymers under shear flow and expected to control water mobility and reduce permeability to the water phase. They are quasi-insensitivity to PH, salinity, temperature and shear stress. They were also found to have good thermo-stability and good propagation ability in porous media (67). Almohsin el at. test the transportation of microgel with diameters ranging from 100 to 285 nanometer in sandstone porous media (68). The plugging efficiency was better when using lower permeability rocks as the permeability could be reduced up to 100 times in a 41 mD core. A test contained oil phase was performed and the oil recovery was improved from 40% to 60% by the treatment(69). Dupuis et al. tested SMG (small microgel) in sandstone porous media with residual oil. Results showed that with an increase in gel concentration or a decrease of flow rate, the microgel could plug cores better (70).

Brightwater®, a type of submicron-sized gel particles, was first developed by Nalco Company, ChevronTexaco and BP. The particle size is initially under 1 micrometer and can expand from 4 to 10 times under reservoir temperature, as shown in Figure 2.5 (71). This feature makes it easier to be injected into the in-depth of porous media. Salehi et al. (2012) tested the Brightwater® particle gel using sand packs. Different from Microgel, such nanogel injection pressure was only slightly higher than the water flooding pressure before gel treatment. This is due to the characteristic that the particles will swell with the high temperature only. After heating the sand pack model, thewater injection pressure after treatment had a significant increase(72). Fabbri et al. (2015) tested the same product into the sand pack with higher permeability (7.3 Darcy). After injection and heating, the permeability was only reduced by a small fraction, proved that Brightwater® particle gel was too small when dealing a porous media with high permeability (73).

Other than the above-mentioned products, there are several other polymeric nanosized and micronized particles being studied for EOR purposes. A typical polymeric nanoparticle (PAMPS-Na nanogel) under SEM is shown in Figure 2.6.

Polyacrylamide (PAM) gels is a type of polymeric particle gel that has been used mostly for reducing water permeability. They are synthesized with a monomer and a crosslinker (74). Crosslinked Polyacrylamide nanoparticles have been studied for their EOR potential by a few researchers (63,75,76). It was found that they are a good candidate for profile control and oil displacement improvement researchers (63). Besides, PAM gel particles can also alter the wettability of porous media researchers (76).

However, in-depth problems were also observed as PAM particles could be retained in the inlet section of the core researchers (75).

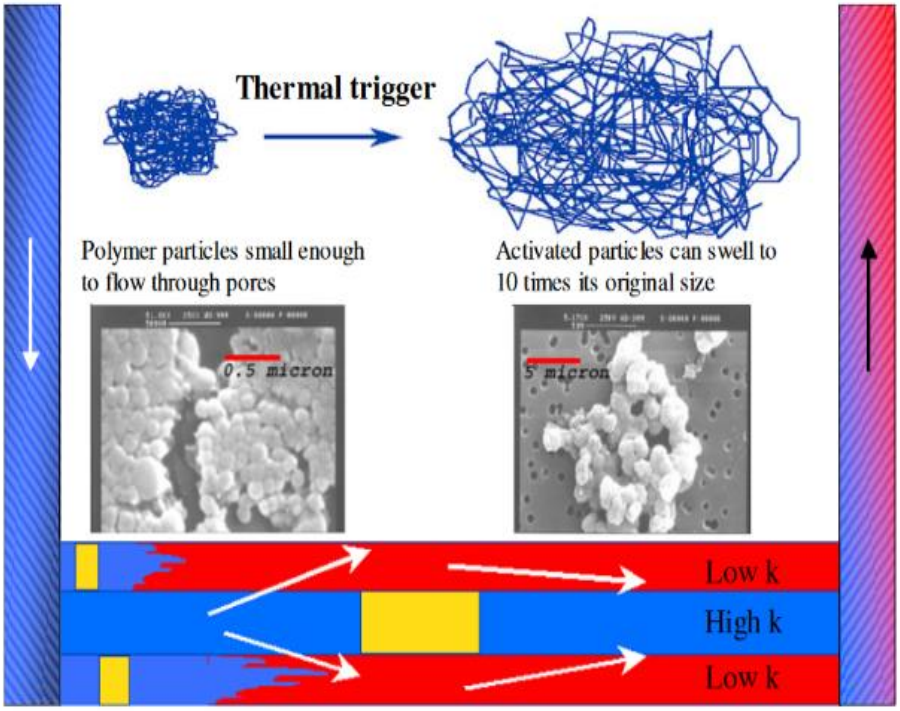

Figure 2.5. Mechanism of conformance control using Brightwater® (71)

Several studies on polymeric nanoparticles with surface charge have done recently. It was revealed that the nanoparticles can reduce oil/water interfacial tension and stabilize oil/water emulsions. The stability of the emulsions is affected by the charge of nanoparticles(77). Meanwhile, the surface charge of nanoparticle also affects the sizes of emulsion droplets and IFT reduction(78). It was also discovered that positive-charged nanoparticle tends to be adsorbed more on sandstone surface compare to neutral and negative charged nanoparticles. these nanoparticles can also alternate rock wettability to a more water-wet condition. Negative-charged particles were proved to be able to change

the contact angle the most. 10% of oil recovery increments can be observed regardless of particle surface charge. The additional oil recovery from post water flooding showed the nanoparticles can also increase oil recovery by diverting water flow to enhance sweep efficiency.

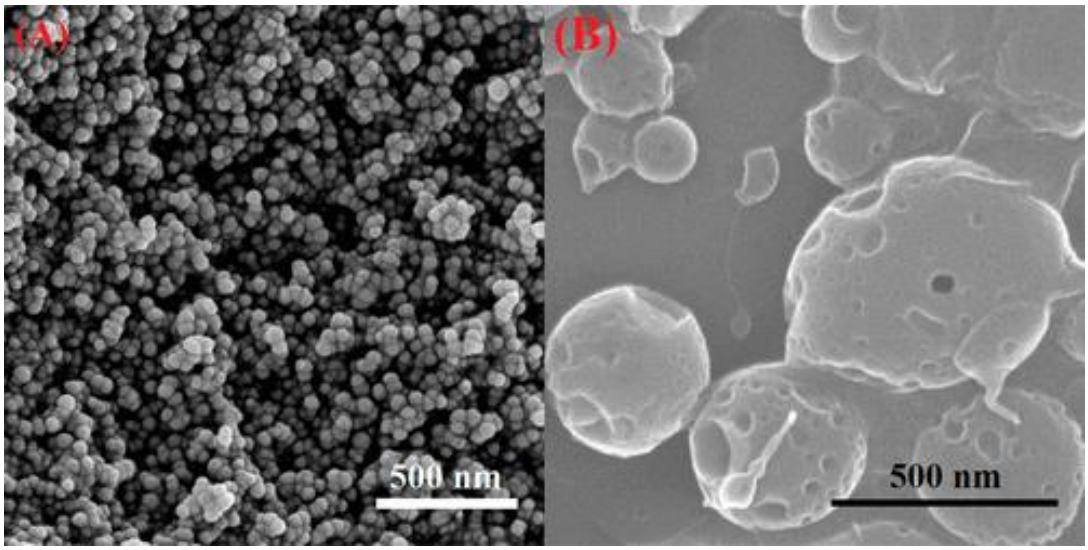

Figure 2.6. SEM micrographs of polymeric nanoparticle (nanogel) before (left) and after (right) fulling swelling (65)

PAPER

I. EXPERIMENTAL DATA ANALYSIS OF NANOPARTICLES FOR ENHANCED OIL RECOVERY

ABSTRACT

Enhanced oil recovery with nano-meter sized particles is an attractive topic in the industry because of the various advantages brought by the size. Since nanoparticles have not been applied widely on a field scale, core flooding tests are the best method to study and evaluate oil recovery improvement mechanisms. Different from previous review papers that discussed this research area case by case, our paper investigated nanoparticle core flooding research from a data statistic perspective. Thirty-nine published studies with a total of 240 laboratory core flooding tests using nanoparticles were included for this study. A dataset was constructed by collecting all relevant information available from those publications. Histograms, the combination of box plots and violin plots, bar charts, and scatter plots were utilized for visualization of the statistical analysis. We displayed the distribution of relevant parameters and the relationship between some of them. Special cases were explained and the uniqueness of the corresponding studies was discussed. Results show that in the laboratory scale, studies reveal an incremental oil recovery as high as 30% of the original oil in place (OOIP). However, the most frequent range is 5%. Wettability alternation and interfacial tension (IFT) reduction were the two most studied mechanisms. The result of contact angle tests and IFT tests could indicate the enhanced oil recovery (EOR) performance of nanoparticles in core flooding tests. In

addition, it was discovered that several aspects of nanoparticles need to be researched further for a better understanding.

1. INTRODUCTION

Nanotechnology has been a hot topic since the end of the last century. It is defined by the National Nanotechnology Initiative (NNI) as the understanding and control of matter with a dimension between 10 to 100 nanometers (1). At this size range, materials have different or enhanced properties (2) such as larger surface area (3) and quantum physics properties (4). Nanotechnology has been studied and applied in many domains such as medical (5), civil engineering (4), food science (6) and the oil and gas industry.

The application of nanoparticles addresses challenges from multiple aspects. Due to their small size, they could be used as sensors to detect reservoir properties such as temperature (7) and heterogeneity (8) inside porous media. During drilling, nanoparticles improve operations at extreme reservoir conditions (9), decrease water invasion (10), and reduce fluid loss (11). When performing hydraulic fracturing, they reduce the leak-off rate and stabilize fluid viscosity under high temperature and high pressure conditions (3).

Among all aspects, enhanced oil recovery (EOR) is one of the most studied areas of nanoparticles. Commonly, only 35%-50% of the original oil in initial can be recovered after the secondary recovery stage (12). Subsequently, a large amount of oil resource is left for EOR stage.

It has been proven that nanoparticle dispersion can change porous media wettability. By controlling the flow and spatial distribution of fluids, the wettability

would affect oil recovery during water flooding (13). Chaudhury (2003) and Wasan & Nikolov (2003) first found that liquid containing nanoparticles could change the wettability of a solid surface (14, 15). Numerous research further confirmed the ability of nanoparticles to alter porous media into a more water-wet condition (16–19). Reducing interfacial tension is another approach to improve oil recovery. When interfacial tension (IFT) decreases, displacement efficiency is improved remarkably regardless of the porous media wettability (20). Studies have shown that nanoparticles can assist surfactants to achieve a higher IFT reduction. Additionally, nanoparticles alone can reduce IFT, due to the adsorption onto the surface of fluids (21). Greater IFT reduction eventually leads to further incremental oil recovery (22–27).

Aside from wettability alternation and IFT reduction, which are the two most proposed EOR mechanisms of nanoparticles, they can also improve polymer properties: polymer flooding enhances oil recovery by improving the mobility ratio between displacing and displaced phases (12). When nanoparticles are added, the polymer fluids improve stability and heighten viscosity. Both results are desirable for a polymer EOR project (21,28). Due to the small size of the nanoparticle, it is easier to be injected into un-fractured low permeability formations as a method to improve reservoir homogeneity and sweep efficiency (29).

Despite all the proposed EOR mechanisms, nanoparticles are not widely applied on a field scale currently (21). This suggests that we still need a better understanding of nanoparticles. Experimental core flooding research is one of the best ways to study the mechanisms, effects, and EOR potentials. Some researchers have reviewed the EOR studies of nanoparticles with a focus on previous core flooding studies.

Agista et al. (2018) summarized the four advantages of nanoparticles: a) high surface area-to-volume ratio; b) the small amount required to enhance oil recovery; c) good stability in extreme conditions; and d) high flexibility. The authors also concluded that nanoparticles are the most used nanomaterial for nano-EOR (21). Likewise, Sun et al. (2017) suggested that nanoparticles can be used to solve problems from traditional methods (30). Olayiwola & Dejam (2019) reviewed the ability to assist low salinity water flooding and surfactant treatment with nanoparticles (31). Bera & Belhaj (2016) stated that 5%-15% incremental oil recovery can be expected from a laboratory core flooding test (32).

Nonetheless, Li et al. (2018) pointed out the two disadvantages of nanoparticles: a) the cost of nanoparticles is high, and b) inconsistent results from different researchers and incomprehension about the mechanisms (33). Cheraghian & Hendraningrat (2015) also suggested that this EOR method was still immature from an application point of view (34).

All the above-mentioned reviews on this topic discussed previous experimental studies case by case. Up to now, no studies have been carried out to analysis the subject from a statistic standpoint.

The objective of this work is to statistically analyze previous nanoparticle core flooding studies. To accomplish this goal, we extracted laboratory data from 39 publications regarding this subject and established a dataset including various parameters. Proper methods were utilized to summarize the current state of nanoparticle EOR studies. Current research interests, popular experimental approaches, and some relationships

between parameters were discovered. In addition, we discussed EOR performances, mechanisms, and experimental material selections.

2. DESCRIPTION OF THE DATASET

This study collected data from 39 publications with nearly 240 experiments (22–29,35–65) recorded laboratory core flooding tests that used nano-meter sized particles. The parameters of the dataset were classified into five categories (Table 1).

Table 1. Parameters in the Dataset

Category	Parameters
Nanoparticle and nanofluid properties	Nanoparticle type, polarity, size, surface area, and bulk density; dispersion salinity, concentration, and viscosity.
Material properties	Core lithology, permeability, porosity, pore volume, and size (section area & length); oil viscosity and API gravity.
Experimental operational properties	Temperature, injection volume, flow rate, injection velocity, injection scenario.
Oil recovery improvement	Original oil in place, oil recovery from water flooding, and incremental oil recovery.
Mechanism studies	Interfacial tension reduction, wettability alternation (contact angle), resistance factor, and residual resistance factor.

Values of the parameters were statistically analyzed in one or multiple dimensions. Information repeated within the same publication was deleted during the data processing. As shown in Figure 1, the numbers of tests per publication were disparate.

We extracted data from 26 core flooding tests from the paper with the most experiments. On the other hand, various papers in our dataset only reported results from less than three experiments. It would lead to a skewed analysis if all experiments were weighted the same. Hence, for categorical data, repeated information from the same study was only taken into account once. For numerical data, only the mean values of parameters were recorded when they were not variable factors in the studies.

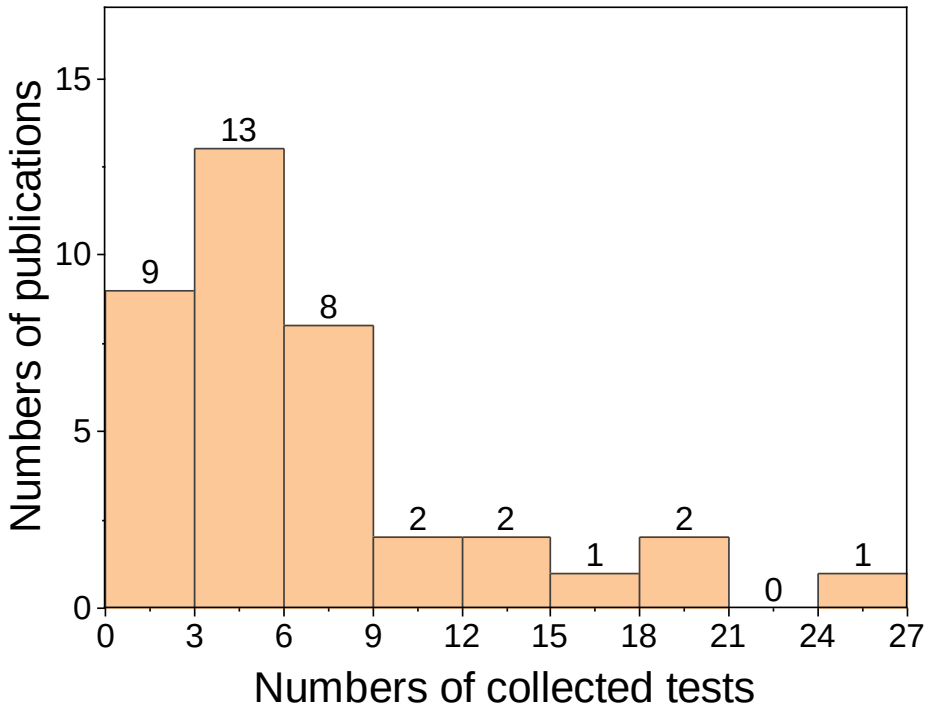

Figure 1. Distribution of the Numbers of Collected Tests from Each Publication

3. DATA VISUALIZATION METHODS

Box plot combined with violin plot: Box plot is the preferred method to visually analyze a single parameter. In a box plot, the minimum, first quartile (Q1), median, third

quartile (Q3), maximum, and mean values of a parameter are demonstrated. The maximum (upper limit) and minimum (lower limit) are defined as [Q3+1.5*(Q3-Q1)] and [Q1-1.5*(Q3-Q1)]. Any values above or below these limits are identified as outliers. In addition, the violin plot is added to enhance the display of distributions. The width of the violin plot at each position represents the frequency at this value. Figure 2 shows a typical combination plot with each element labeled.

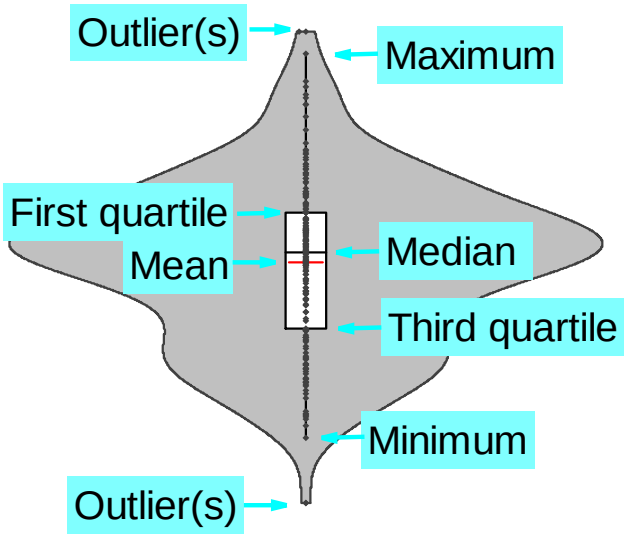

Figure 2. Schematic of a Combination Plot of Box Plot and Violin Plot

Histogram: When the variance is too small or too large, a histogram is preferred to show the distribution of a numerical parameter. A histogram shows the numbers of values within an interval on vertical and variable on horizontal.

Bar chart: Similar to the histogram, a bar chart is a plot of categorical variables. It shows comparisons among categories.

Scatter plot: A scatter plot visualizes the values of multiple different variables. It can show the relationships between different parameters.

4. RESULTS AND DISCUSSIONS

4.1. NANOPARTICLE PROPERTIES

Figure 3 summarizes some key properties of nanoparticles in the dataset.

As shown in Figure 3 (a), multiple nanoparticle types were featured in different studies. The most widely used type was silicon (silicon dioxide). Metallic oxide nanoparticles were the second most frequent type, which includes Al_2O_3, Fe_2O_3, MgO, Ni_2O_3, NiO, SnO, TiO_2, ZnO, ZrO_2 particles. In spite of not being commonly studied, clay nanoparticles and polymer nanoparticles (including polymer-coated nanoparticles) were studied in a few articles as well. In addition, nanoparticle polarities were reported in 23 publications. As Figure 3 (a) reveals, there are three types of polarity: hydrophilic, lipophilic, and neutral. Hydrophilic is the most frequently seen category. For particles with unreported polarity, we can safely assume that they were all hydrophilic or natural because of their solvent being deionized (DI) water and brine.

Figure 3(b) demonstrates the distribution of particle sizes. Most of the particles being studied were smaller than 60 nm in diameter. Both the smallest and biggest nanoparticles were silicon particles (5nm and 140 nm in diameter). For all but polymer particles, the sizes would not change significantly when dispersed in a solvent. For polymer particles, we collected values of the swelling particle diameter to the dataset.

Statistics of surface area values are shown in Figure 3(c). As stated earlier, a higher surface area is often considered as an advantage of nanoparticles (21). A higher surface area could lead to a stronger adsorption to the rock surface (31), more dominant behavior of atoms on the surface of particles, and greater interactions with other particles

(66). The lowest surface area value was 6 m^2/g, the highest was 650 m^2/g, and the mean value was 176 m^2/g. This parameter of the most particles was lower than 200 m^2/g, and few were higher than 400 m^2/g. The relationship between particle size and surface area is revealed in Figure 3(d); smaller particles would have a relatively higher surface area at the same weight.

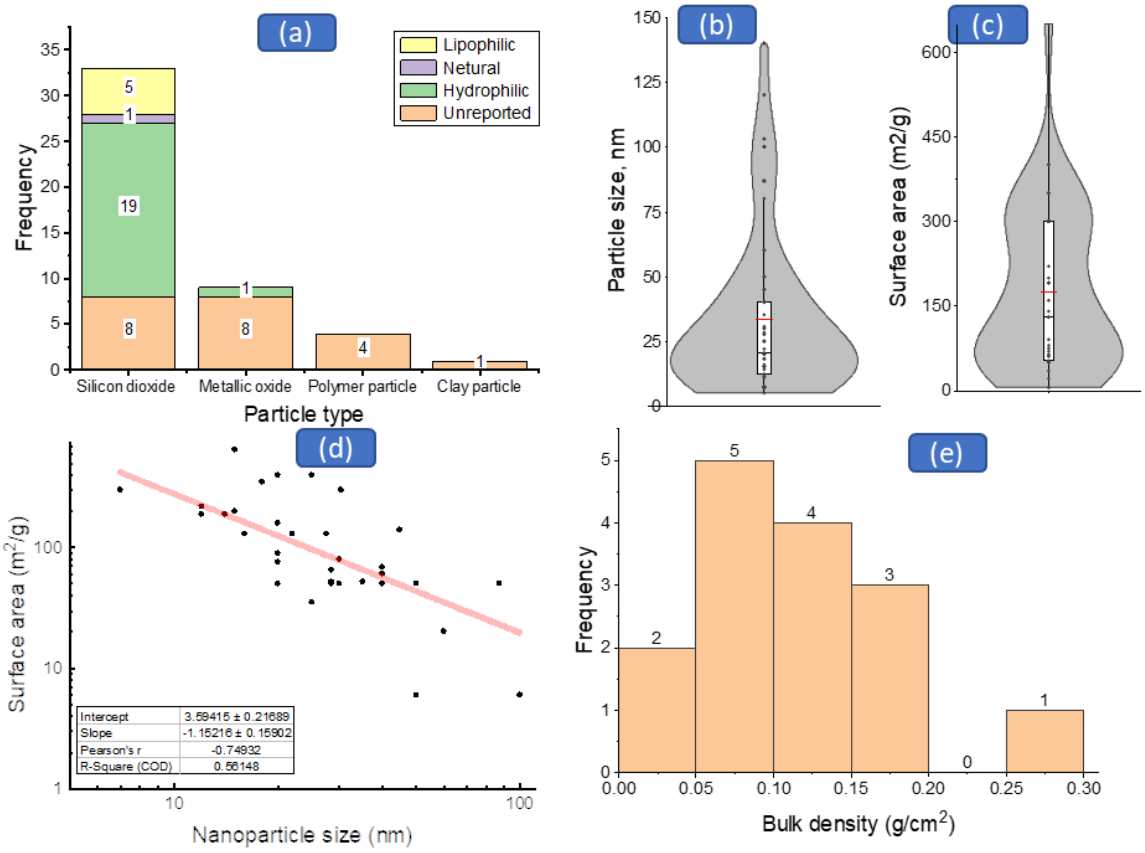

Figure 3. Distributions of Important Nanoparticle Properties
(a) Particle Type (and Polarity); (b) Particle Size (in Diameter); (c) Surface Area; (e) Bulk Density; and Relationship Between (d) Surface Area and Size

The bulk densities of only 15 different nanoparticles from 8 publications were reported. As shown in Figure 3(e), most of the bulk densities were between 0.05 to 0.2

g/cm^2. Both median and mean value were around 0.1 g/cm^2. The lowest and highest densities were 0.04 g/cm^2 and 0.295 g/cm^2, respectively.

4.2. DISPERSION PROPERTIES

Figure 4 shows the properties of nanoparticle dispersions in the dataset. Figure 4(a) depicts the distribution of nanoparticle concentration. It shows that despite a few cases with high concentrations, in most studies, a concentration lower than 1,000 ppm was used and the lowest was 50 ppm. The highest concentration appeared in the study by Qiu & Mamora (2010). The authors selected a concentration of 47,600 ppm to thicken the fluid for heavy oil recovering (38).

Figure 4(b) displays salinity distribution; the most frequent salt concentration range was between 3 % to 4%. Four studies used DI water where the salinity was 0. Figure 4 (c) reveals that Xylene or Ethanol was selected as solvents in studies focused on lipophilic particles, which require organic solvents (27,38,42,50,60). As shown in Figure 4(d), in 16 studies, NaCl alone was used to synthesize the brine. In the other 9 studies, the brines were either synthetic sea water or formation water containing multiple salt content.

Figure 4(e) summarizes dispersion viscosity information. Among the reported viscosity values from only 10 publications, the majority of nanoparticle dispersion viscosities were between 1 cp to 1.1 cp, which was not much higher than their solvent (DI water or brine).

4.3. MATERIALS PROPERTIES

Figure 5 and Figure 6 illustrate parameters regrading experimental materials (cores and oil).

The following core models were selected for core flooding tests: core, sand pack, and glass micromodel, as shown in Figure 5(a). Lithology details are also demonstrated: most of the models were sandstone cores, while only 5 were carbonate cores.

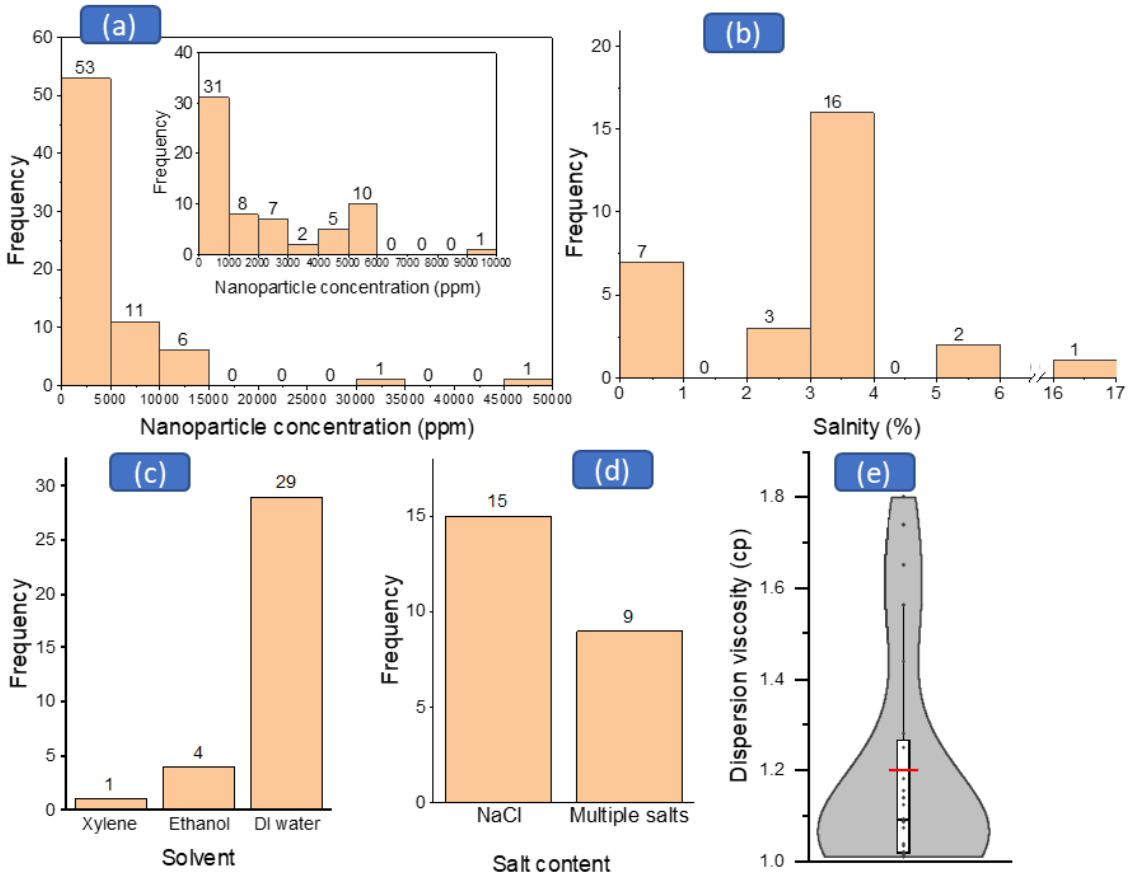

Figure 4. Summary of Nanoparticle Dispersion Properties
(a)Nanoparticle Concentration; (b) Salinity; (c) Solvent; (d) Salt Content; and (e)Dispersion Viscosity

Figure 5(b) describes the porosity distribution of the cores in this dataset. The most frequent porosity range was 15% to 20%. A handful of core models had a porosity higher than 35% and the most porous model was a glass micromodel with a porosity of 52.2% (40). In fact, all core models with a porosity higher than 30% were either sand pack model or glass model. The highest porosity of a natural core model was 30% (36). As discussed previously, one of the advantages of nanoparticles is the ability of transportation in low permeability formations. Accordingly, as shown in Figure 5(c), all but six models had permeability lower than one Darcy. The lowest average permeability of a study was 0.245 mD, as a simulation of a low permeability reservoir (65). The objective silicon nanoparticle showed great EOR potential and injectivity at this permeability. The most permeable core model was also a glass micromodel with a permeability of 25,000 mD (23). The highest permeability of a natural core was 2.6 Darcy (54). Figure 5(d) displays the log-linear relationship between porosity and corresponding permeability in the dataset. As the porosity of glass micromodels are relative higher compare to other models, these cases were highlighted in red in the plot.

Figure 5(e) through (g) show the distribution of parameters regarding the core dimension. Every core model in the dataset was either cylindrical or cuboid. Data from studies using micromodels were excluded due to the extreme small sectional area (0.04 and 0.039 cm^2). The longest core used was 48 cm long and the shortest was 3.26 cm long. As Figure 5(e) indicates, most cores were shorter than 15 cm, and only a few of them were longer than 20 cm. Most core sectional area values fell into the range between 10 cm^2 to 15 cm^2. A cylindrical core model at this range would have a diameter between 3.6 cm to 4.4 cm. The smallest sectional area of a natural core or sand pack was 2.85 cm^2.

Pore volumes (PV) of most cores were lower than 20 cm^3. The smallest pore volume was 2.6 cm^3 and the biggest pore volume was 95 cm^3.

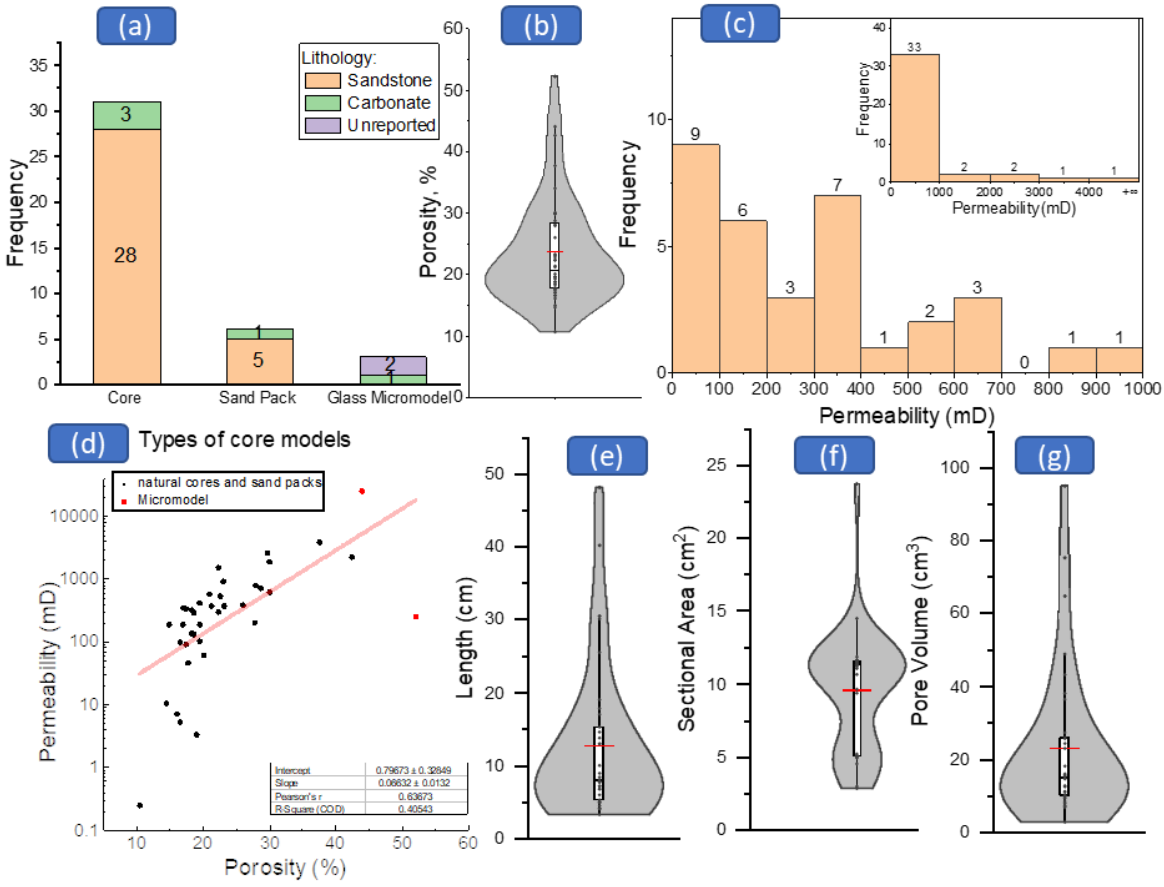

Figure 5. Distribution (and Relationships) of Various Core Properties
(a) Model Type and Lithology; (b) Porosity; (c) Permeability; (d) Relationship Between Porosity and Permeability; (e) Length; (f) Sectional Area; and (g) Pore Volume

As shown in Figure 6(a), at experimental conditions, most oils selected for the studies were lower than 25 cp in viscosity. The least viscous oil was n-decane, whose viscosity was only 0.92cp (49). It is worth noting that the three highest viscosity values (as shown in the far right of the histogram) were all way above 250cp. The highest viscosity at experimental condition was 61637 cp. This study ran experiments at both

room temperature and high temperature. When the temperature reached 70 ℃, the oil viscosity dropped to 511 cp (35). The distribution of the oil viscosity at room temperature is not shown because of the similarity between distribution of viscosity at room temperature and experimental condition. This is due to the fact that most of the studies were conducted at room temperature only. The highest viscosity at room temperature in the dataset was 66,000 cp (62). However, this study was conducted under a high temperature condition and the viscosity at the experimental temperature was not reported.

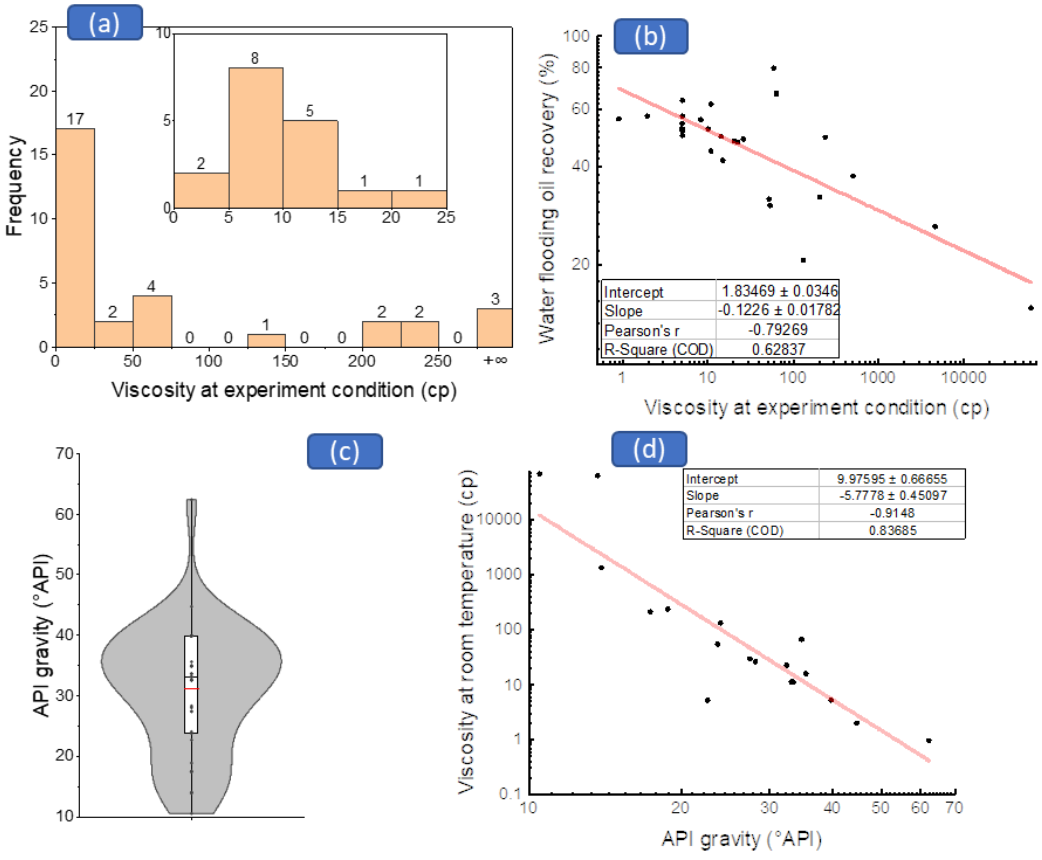

Figure 6. Distribution and Relationships of Parameters Regarding Oil Properties (a) Viscosity (at Experiment Condition); (b) the Relationship Between Oil Recovery and Viscosity; (c) API Gravity; (d) the Relationship Between API Gravity and Viscosity

Oil viscosity plays a major role in water flooding recovery. As demonstrated in Figure 6(b), less water flooding oil recovery would be observed with a higher oil viscosity at the experimental condition. Measured in American Petroleum Institute (API) gravity, 30° API to 40° API (0.825g/ml – 0.876 g/ml) was the most frequent range of oil gravity, see Figure 6(c). Figure 6(d) displays the negative relationship between gravity and viscosity.

4.4. EXPERIMENT APPROACH

Figure 7(a) depicts that most of the experiments were conducted at room temperature. The temperature in 14 studies was between 20 to 30 degrees Celsius. The lowest was 17 degrees, which is room temperature as well. Eighteen papers did not report the temperature. It is likely that those core flooding tests were conducted at room temperature as well. Most of the higher temperature cases studied the impact of temperature on the EOR performance of nanoparticles. Five of the studies reported experiments at high temperatures only. The highest value was 240 degrees Celsius, which was the experiment condition for a nanoparticle-assisted steam flooding project (62). At this high temperature condition, the authors placed nanoparticles inside the sand pack prior to the steam injection process and observed incremental oil recovery up to 10%. All other studies were conducted under a temperature below 100 degrees Celsius.

Figure 7(b) and (c) summarize the distributions of injection flow rate and interstitial velocity. Interstitial velocity is the speed at which water is progressing in the direction of movement. It is calculated as the volumetric flow rate divided by the cross-sectional area and the porous medium porosity. Lower flow rates were selected by most

researchers as 0 - 0.25 mL/min is the most frequent range. The highest flow rate was 3.3 mL/min, and the lowest was only 0.0008 mL/min from the study by Mohajeri et al. However, due to the small sectional area in this work (0.039 cm2), the interstitial velocity was 1.86 ft/day (40). The interstitial velocities in the data set were mostly lower than 10 ft/day. The lowest value was 1.3 ft/day. The two highest interstitial velocities are not shown in the box plot due to their extremely high values. In the study by Hendraningrat et al, the sectional area of the micromodel was only 0.04 cm^2. Flow rates of this study were 0.1 and 0.5 ml/min. Hence, the interstitial velocities were 268 and 1342 ft/day. The maximum interstitial velocity excluding this study was 43 ft/day.

Average injection volumes by PV (pore volume) from every study are summarized in Figure 7(d). The highest and lowest injection volumes were 12 PV and 0.2 PV. Since most of the studies stopped nanoparticle injection only after the water cut reached 100% (no more oil production), it was a good indicator of the amount of nanoparticle dispersion required for an EOR procedure. Figure 7(e) shows the connection between the nanoparticle concentration and the injection volume of each study: with higher nanoparticle concentration, less injection volume would be needed for the EOR process.

In addition, five of the studies in the dataset reported tests in a single phase (water only) condition. Their focuses were on the injectivity and plugging efficiency of nanoparticles. However, the majority of the experiments were performed in water-oil two-phase conditions. As depicted in Figure 7(f), experiments in two-phase condition can be further divided into two categories by the injection scenario. The “secondary stage” represents cases in which nanoparticles were injected right after oil saturation. There was

no water flooding prior to the nanoparticle flooding. In contrast, the “tertiary stage” means that nanoparticle flooding was performed after water flooding. Worth noting, the incremental oil recovery for the secondary injection scenario could be negative because of the possibility that nanoparticle flooding recovers less oil than water flooding. Nine studies performed subsequent water flooding after nanoparticle flooding as an effort to recover more oil.

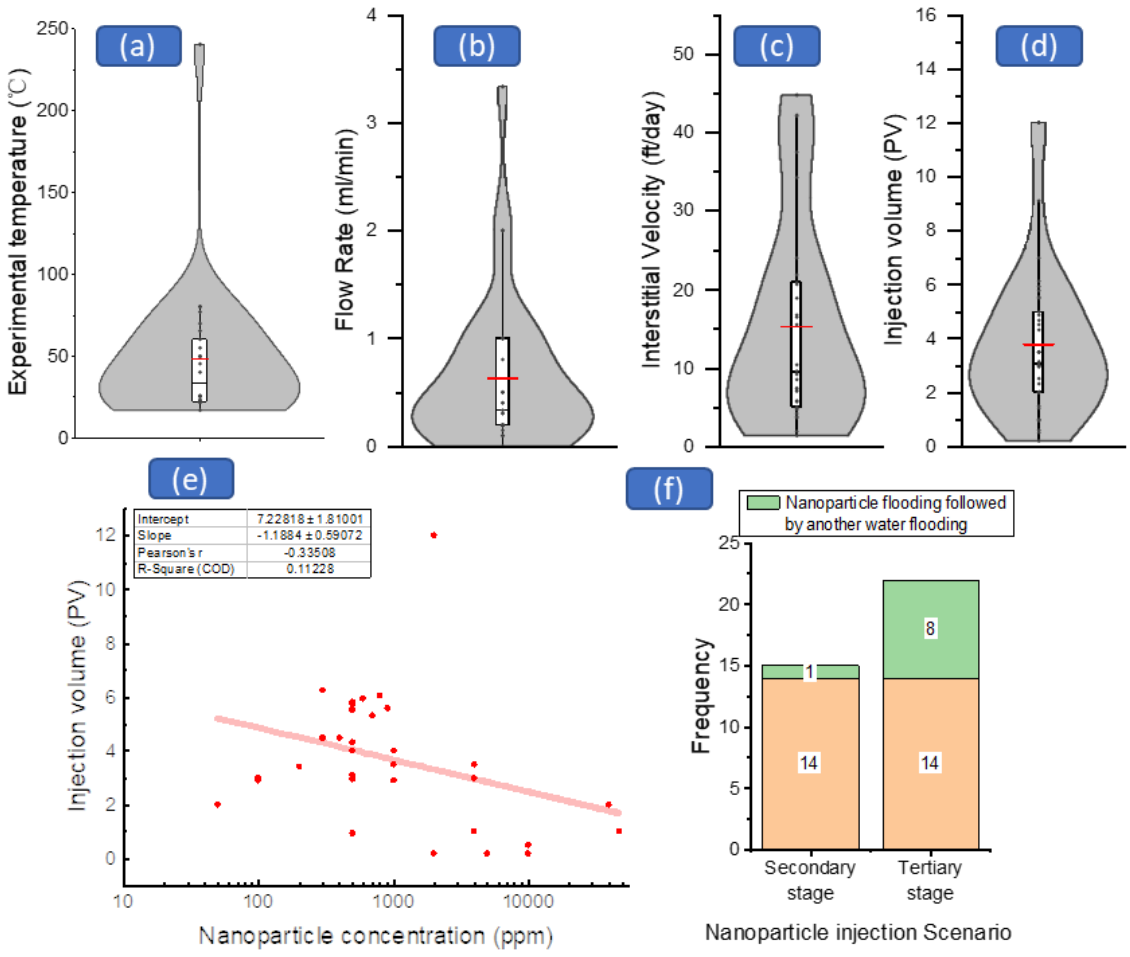

Figure 7. Parameters Regarding Core Flooding Approach
(a) Temperature; (b) Flow Rate; (c) Interstitial Velocity; (d) Injection Volume; (e) Relationship Between Injection Volume and Nanoparticle Concentration; (f) Injection Scenario; and (g) Other Injected Components

4.5. OIL RECOVERY IMPROVEMENT

Incremental oil recovery is the most important evaluation criterion for a nanoparticle EOR study. Figure 8 summarizes the results from the dataset. Figure 8(a) displays the average oil recovery before and after nanoparticle treatments. The average initial oil recovery (oil recovery after water flooding) is 51% and the average final oil recovery is 60%. The incremental oil recovery data are shown in Figure 8(b). Most of the increments were lower than 10%, also the most frequent range of this parameter. The lowest increment was only 0.97%. The objective nanoparticle in this study (54) improved oil recovery by conformance control. However, due to the small scale of the core model heterogeneity, only a marginal incremental recovery was observed. The highest increment was over 30% as the objective nanoparticles were able to reduce IFT greatly by 24.15 mN/m. (60).

4.6. EOR MECHANISMS STUDIES

As discussed earlier, interfacial tension reduction and wettability alternation are the two most studied and proposed EOR mechanisms of nanoparticles. Figure 9 and Figure 10 summarize the studies regarding these two mechanisms.

As discussed earlier, the reduction in the interfacial tension (IFT) would benefit the displacement efficiency in both water-wet and oil-wet systems and lead to an increase in oil recovery accordingly (20). This was the EOR mechanism proposed in many nanoparticle EOR studies. Besides core flooding experiments, 16 studies conducted IFT tests to understand this EOR mechanism. Figure 9(a) demonstrates the distributions of oil-water IFT in the base fluids (brine/DI water) and nanoparticle dispersions. The IFT

after applying nanoparticles is significantly lower than the initial IFT, as the mean values are 12 and 26.3 mN/m, respectively. Figure 9(b) reveals the distribution of the average IFT reduction from each study. The highest reduction was 36.7 mN/m.

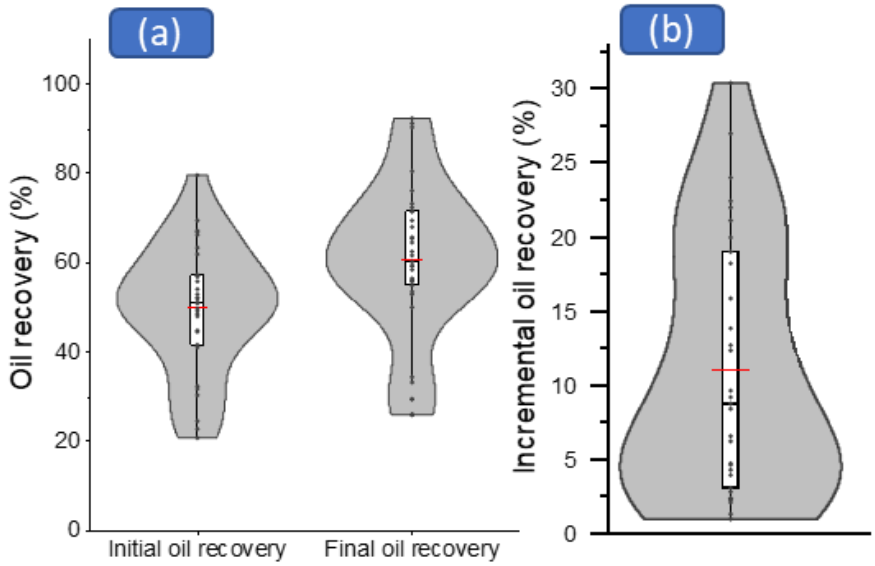

Figure 8. Distribution of (a) Initial Oil Recovery and Final Oil Recovery; and (b) Incremental Oil Recovery

As pointed out by the arrow in Figure 9(b), Roustaei, et al. (2015) suggested that the nanoparticle of their study increased oil recovery mainly by wettability reversal (from oil-wet to water-wet) (55). The IFT was increased by 11 mN/m (the reduction was -11 mN/m). This was due to a large amount of residual oil left after initial water flooding since the system was initially oil-wet. IFT increases would result in higher capillary pressure and benefit imbibition. All other studies observed IFT reduction after the application of nanoparticles into the water phase.

Figure 9(c) and (d) display the IFT reduction in relation to nanoparticle concentration and oil recovery increment. The two scatter plots indicate that higher nanoparticle concentration would lead to a larger IFT reduction. At the same time, incremental oil recovery increased with IFT reduction. Both arrows in the scatter plots in Figure 9(c) and (d) point out the outlying data from Roustaei et al. (2015) where nanoparticles increased the IFT.

As wettability being another important function of oil recovery, when a system becomes more water-wet, oil recovery increase (13). The measurement of the contact angle was performed in most studies in our dataset. The contact angle in a water-oil-solid system is defined as the angle measured through the water phase when oil is less dense than water. However, some studies measured contact angles of the wrong side. Those results were re-calculated before being recorded into the dataset. A system is defined as water-wet if the angle is lower than 75 degrees, oil-wet if the angle is higher than 105 degrees, and neutrally-wet if the angle is in the middle range (67).

Figure 10(a) shows the distribution of contact angles of water-oil and nanoparticle dispersion-oil systems. As the box plot on the left indicates, most of the systems were initially water-wet while the range between 45 to 60 degrees is the most frequent. When spreading nanoparticles, the most frequent range became 20 to 40 degrees. Figure 10(b) illustrates the contact angle reduction distribution. The more a contact angle is reduced, the more a system is altered to water-wet. Most systems became more water-water after adding nanoparticles. However, a few studies suggested that a more neutral system is favorable for oil movement compared to a strong water-wet system (27,42,60). The goal

of these studies is to create a more neutral-wet system which could reduce capillary pressure and make oil drop move easier.

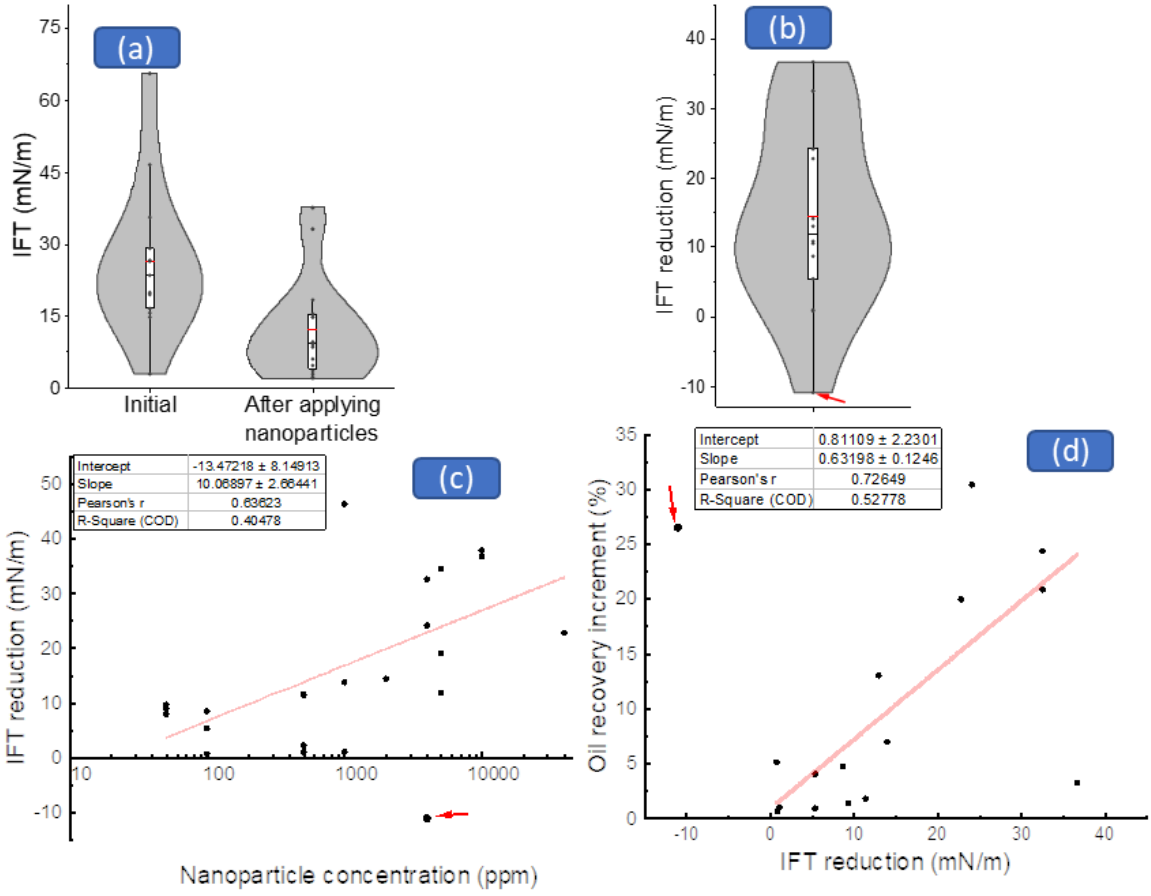

Figure 9. Distribution of IFT Tests Results and the Relationship to Other Parameters (a) Initial and Post-treatment IFT; (b) IFT Reduction; (c) Relationship Between Nanoparticle Concentration and IFT Reduction; and (d) Relationship Between IFT Reduction and Incremental Oil Recovery

Figure 10(c) and (d) reveal the impact of nanoparticle concentration on contact angle alternation and the impact of alternation on EOR performance. Above mentioned studies that observed contact angle increases are excluded. Similar to the previous results

regarding IFT reduction, dispersions with higher concentration can alter wettability better. A greater alternation can result in higher incremental oil recovery.

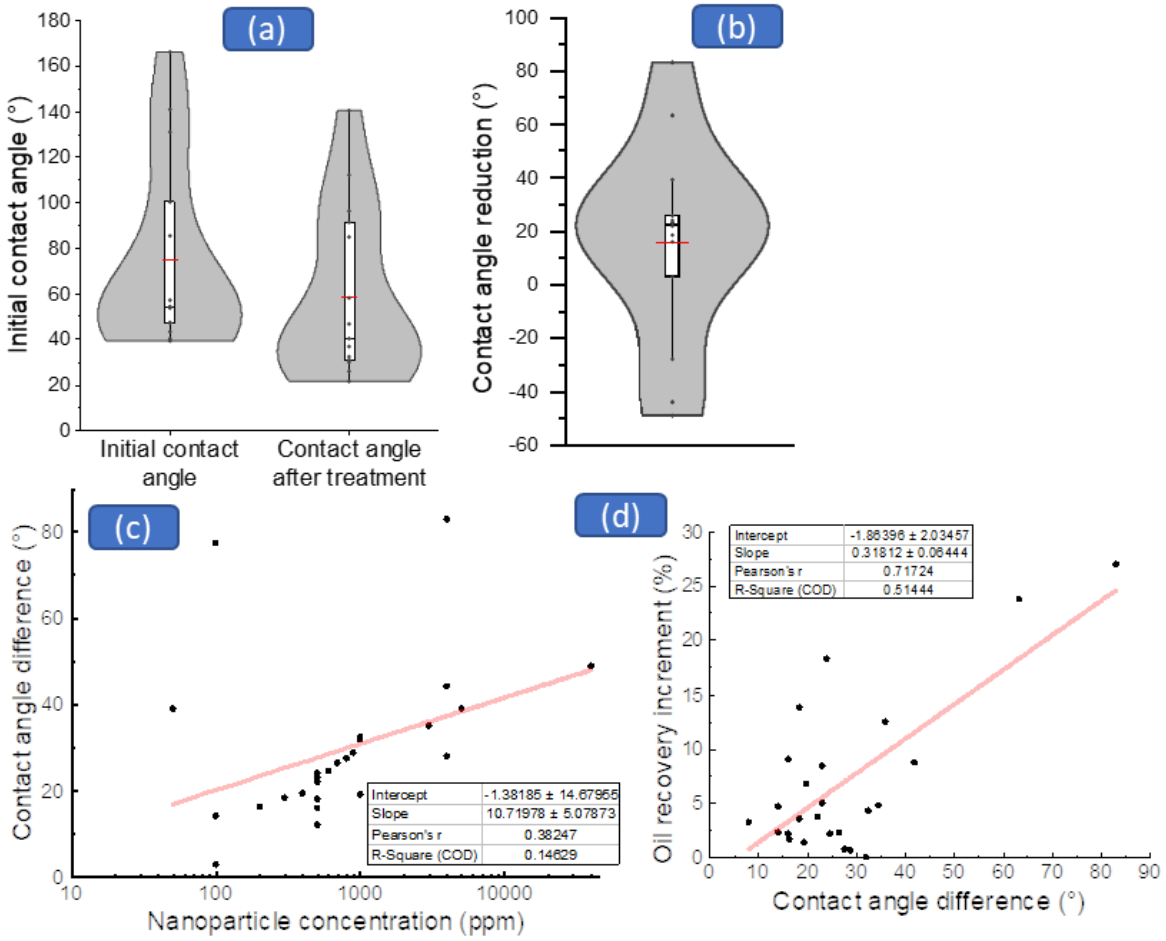

Figure 10. Distribution of Wettability Tests Results and the Relationship to Other Parameters (a) Initial and Post-treatment Contact Angle; (b) Contact Angle Reduction; (c)Relationship Between Nanoparticle Concentration and Contact Angle Reduction; and (d) Relationship Between Contact Angle Reduction and Incremental Oil Recovery

Aside from IFT reduction and wettability alternation, some researchers studied the injectivity of nanoparticles. Due to the size advantage of nanoparticles, they are easily injected and can improve reservoir homogeneity by plugging porous media. Resistance

factor (RF) and residual resistance factor (RRF) are the common parameters for evaluating conformance control. RF is defined as the ratio between water mobility and treatment fluids mobility. Mathematically, it could be calculated as the ratio between nanoparticle dispersion injection pressure and pre-treatment water flooding pressure. RFF is defined as the ratio between water mobility before and after treatment. It represents how many times the permeability is being reduced. Figure 11 shows the distributions of RF and RRFs in the dataset. Data were either collected directly from publication or captured from pressure plots.

In most studies, RF and RRF were lower than 5. However, in Li et al. (2015), the authors observed both RF and RRF with extremely high values (over 10, 000) as a result of the core surface being completely blocked (43). The strong adsorption caused the plugging effect in spite of the large difference between particle size and pore size (particle diameter was 7 nm and porous media permeability were between 100 mD to 260 mD). For better visualization, these outliers are not shown in the plot. The lowest values of both RF and RRF were from the research by Xu et al. (65). RF was 0.89 and RRF was 0.53, which were caused by the particle's strong IFT reduction ability.

4.7. FACTORS THAT AFFECT THE EOR OF NANOPARTICLES

As stated in the earlier section (4.4), there are two scenarios for a nanoparticle EOR project: secondary stage injection scenario and tertiary stage injection scenario. For the first scenario, incremental oil recovery is calculated as the oil recovery difference between nanoparticle flooding (and subsequent water flooding) and water flooding alone. Due to the possibility that nanoparticle flooding could recover less compared to water

flooding, the increment could be negative in this scenario. For the latter scenario, the increment is the oil recovery from the nanoparticle flooding (and subsequent water flooding). Figure 12(a) demonstrates the average incremental oil recovery by scenario. The existence of cases with negative increment led to the smaller increment in the secondary scenario. Meanwhile, the second distribution peak in the left box plot indicates that there were more cases with better EOR performance in the tertiary scenario.

Figure 12(b) shows the nanoparticle dispersion injection volume by injection scenario. The mean injection volume value of the secondary scenario is higher than the tertiary stage scenario by a small margin. For the tertiary scenario, less injection volume was required due to the existence of water flooding before nanoparticle flooding. However, even in the secondary scenario, it only took a small amount of injection volume for most cases to reach the breakthrough point. At that point, the oil recovery which was supposed to be produced by water flooding was reached. Thus, the difference in injection volume between scenarios was not significant.

Figure 13 reveals the average incremental oil recovery improved by different particle types and polarities. Due to small sample size, polymer particles and clay particles were excluded from this comparison. As shown in Figure 13(a), core flooding tests with silicon dioxide had much better EOR results compared to tests with metallic oxide particles. The mean incremental oil recoveries were 4.3% and 12%. This explained the reason for the popularity of nano-silica in nanoparticle EOR research. Lipophilic particles improved oil recovery even more as the mean increment was over 20%. One reason was oil-wet porous media being selected in lipophilic particles studies. An oil-wet system is unfavorable for water flooding. Hence, it would leave plenty of room for EOR

processes. Secondly, all lipophilic particles were dispersed in organic solvents, which can recover more oil compared to brine or DI water regardless of the presence of nanoparticles (50).

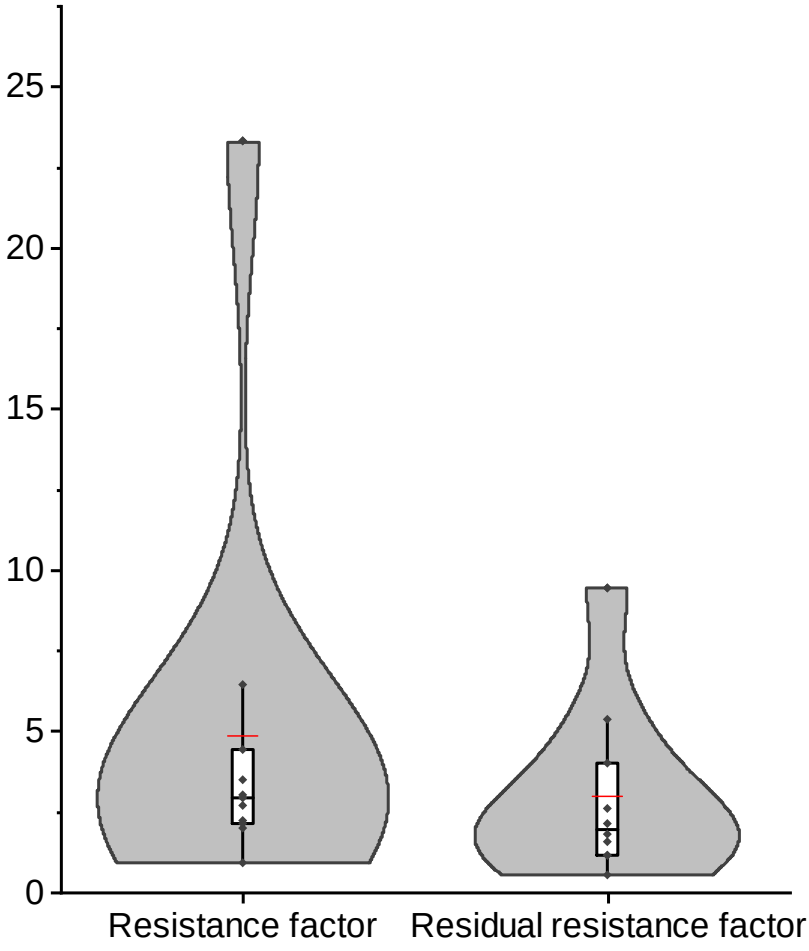

Figure 11. Resistance Factor and Residual Resistance Factor Distributions

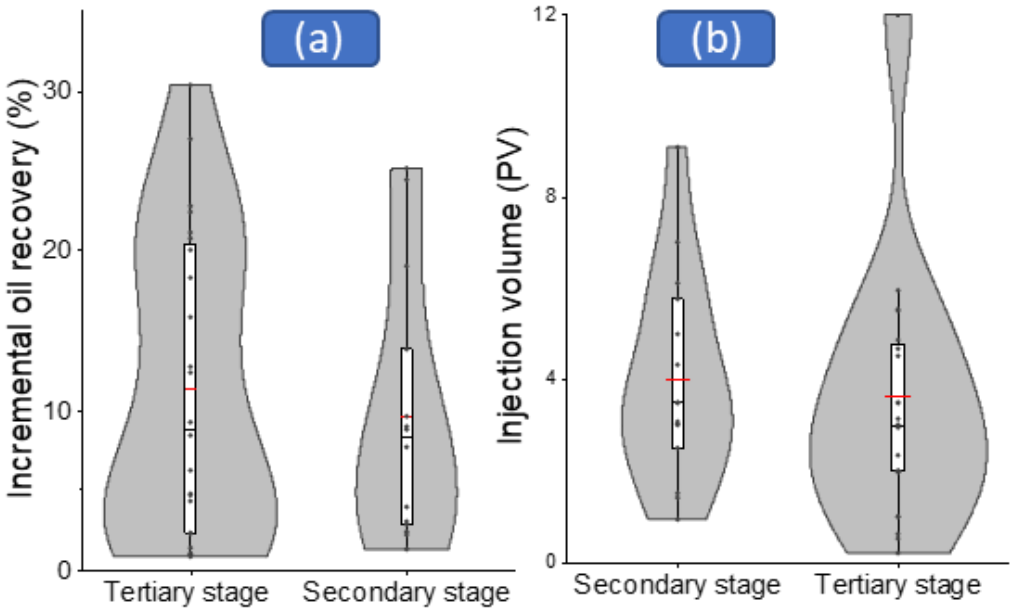

Figure 12. Effect of Injection Scenario on (a) Incremental Oil Recovery and (b) Nanoparticle Dispersion Injection Volume

Concentration was another key parameter to nanoparticle EOR. Figure 14 illustrates that the higher the nanoparticle concentration, the higher the incremental oil recovery would be observed. As shown in the last section, higher nanoparticle concentration can lead to better wettability alternation and IFT reduction. Consequently, incremental oil recovery increased with concentration.

Particle size is proposed to be a key factor of EOR performance (21). Unfortunately, as displayed in Figure 15(a), in our dataset, the relationship between particle size and incremental oil recovery was not clear. The Pearson correlation coefficient of only 0.17 indicated that the correlation between these two parameters was neglectable (68). However, Figure 15（b） proves that a higher surface area was favorable for improving oil recovery. As mentioned in Figure 3, the surface area increased with a decrease in particle size. Hence, this observation reflects that particle

size had an impact on EOR. In fact, higher surface area due to smaller particle size was one of the proposed nanoparticle advantages over other EOR agent s (3).

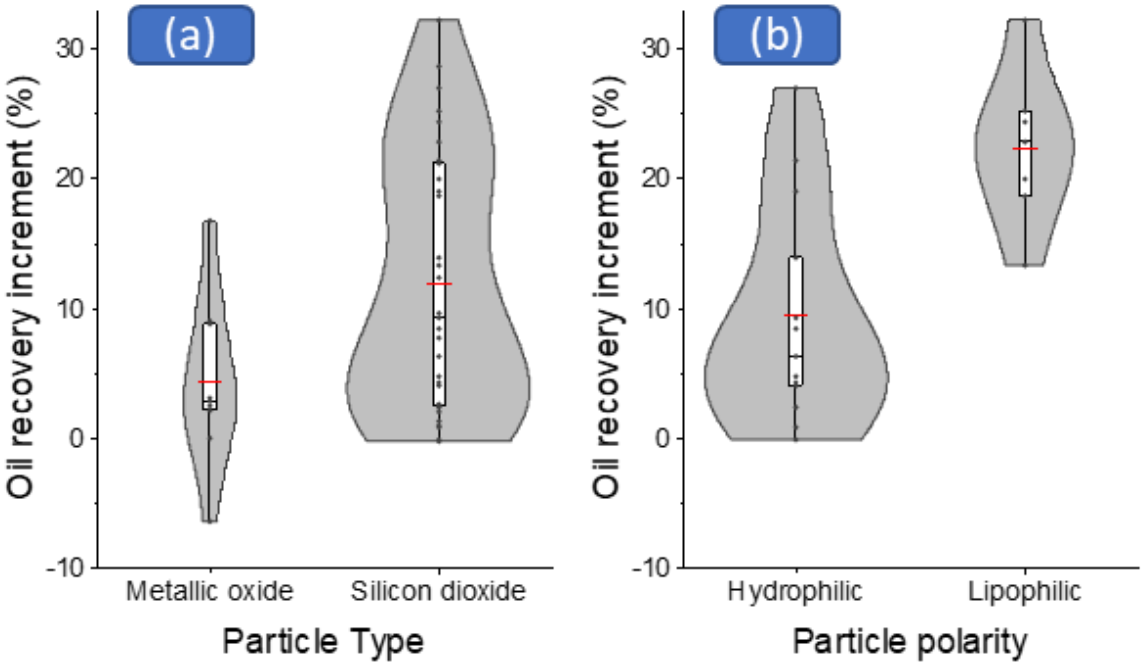

Figure 13. Impacts of (a) Particle Type and (b) Particle Polarity on Incremental Oil Recovery

5. UNDER-RESEARCHED TOPICS

In our dataset, in over 80% of the studies, the silicon dioxide particle was chosen as the main research objective or contrast object. Such popularity was due to its well-known properties, mechanism and the fact that it can be easily produced (21). The metallic nanoparticle is the second popular type and was often prepared combined with silica nanoparticle. However, few studies focused on other types of nanoparticles. Polymer-nanoparticle was one of the promising nanoparticle categories as it could

improve sweep efficiency and injection fluids viscosity (29). The difference between polymer particle and silica/metallic particles is notable; unlike the others, polymer particles are deformable and swellable when being dispersed in water or brine. Such properties give particles better in-depth transportation properties (69). On the other hand, the in-depth transportation of nanoparticles has not been well-studied. Before the application on a field scale, we must guarantee successful transportation of the nanoparticles in the reservoir.

There were fewer studies conducting experiments in high-temperature conditions. It was proven that nanoparticles can play an important role in steam EOR processes (62). However, the impact of temperature on the performance of nanoparticles is still unclear (21).

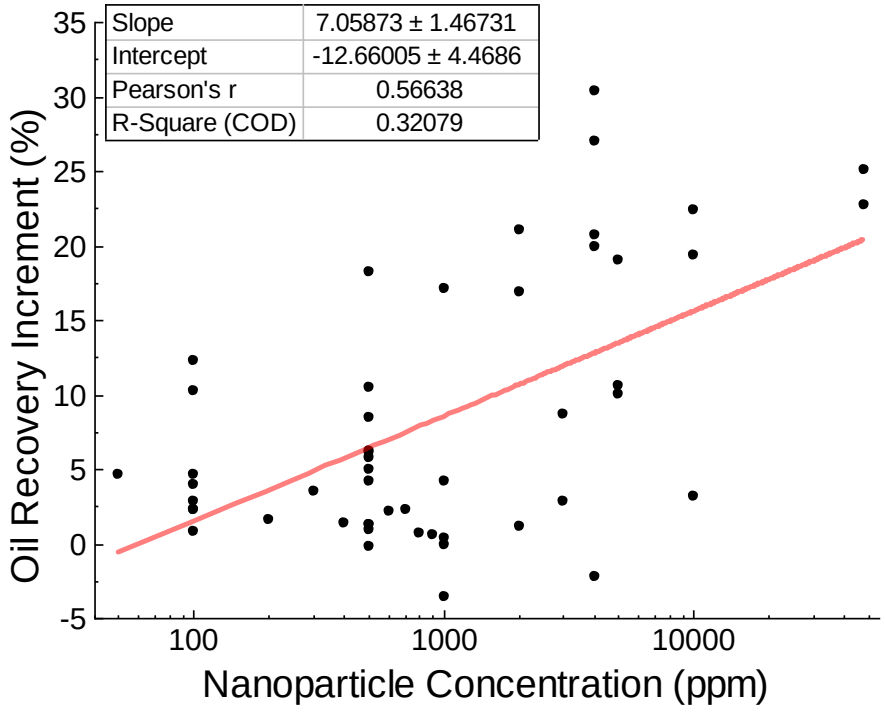

Figure 14. Impacts of Nanoparticle Concentration on Incremental Oil Recovery

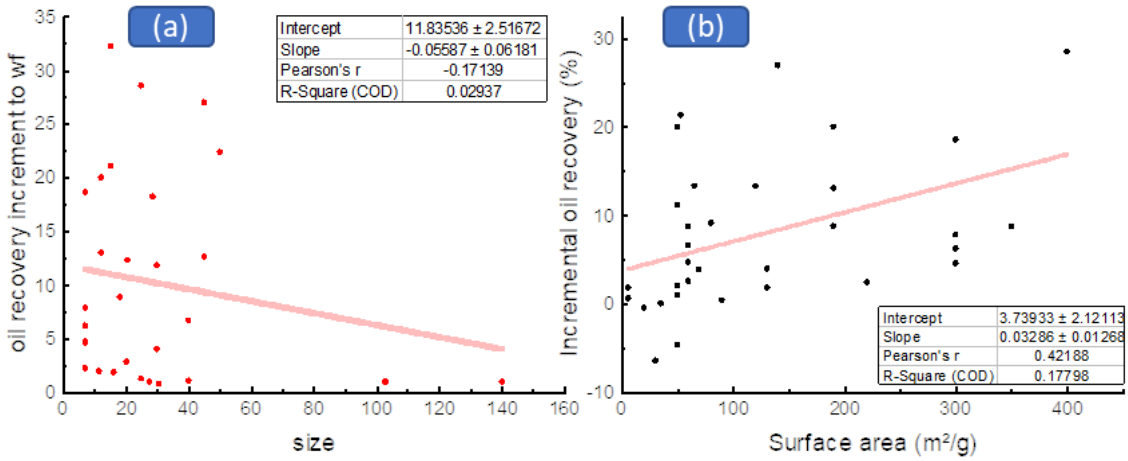

Figure 15. Impacts of Surface Area on Incremental Oil Recovery

With IFT reduction and wettability alternation being the most investigated mechanisms, the understanding of other mechanisms is still crucial. As stated earlier, since it is easier for nanoparticles to be injected into a low permeability formation, they might be used as conformance control agents to improve reservoir homogeneity. However, this impact was neglected by many studies. Polymer particles were often proposed for conformance control (70). The ability of micron and sub-micron size polymer particles to improve injection profile at low permeability porous media has been proven (69,71,72). However, the injectivity of such particles was fairly low when the target permeability became lower than 100 mD (72). Nano-meter sized polymer particle would be a good candidate for treatment at this situation. Thus, more studies on polymer particles would benefit the understanding of such mechanisms as well.

6. CONCLUSIONS

- This work built a dataset consisting of core flooding tests from nanoparticles for EOR studies;
- Key parameters in six categories were collected and analyzed from a statistical aspect;
- Parameter distributions revealed the popular (and unpopular) selections of research topics, materials, and approaches;
- Grouped box plots and scatter plots discovered and proved the connection between different parameters;
- On a laboratory scale, nanoparticles showed promising EOR performance;
- IFT reduction and wettability alternation were the EOR mechanisms studied by most researchers. The results of IFT and contact angle tests can indicate incremental oil recovery;
- There are several research areas that are currently under-researched. To fully understand the nanoparticles, more research is still necessary.

REFERENCES

1. National Nanotechnology Initiative (NNI). What It Is and How It Works | Nano [Internet]. Available from: https://www.nano.gov/nanotech-101/what

2. Dowling A, Clift R, Grobert N, Hutton D, Oliver R, O'Neill O, et al. Nanoscience and nanotechnologies : opportunities and uncertainties. London R Soc R Acad Eng Rep. 2004;

3. Al-Muntasheri GA, Liang F, Hull KL. Nanoparticle-Enhanced Hydraulic-Fracturing Fluids: A Review. SPE Prod Oper [Internet]. 2017;32(02):186–95. Available from: https://doi.org/10.2118/185161-PA

4. Ganesh VK. Nanotechnology in civil engineering. Eur Sci Journal, ESJ. 2012;8(27).

5. Kubik T, Bogunia-Kubik K, Sugisaka M. Nanotechnology on duty in medical applications. Curr Pharm Biotechnol. 2005;6(1):17–33.

6. Duncan T V. Applications of nanotechnology in food packaging and food safety: barrier materials, antimicrobials and sensors. J Colloid Interface Sci. 2011;363(1):1–24.

7. Alaskar MN, Ames MF, Connor ST, Liu C, Cui Y, Li K, et al. Nanoparticle and Microparticle Flow in Porous and Fractured Media--An Experimental Study. SPE J [Internet]. 2012;17(04):1160–71. Available from: https://doi.org/10.2118/146752-PA

8. Rahmani AR, Bryant SL, Huh C, Ahmadian M, Zhang W, Liu QH. Characterizing Reservoir Heterogeneities Using Magnetic Nanoparticles [Internet]. SPE Reservoir Simulation Symposium. Houston, Texas, USA: Society of Petroleum Engineers; 2015. p. 29. Available from: https://doi.org/10.2118/173195-MS

9. Aftab A, Ismail AR, Ibupoto ZH, Akeiber H, Malghani MGK. Nanoparticles based drilling muds a solution to drill elevated temperature wells: A review. Renew Sustain Energy Rev [Internet]. 2017 Sep 1 [cited 2019 Feb 11];76:1301–13. Available from: https://www.sciencedirect.com/science/article/pii/S1364032117303623

10. Cai J, Chenevert ME, Sharma MM, Friedheim JE. Decreasing Water Invasion Into Atoka Shale Using Nonmodified Silica Nanoparticles. SPE Drill Complet [Internet]. 2012;27(01):103–12. Available from: https://doi.org/10.2118/146979-PA

11. Vryzas Z, Mahmoud O, Nasr-El-Din HA, Kelessidis VC. Development and testing of novel drilling fluids using Fe 2 O 3 and SiO 2 nanoparticles for enhanced drilling operations. In: International Petroleum Technology Conference. International Petroleum Technology Conference; 2015.

12. Green DW, Willhite GP. Enhanced oil recovery. Vol. 6. Henry L. Doherty Memorial Fund of AIME, Society of Petroleum Engineers …; 1998.

13. Anderson WG. Wettability Literature Survey-Part 6: The Effects of Wettability on Waterflooding. J Pet Technol [Internet]. 1987;39(12):1605–22. Available from: https://doi.org/10.2118/16471-PA

14. Chaudhury MK. Spread the word about nanofluids. Nature [Internet]. 2003 May 8;423:131. Available from: https://doi.org/10.1038/423131a

15. Wasan DT, Nikolov AD. Spreading of nanofluids on solids. Nature [Internet]. 2003 May 8;423:156. Available from: https://doi.org/10.1038/nature01591

16. Mohammed MA, Babadagli T. Experimental Investigation of Wettability Alteration in Oil-Wet Reservoirs Containing Heavy Oil. SPE Reserv Eval Eng [Internet]. 2016;19(04):633–44. Available from: https://doi.org/10.2118/170034-PA

17. Roustaei A. An Evaluation of Spontaneous Imbibition of Water into Oil-Wet Carbonate Reservoir Cores Using Nanofluid. Petrophysics [Internet]. 2014;55(01):31–7. Available from: https://doi.org/

18. Cao N, Mohammed MA, Babadagli T. Wettability Alteration of Heavy-Oil-Bitumen-Containing Carbonates by Use of Solvents, High-pH Solutions, and Nano/Ionic Liquids. SPE Reserv Eval Eng [Internet]. 2017;20(02):363–71. Available from: https://doi.org/10.2118/183646-PA

19. Cheraghian G, Hendraningrat L. A review on applications of nanotechnology in the enhanced oil recovery part A: effects of nanoparticles on interfacial tension. Int Nano Lett [Internet]. 2016;6(2):129–38. Available from: https://doi.org/10.1007/s40089-015-0173-4

20. Wagner OR, Leach RO. Effect of Interfacial Tension on Displacement Efficiency. Soc Pet Eng J [Internet]. 1966;6(04):335–44. Available from: https://doi.org/10.2118/1564-PA

21. Agista MN, Guo K, Yu Z. A State-of-the-Art Review of Nanoparticles Application in Petroleum with a Focus on Enhanced Oil Recovery. Appl Sci [Internet]. 2018;8(6). Available from: http://www.mdpi.com/2076-3417/8/6/871

22. Alomair OA, Matar KM, Alsaeed YH. Nanofluids application for heavy oil recovery. In: SPE Asia Pacific Oil & Gas Conference and Exhibition. Society of Petroleum Engineers; 2014.

23. Hendraningrat L, Shidong L, Torsaeter O. A glass micromodel experimental study of hydrophilic nanoparticles retention for EOR project. In: SPE Russian Oil and Gas Exploration and Production Technical Conference and Exhibition. Society of Petroleum Engineers; 2012.

24. Li S, Genys M, Wang K, Torsæter O. Experimental study of wettability alteration during nanofluid enhanced oil recovery process and its effect on oil recovery. In: SPE Reservoir Characterisation and Simulation Conference and Exhibition. Society of Petroleum Engineers; 2015.

25. Li S, Hendraningrat L, Torsaeter O. Improved oil recovery by hydrophilic silica nanoparticles suspension: 2 phase flow experimental studies. In: IPTC 2013: International Petroleum Technology Conference. 2013.

26. Li S, Torsæter O. Experimental Investigation of the Influence of Nanoparticles Adsorption and Transport on Wettability Alteration for Oil Wet Berea Sandstone [Internet]. SPE Middle East Oil & Gas Show and Conference. Manama, Bahrain: Society of Petroleum Engineers; 2015. p. 16. Available from: https://doi.org/10.2118/172539-MS

27. Shahrabadi A, Bagherzadeh H, Roostaie A, Golghanddashti H. Experimental investigation of HLP nanofluid potential to enhance oil recovery: A mechanistic approach. In: SPE International Oilfield Nanotechnology Conference and Exhibition. Society of Petroleum Engineers; 2012.

28. Ye Z, Qin X, Lai N, Peng Q, Li X, Li C. Synthesis and performance of an acrylamide copolymer containing nano-SiO 2 as enhanced oil recovery chemical. J Chem. 2013;2013.

29. Wang L, Zhang G, Li G, Zhang J, Ding B. Preparation of microgel nanospheres and their application in EOR. In: International Oil and Gas Conference and Exhibition in China. Society of Petroleum Engineers; 2010.

30. Sun X, Zhang Y, Chen G, Gai Z. Application of nanoparticles in enhanced oil recovery: a critical review of recent progress. Energies. 2017;10(3):345.

31. Olayiwola SO, Dejam M. A comprehensive review on interaction of nanoparticles with low salinity water and surfactant for enhanced oil recovery in sandstone and carbonate reservoirs. Fuel [Internet]. 2019;241:1045–57. Available from: http://www.sciencedirect.com/science/article/pii/S0016236118321914

32. Bera A, Belhaj H. Application of nanotechnology by means of nanoparticles and nanodispersions in oil recovery - A comprehensive review. J Nat Gas Sci Eng [Internet]. 2016;34:1284–309. Available from: http://www.sciencedirect.com/science/article/pii/S1875510016305704

33. Li K, Wang D, Jiang S. Review on enhanced oil recovery by nanofluids. Oil Gas Sci Technol d'IFP Energies Nouv. 2018;73:37.

34. Cheraghian G, Hendraningrat L. A review on applications of nanotechnology in the enhanced oil recovery part B: effects of nanoparticles on flooding. Int Nano Lett [Internet]. 2016;6(1):1–10. Available from: https://doi.org/10.1007/s40089-015-0170-7

35. Agrawal D, Xu K, Darugar Q, Khabashesku V. Enhanced Oil Recovery by Nanoparticle-Induced Crude Oil Swelling: Pore-Scale Experiments and Understanding [Internet]. SPE Asia Pacific Oil and Gas Conference and Exhibition. Brisbane, Australia: Society of Petroleum Engineers; 2018. p. 10. Available from: https://doi.org/10.2118/191971-MS

36. Xu D, Bai B, Meng Z, Zhou Q, Li Z, Lu Y, et al. A Novel Ultra-Low Interfacial Tension Nanofluid for Enhanced Oil Recovery in Super-Low Permeability Reservoirs [Internet]. SPE Asia Pacific Oil and Gas Conference and Exhibition. Brisbane, Australia: Society of Petroleum Engineers; 2018. p. 16. Available from: https://doi.org/10.2118/192113-MS

37. Ding Y, Zheng S, Meng X, Yang D. Low Salinity Hot Water Injection with Addition of Nanoparticles for Enhancing Heavy Oil Recovery under Reservoir Conditions [Internet]. SPE Western Regional Meeting. Garden Grove, California, USA: Society of Petroleum Engineers; 2018. p. 18. Available from: https://doi.org/10.2118/190132-MS

38. Salem Ragab AM, Hannora AE. A Comparative Investigation of Nano Particle Effects for Improved Oil Recovery–Experimental Work. In: SPE Kuwait Oil and Gas Show and Conference. Society of Petroleum Engineers; 2015.

39. Hendraningrat L, Li S, Torsater O. Effect of some parameters influencing enhanced oil recovery process using silica nanoparticles: An experimental investigation. In: SPE Reservoir Characterization and Simulation Conference and Exhibition. Society of Petroleum Engineers; 2013.

40. Qiu F, Mamora DD. Experimental study of solvent-based emulsion injection to enhance heavy oil recovery in Alaska north slope area. In: Canadian Unconventional Resources and International Petroleum Conference. Society of Petroleum Engineers; 2010.

41. Wang W, Yuan B, Su Y, Wang K, Jiang M, Moghanloo RG, et al. Nanoparticles adsorption, straining and detachment behavior and its effects on permeability of berea cores: Analytical model and lab experiments. In: SPE Annual Technical Conference and Exhibition. Society of Petroleum Engineers; 2016.

42. Mohajeri M, Hemmati M, Shekarabi AS. An experimental study on using a nanosurfactant in an EOR process of heavy oil in a fractured micromodel. J Pet Sci Eng. 2015;126:162–73.

43. Yu J, An C, Mo D, Liu N, Lee RL. Study of adsorption and transportation behavior of nanoparticles in three different porous media. In: SPE improved oil recovery symposium. Society of Petroleum Engineers; 2012.

44. Roustaei A, Saffarzadeh S, Mohammadi M. An evaluation of modified silica nanoparticles' efficiency in enhancing oil recovery of light and intermediate oil reservoirs. Egypt J Pet. 2013;22(3):427–33.

45. Li S, Torsaeter O. The impact of nanoparticles adsorption and transport on wettability alteration of intermediate wet berea sandstone. In: SPE Middle East Unconventional Resources Conference and Exhibition. Society of Petroleum Engineers; 2015.

46. Zargartalebi M, Kharrat R, Barati N. Enhancement of surfactant flooding performance by the use of silica nanoparticles. Fuel. 2015;143:21–7.

47. Hendraningrat L, Torsaeter O. Unlocking the potential of metal oxides nanoparticles to enhance the oil recovery. In: offshore technology conference-Asia. Offshore Technology Conference; 2014.

48. Li S, Torsæter O. The Impact of Nanoparticles Adsorption and Transport on Wettability Alteration of Water Wet Berea Sandstone [Internet]. SPE/IATMI Asia Pacific Oil & Gas Conference and Exhibition. Nusa Dua, Bali, Indonesia: Society of Petroleum Engineers; 2015. p. 11. Available from: https://doi.org/10.2118/176256-MS

49. Hendraningrat L, Torsæter O. Effects of the initial rock wettability on silica-based nanofluid-enhanced oil recovery processes at reservoir temperatures. Energy & Fuels. 2014;28(10):6228–41.

50. Torsater O, Engeset B, Hendraningrat L, Suwarno S. Improved oil recovery by nanofluids flooding: an experimental study. In: SPE Kuwait international petroleum conference and exhibition. Society of Petroleum Engineers; 2012.

51. Yoon KY, Son HA, Choi SK, Kim JW, Sung WM, Kim HT. Core Flooding of Complex Nanoscale Colloidal Dispersions for Enhanced Oil Recovery by in Situ Formation of Stable Oil-in-Water Pickering Emulsions. Energy & Fuels. 2016;30(4):2628–35.

52. Ogolo NA, Olafuyi OA, Onyekonwu MO. Enhanced oil recovery using nanoparticles. In: SPE Saudi Arabia section technical symposium and exhibition. Society of Petroleum Engineers; 2012.

53. Hendraningrat L, Zhang J. Polymeric nanospheres as a displacement fluid in enhanced oil recovery. Appl Nanosci. 2015;5(8):1009–16.

54. Cheraghian G, Khalilinezhad SS. Effect of nanoclay on heavy oil recovery during polymer flooding. Pet Sci Technol. 2015;33(9):999–1007.

55. El-Diasty AI. The potential of nanoparticles to improve oil recovery in bahariya formation, Egypt: An experimental study. In: SPE Asia Pacific Enhanced Oil Recovery Conference. Society of Petroleum Engineers; 2015.

56. Lenchenkov NS, Slob M, van Dalen E, Glasbergen G, van Kruijsdijk C. Oil Recovery from Outcrop Cores with Polymeric Nano-Spheres. In: SPE Improved Oil Recovery Conference. Society of Petroleum Engineers; 2016.

57. Roustaei A, Bagherzadeh H. Experimental investigation of SiO2 nanoparticles on enhanced oil recovery of carbonate reservoirs. J Pet Explor Prod Technol. 2015;5(1):27–33.

58. Skauge T, Spildo K, Skauge A. Nano-sized particles for EOR. In: SPE improved oil recovery symposium. Society of Petroleum Engineers; 2010.

59. Cheraghian G. An experimental study of surfactant polymer for enhanced heavy oil recovery using a glass micromodel by adding nanoclay. Pet Sci Technol. 2015;33(13–14):1410–7.

60. Ragab AMS, Hannora AE. An experimental investigation of silica nano particles for enhanced oil recovery applications. In: SPE North Africa Technical Conference and Exhibition. Society of Petroleum Engineers; 2015.

61. Hendraningrat L, Li S, Torsaeter O. Enhancing oil recovery of low-permeability berea sandstone through optimised nanofluids concentration. In: SPE Enhanced Oil Recovery Conference. Society of Petroleum Engineers; 2013.

62. Roustaei A, Moghadasi J, Bagherzadeh H, Shahrabadi A. An experimental investigation of polysilicon nanoparticles' recovery efficiencies through changes in interfacial tension and wettability alteration. In: SPE International Oilfield Nanotechnology Conference and Exhibition. Society of Petroleum Engineers; 2012.

63. Esfandyari Bayat A, Junin R, Samsuri A, Piroozian A, Hokmabadi M. Impact of metal oxide nanoparticles on enhanced oil recovery from limestone media at several temperatures. Energy & Fuels. 2014;28(10):6255–66.

64. Farooqui J, Babadagli T, Li HA. Improvement of the recovery factor using nano-metal particles at the late stages of cyclic steam stimulation. In: SPE Canada Heavy Oil Technical Conference. Society of Petroleum Engineers; 2015.

65. Tarek M. Investigating nano-fluid mixture effects to enhance oil recovery. In: SPE Annual Technical Conference and Exhibition. Society of Petroleum Engineers; 2015.

66. Singh SK, Ahmed RM, Growcock F. Vital Role of Nanopolymers in Drilling and Stimulations Fluid Applications [Internet]. SPE Annual Technical Conference and Exhibition. Florence, Italy: Society of Petroleum Engineers; 2010. p. 7. Available from: https://doi.org/10.2118/130413-MS

67. Anderson W. Wettability Literature Survey- Part 2: Wettability Measurement. J Pet Technol [Internet]. 1986;38(11):1246–62. Available from: https://doi.org/10.2118/13933-PA

68. Hinkle DE, Wiersma W, Jurs SG. Applied statistics for the behavioral sciences. 1988;

69. Almohsin A, Ding H, Bai B. Experimental Study on the Transport and Improved Oil Recovery Mechanism of Submicron Particle Gel [Internet]. SPE EOR Conference at Oil and Gas West Asia. Muscat, Oman: Society of Petroleum Engineers; 2018. p. 14. Available from: https://doi.org/10.2118/190364-MS

70. Geng J, Ding H, Han P, Wu Y, Bai B. Transportation and Potential Enhanced Oil Recovery Mechanisms of Nanogels in Sandstone. Energy & Fuels [Internet]. 2018 Aug 16;32(8):8358–65. Available from: https://doi.org/10.1021/acs.energyfuels.8b01873

71. Kong X, Ohadi M. Applications of Micro and Nano Technologies in the Oil and Gas Industry - Overview of the Recent Progress [Internet]. Abu Dhabi International Petroleum Exhibition and Conference. Abu Dhabi, UAE: Society of Petroleum Engineers; 2010. p. 11. Available from: https://doi.org/10.2118/138241-MS

72. Almohsin AM, Bai B, Imqam AH, Wei M, Kang W, Delshad M, et al. Transport of nanogel through porous media and its resistance to water flow. In: SPE Improved Oil Recovery Symposium. Society of Petroleum Engineers; 2014.

II. AN INVESTIGATION OF FACTORS INFLUENCING THE NEAR-WELLBORE TRANSPORT OF NANOGEL

ABSTRACT

Nanogel (crosslinked polymeric nanoparticle) is considered as an EOR method to handle reservoir heterogeneity problems and improve oil recovery in low permeability formations. It has unique properties different from both traditional polymer gel and other EOR nanoparticles. Hence, for a comprehensive understanding of such an EOR agent, near-wellbore transport behaviors of nanogel are crucial.

Various previous works have studied this aspect by conducting filtration experiments using filter membranes. The use of membranes allows researchers to focus more on its injectivity and have better control of porous media permeability, pore size, and homogeneity. In contrast, using core chips makes a study focus more on transport behavior and creates a condition that is closer to real case scenarios. In this work, core chips made from homogeneous Berea sandstone were used as porous media to study near-wellbore transport of partially hydrolyzed polyacrylamide (HPAM) based nanogel. Constant pressure-driven filtration tests were performed at different conditions.

Multiple factors were considered including salt concentration, core permeability, nanogel concentration, and driven pressure. It was found that higher salinity induces lower nanogel swelling ratio and viscosity. During filtration tests, nanogel dispersed in lower salinity environment result in higher resistance factors, indicating particle size dominate its transport behavior over nanogel strength. Higher nanogel concentration also results in higher viscosity and consequently, higher resistance factors. In porous media

with different permeability, resistance factors decrease with higher permeability. Above certain value, the permeability has little impact on nanogel transport. When filtration tests were under different driven pressure, the differences among tests were not distinguishable. Meanwhile, the results of all tests can be well fitted by the intermediate blocking model and standard blocking model. Nanogel dispersion viscosity was taken into consideration when using these models. It was found that most of the differences among tests under different salinity and nanogel concentration were caused by the viscosity difference.

1. INTRODUCTION

Nanogel (crosslinked polymeric nanoparticle) is considered as an EOR method to handle reservoir heterogeneity problems and improve oil recovery (1–4). It is capable of reducing reservoir permeability, diverting injection fluids to upswept zones (5). In addition, from previous laboratory studies, nanogel has found to be capable of reducing interfacial tension and modify reservoir wettability (6–8). Due to the advantage of the small particle size and deformability, it has often been proposed for treatment in a low permeability reservoir, as it is able to pass through narrow pore throats and transport deep into reservoirs (5,9,10). Hence, the understanding of nanogel transport is crucial for nanogel research and its potential for field scale applications.

Various factors could impact the transport of nanogel and other types of particles. For polymeric particles, it was found that high salinity often results in lower swelling ratio but better strength (5,11,12). For some particles, particle size dominates their

transport behavior as a higher swelling ratio would cause more resistance towards their movement (5). On the other hand, for some other types of polymeric particles, more rigid ones (less swelled) would result in higher resistance factors. For dispersions at different concentrations, the most significant influence is the higher viscosity brought by concentration due to the increasing volumetric fraction (13). Higher concentration also increases the chance of agglomeration among particles, which would ultimately lead to poorer injectivity (14). In porous media with different permeability, the different size ratio between pore and particles plays an important role in transport behaviors. Different size matches between particle and pore throat could influence the way particles passing through. It was also found that the transport of nanogel would be hindered in low permeability conditions (11).

Previously, researchers have studied the near-wellbore transport of nanogel and other nano or micro material fluids with filtration tests using filter membrane(5,15,16). By using a filter membrane, the permeability, pore size, and homogeneity will be well controlled by researchers. On the other hand, membranes only represent an ideal scenario, various factors like adsorption behavior between porous media and particles are ignored. Moreover, conducting experiments using membranes focuses more on particle dispersion injectivity rather than their transport behavior. Hence, in this study, core chips made from homogeneous Berea sandstone were used as porous media to study near-wellbore transport of partially hydrolyzed polyacrylamide (HPAM) based nanogel. Impacts of salinity, core permeability, nanogel concentration, and driven pressure have been studied. Nanogel properties at certain conditions have been investigated.

Intermediate blocking model and standard blocking model are utilized for further explanation of the results from each test.

2. STUDY DESCRIPTION

2.1. MATERIAL

The objective partially hydrolyzed polyacrylamide (HPAM) based nanogel was prepared by suspension polymerization with acrylamide (AM, 13.5g, 0.19mol), acrylic acid (AA, 1.5g, 0,02mol), and the organic crosslinker N,N'-Methylenebisacrylamide (MBAA, 2.25mg, 1.4*10-5mol) (7). All chemicals were purchased from Sigma-Aldrich Corp. (St. Louis, Missouri) and used as received. To prepare a nanogel dispersion, the nanogel dry powders were stirred and heated properly for fully dispersing. The 1 wt.% sodium chloride (NaCl) solution was used throughout the study as the nanogel solvent.

2.2. FILTRATION EXPERIMENTS

The setup of experiments is shown in Figure 1: A syringe pump (#2) filled with DI water (#1) was used to inject brine and nanogel dispersion from the accumulator (#3) into core chips at a constant pressure. The core holder (#5) held core chips with a diameter of 2.51 cm and a length of 1.1 cm. The confining pressure system (#6) is set 400 psi above the injection. A pressure sensor (#4) was connected to the inlet of the core holder to monitor and ensure the injection pressure being constant at the selected value. Test tubes (#7) are kept at the outlet to collect effluents and determine the production flow rate.

During each experiment, after measuring the permeability of core chips, selected nanogel dispersion would be injected into porous media at a constant driven pressure set by the pump. Production flow rates were recorded. Each test was run for 70 minutes.

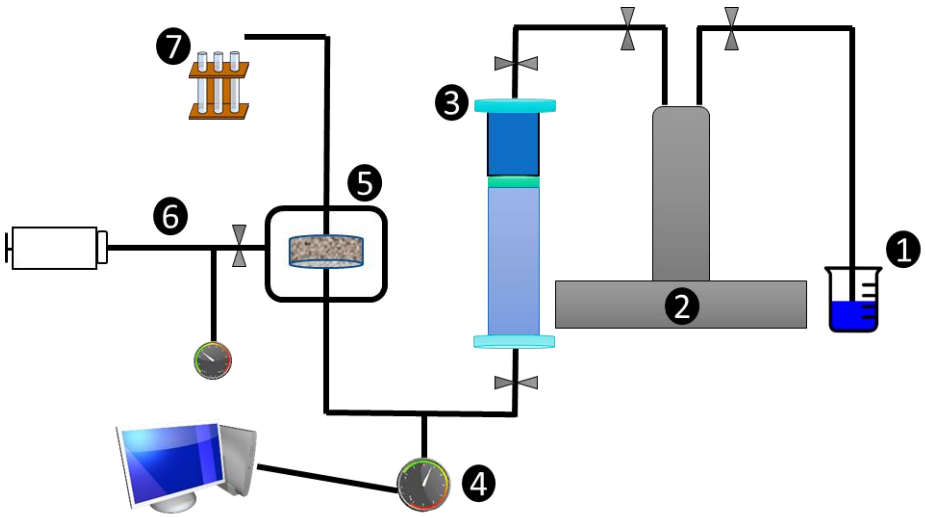

Figure 1. Schematic Diagram of the experimental setup

The full list of performed filtration tests is shown in Table 1. Four factors were studied: brine concentration, porous media permeability, nanogel concentration, and driven pressure. Test #1 was performed at the default condition. Test #1, 9, and 10 were performed at different brine concentrations. Test #1, 11, and 12 were performed at different driven pressures. Test #1-5 were performed in porous media with different permeability. Test #1,6, 7, and 8 were performed with nanogel dispersion at different concentrations.

2.3. NANOGEL CHARACTERIZATION

Particle size and surface charge determination: At different brine concentrations, the different number of ions would affect the electrostatic repulsion differently and result in different nanogel swelling ratio and dispersion surface charge. Dynamic light scattering (DLS) was performed to determine the hydrodynamic diameter of nanogel particles in dispersions. Zeta potential of nanogel dispersions was tested by electrophoretic light scattering (ELS). Both DLS and ELS tests were conducted using a Malvern ZS90 Nanosizer.

Table 1. Filtration tests to be conducted in this task

Test id	NaCl concentration	Nanoparticle concentration, ppm	Permeability, mD	Injection pressure, psi
1	1%	1000	140.7507	10
2	1%	1000	10.4	10
3	1%	1000	26	10
4	1%	1000	90.8	10
5	1%	1000	371	10
6	1%	500	100.9119	10
7	1%	2000	130.7896	10
8	1%	3000	119.3979	10
9	0.25%	1000	145.75	10
10	5%	1000	105.2631	10
11	1%	1000	137.5	15
12	1%	1000	119.1	20

Rheological properties: At different swelling ratio or nanogel concentration, the dispersion viscosity varies due to the change in volumetric fraction (17). A Brookfield DV3T rheometer with a ULA spindle was used to measure dispersion viscosity at different conditions (salinity and nanogel concentration) from low to high shear rate. All tests were performed at room temperature.

3. RESULTS AND DISCUSSIONS

3.1. NANOGEL CHARACTERISTICS

Salinity would affect nanogel dispersion in many ways. Hydrodynamic diameters and zeta potential of nanogel in brine with different NaCl concentrations are demonstrated in Figure 2. Each DLS and ELS tests were performed multiple times to ensure the most reliable data. Each scatters represents the mean value from those tests with error bars being presented.

As shown in the plot on the left, the particle size decreases with higher salinity logarithmically. This is due to the different numbers of ions, which reduce the electrostatic repulsion among the polymer chain and result in particle shrinkage (6). In addition, it is believed that a nanogel particle would be more rigid and strong at higher salinity because of the lower swelling ratio (18). In addition, it is also shown that there was less negative surface charge at higher NaCl concentration. Likewise, it is caused by different numbers of ions, which can compress particles and reduce diffusion layer thickness (19).

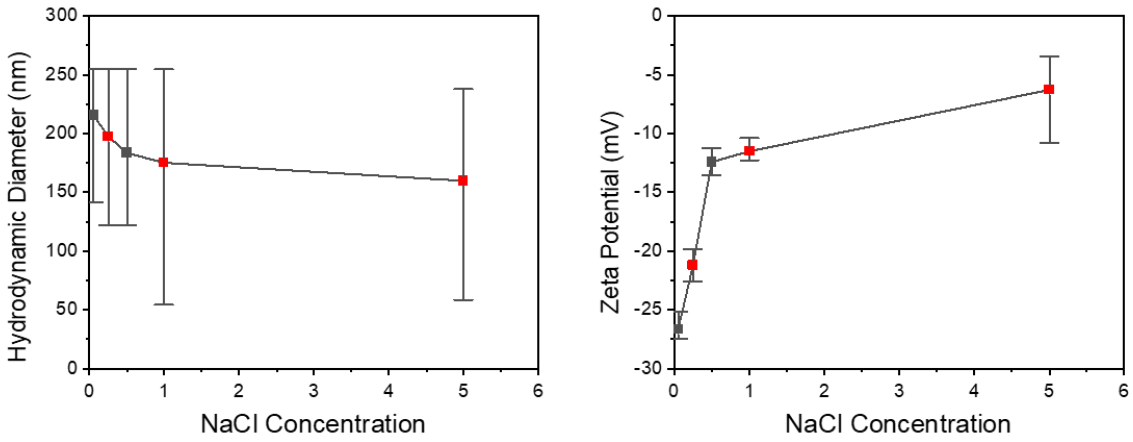

Figure 2. Hydrodynamic diameter (left) and zeta potential (right) of nanogel at different brine concentration

In addition, nanogel dispersion viscosity is affected greatly by both NaCl concentration and nanogel concentration. For each nanogel dispersion, the apparent viscosities were tested with the shear rate being increased gradually. As shown in Figure 3, the shear-thinning effect was observed at lower shear rates. At higher rates, the shear-thinning became minimum, which could be caused by the breakage of the interparticle structure at higher shear rates (8). For nanogel dispersion with different brine concentration, viscosity is generally higher at low salinity. Meanwhile, at the same brine condition, higher nanogel concentration leads to higher viscosity. The difference among dispersion viscosities is an outcome of different volumetric fractions (20,21). Both swollen particle size (affected by NaCl concentration) and nanogel concentration influence volumetric fraction, which ultimately leads to different dispersion viscosity.

Since the apparent viscosities were relatively constant when shear rates were higher than 100 1/S, the apparent viscosities at 160 1/s were selected for comparison among dispersions, except for the case where viscosity was unable to be measured due to

high torque (1% salinity and 5,000 mg/L nanogel concentration). As demonstrated in Figure 4, dispersion viscosity decreases with NaCl concentration logarithmically but increases with nanogel concentration linearly.

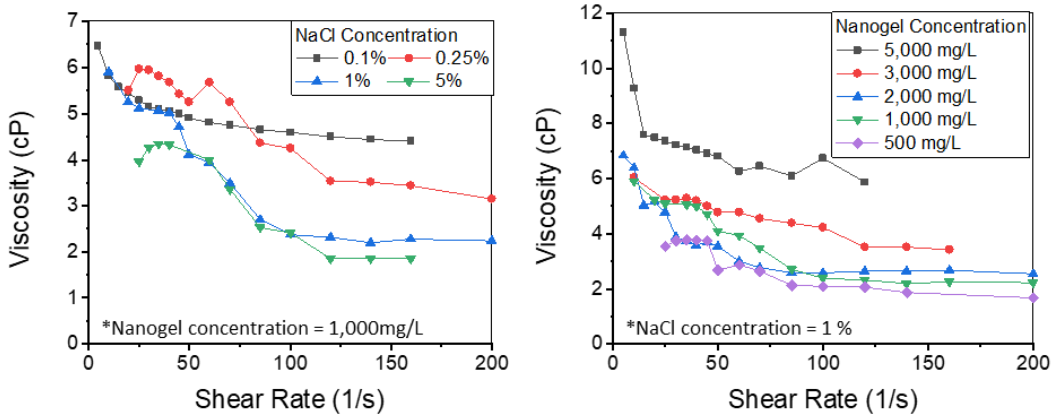

Figure 3. Viscosity of nanogel dispersions at different NaCl concentration (left) and nanogel concentration (right)

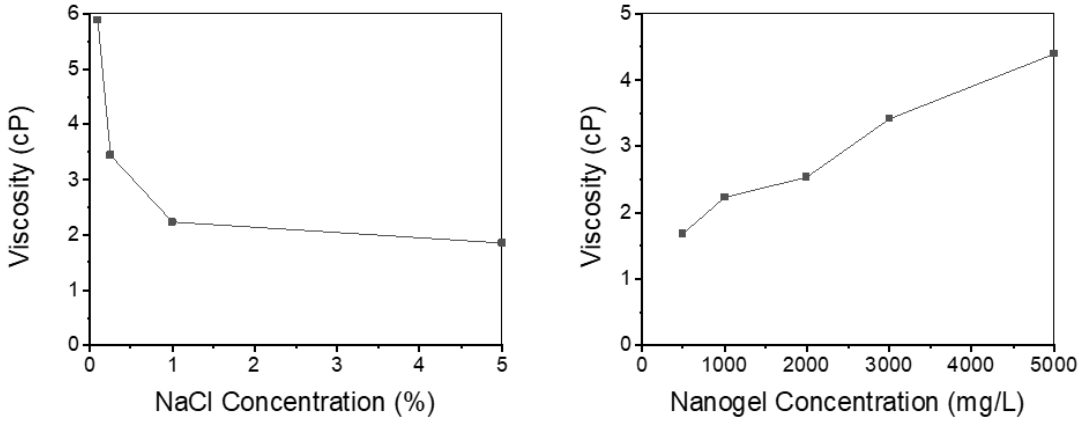

Figure 4. Viscosity at 160 1/s (except 5,000 mg/L dispersion) of nanogel dispersion at different NaCl concentration (left) and nanogel concentration (right)

Equivalent flow rates in porous media with different permeability are displayed in Figure 5. Each scatters represents the equivalent flow rates of such shear rate. The calculation is base on the following equation:

$$\dot{\gamma}_{eq} = 4v\left(\frac{\emptyset}{8k}\right)^{1/2} = \frac{4q}{A\sqrt{8k\phi}}$$

where A is area (cm^2), q is the flow rate (cm^3/min), and k and Φ are permeability (cm^2) and porosity. In all tests, the production flow rates were higher than the equivalent flow rates at 160 1/s during most of the time. Therefore, the viscosity data shown in Figure 4 could be used for calculating the initial production rate for each filtration test in the following sections.

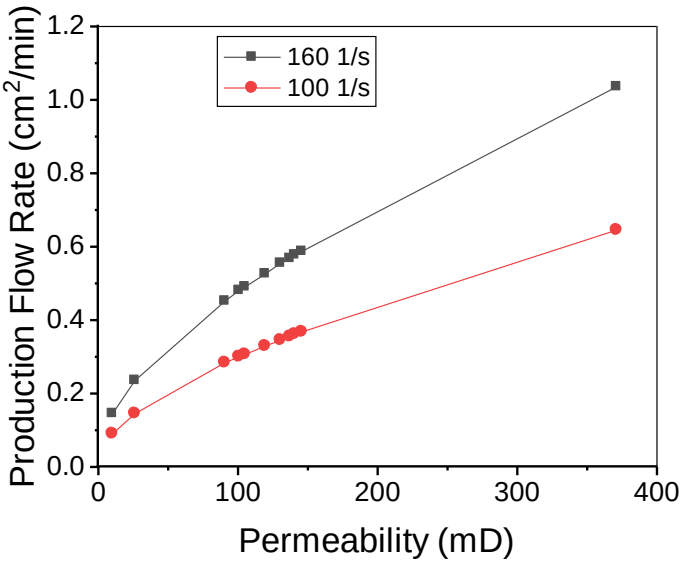

Figure 5. Equivalent flow rates of 100 1/s and 160 1/s shear rates

3.2. FILTRATION EXPERIMENTS

12 filtration experiments have been performed with four factors being studied. During each experiment, the production rate would fall during filtration. The decrease in production rate would be slower with longer experiment period. Various blocking models could be used to analyze the results (22,23):

Complete blocking model: $J_v(t) = J_v(0)e^{-k_{com}J_v(0)t}$

Other models: $J_v(t) = J_v(0)[1+KJ_v(0)t]^n$

where Jv(t) and Jv(0) represent permeate flux at each moment and initial value. The permeate flux is defined as the flow rate per unit area (superficial velocity). For the first model, K_{com} is the complete blocking constant and t is time. For the second equation, n is -0.5, -1, -2, and 4 for cake filtration, intermediate blocking, standard blocking, and adsorptive fouling models, respectively. K is the blocking constant of each model. For this study, it is found that experimental results were fitted well by intermediate blocking and standard blocking with high coefficients of determination. Hence, in addition, to visualize results traditionally (production rate versus time), all results were fitted by both models for further explanation.

3.2.1. Filtration of Nanogel in Different Salinity. Three tests with different brine concentrations were performed to study the impacts of salinity and nanogel swelling ratio on nanogel transport. As discusses in the previous section, change in brine salinity would result in different nanogel properties. There are lower surface charge and swelling ratio in brine that is high in salt concentration. In addition, the dispersion viscosity is higher at lower salinity.

As shown in Figure 6(A), at the highest salinity, the production rate at the end of the filtration test was 5 mL/min. When NaCl concentration was decreased to 0.25%, the final production rate dropped to only 2.6mL/min.

Resistance factor is often used to evaluate gel injectivities. It is the mobility ratio between water injection and the nanogel injection and is calculated as

$$RF = \frac{\lambda_{water}}{\lambda_{nanogel}} = \frac{k_{water} / \mu_{water}}{k_{nanogel} / \mu_{nanogel}} = \frac{q_{water}}{q_{nanogel}}$$

Figure 6(B) displayed the resistance factors calculated with the final production rates of each test. The lower injectivity of nanogel in high salinity conditions is consistent with the nanogel rheology properties. Meanwhile, despite the better strength, at a lower swelling ratio, a smaller size would make nanogel transport through porous media without too much resistance. This is result shows that the impact of particle size is more significant compared to particle strength during nanogel transport.

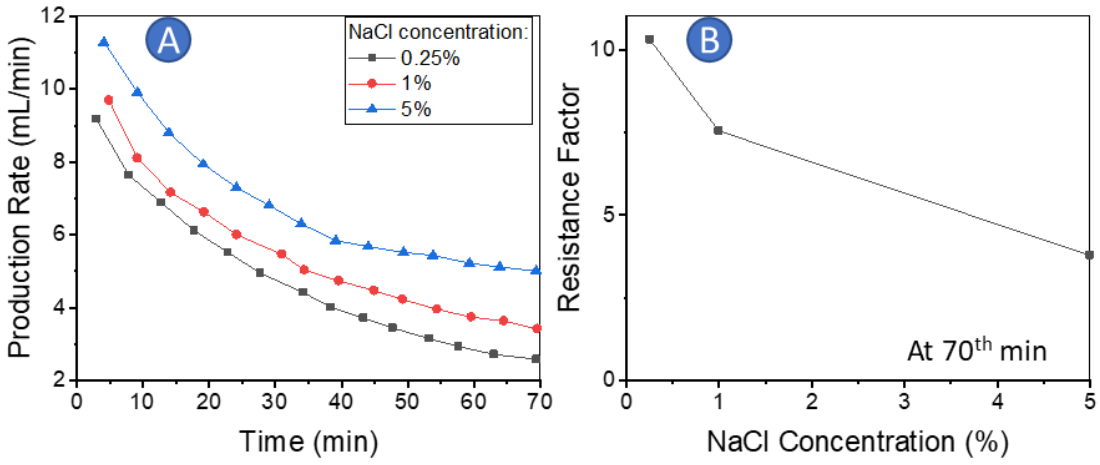

Figure 6. Production rates over time (A) and resistance factor at 70th min (B) at different salinity

The intermediate blocking model and standard blocking model are used to fit the results. As previously discussed, these two models are described as the following equations:

Intermediate blocking model: $J_v(t) = \frac{J_v(0)}{1 + K_i J_v(0) t}$

Standard blocking model: $J_v(t) = \frac{J_v(0)}{(1 + K_s J_v(0) t)^2}$

where K_i and K_s are Intermediate blocking constant and standard blocking constant. In theory, the standard blocking model suggests that particles would be deposited onto the core surface and eventually lead to complete blockage. On the other hand, the intermediate blocking model suggests that particles would directly block a portion of pores and result in partial blockage (22).

Consequently, the two models can be converted to linear equations for better visualization:

Intermediate blocking model: $\frac{q(0)}{q(t)} - 1 = \frac{K_i q(0)}{A} * t$

Standard blocking model: $\sqrt{\frac{q(0)}{q(t)}} - 1 = \frac{K_s q(0)}{A} * t$

q(0) and q(t) are the initial flow rate and flow rate at any moment during filtration tests. Q(0) is calculated by Darcy's law with the permeability, length, surface area of the core chip and nanogel dispersion viscosity (as shown in Figure 4).

The filtration results of the three tests with different salinity fitted by both models are demonstrated in Figure 7. Different from the resistance factor, nanogel dispersion viscosity was considered in this circumstance. Hence, the "1% salinity" test results in the

largest slope, which means the core chip was blocked the most among all tests. Parameters regarding the two models are displayed in Table 2. Block constants of both models are higher with lower salinity.

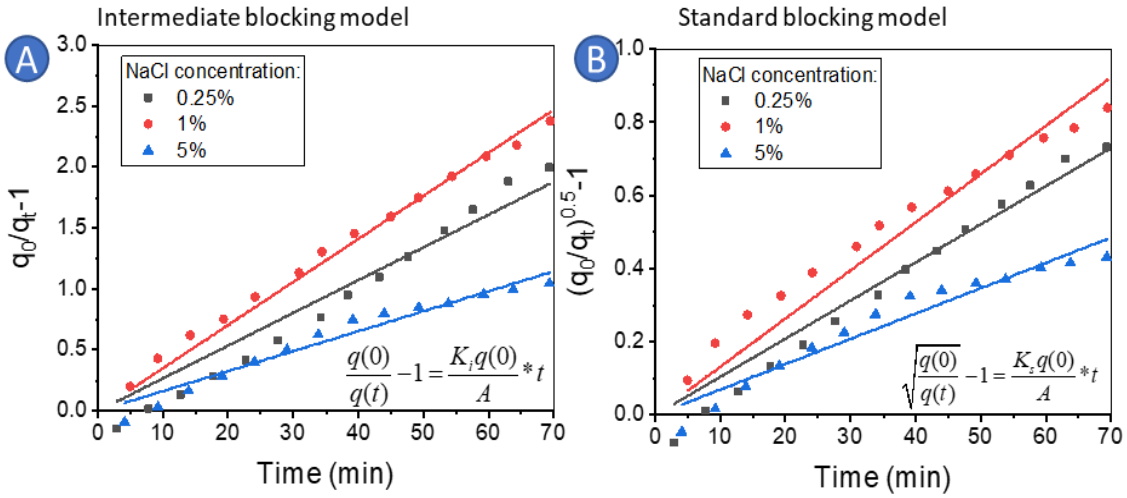

Figure 7. Filtration results fitted by (A) intermediate blocking model and (B)Standard blocking model at different salinity

Table 2. Fitting parameters of blocking models at different salinity

NaCl Concentration	Intermediate blocking model			Standard blocking model		
	Slope	Adj. R-Square	blocking constant, 1/cm	Slope	Adj. R-Square	blocking constant, 1/cm
0.25%	0.027	0.979	0.0170	0.010	0.987	0.0066
1%	0.035	0.998	0.0150	0.013	0.989	0.0056
5%	0.016	0.987	0.0079	0.007	0.983	0.0033

3.2.1. Filtration of Nanogel at Different Dispersion Concentration. Four filtration tests were conducted using nanogel dispersions from a concentration of 500

mg/L to 3,000 mg/L. For most of the EOR agents (e.g. polymer, silica nanoparticle), increased concentration often leads to lower injectivity (18,79). Other than viscosity, nanogel dispersion at different concentrations would also affect how the particles agglomerate with each other and being adsorbed onto the rock surface (80).

As illustrated in Figure 8, higher production rate and lower resistance factors were observed in tests with dispersions in a lower concentration. The resistance factor was nearly doubled as nanogel concentration being raised from 500 mg/L to 3,000 mg/L: at 500 mg/L, the final production rate was 4.5 mL/min, as a comparison to the 2.5 mL/min at 3,000 mg/L. Such results are predictable since nanogel dispersions are more viscous at a higher concentration.

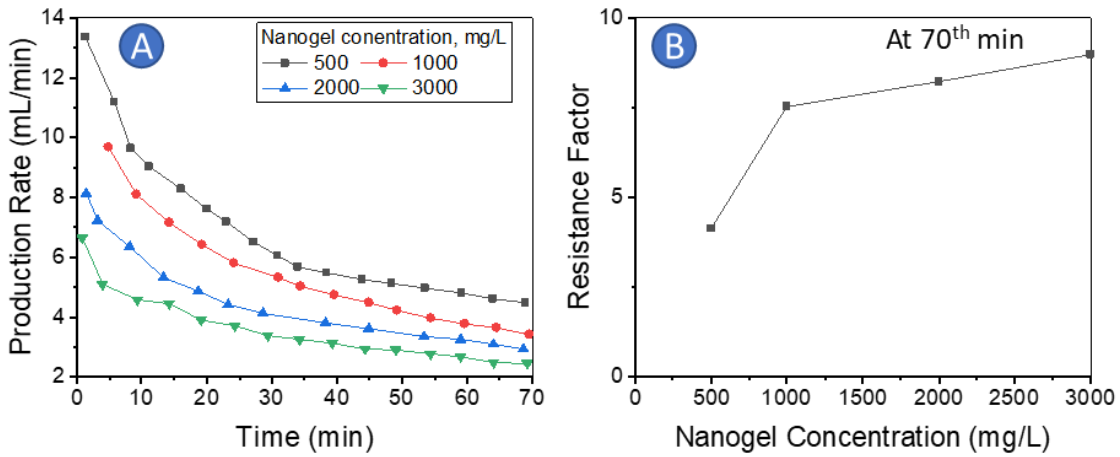

Figure 8. Production rates over time (A) and resistance factor at 70th min (B) at different nanogel concentration

Filtration results fitted by the two models are displayed in Figure 9. When the viscosity was taken into consideration, no obvious trend was observed among all four tests: at 1000 and 2000 mg/L concentration, the slopes of the two fitted regressions are

almost the same. They are also higher than the slopes of the regression of the other two tests. As shown in Table 3, both blocking constants increase with nanogel concentration.

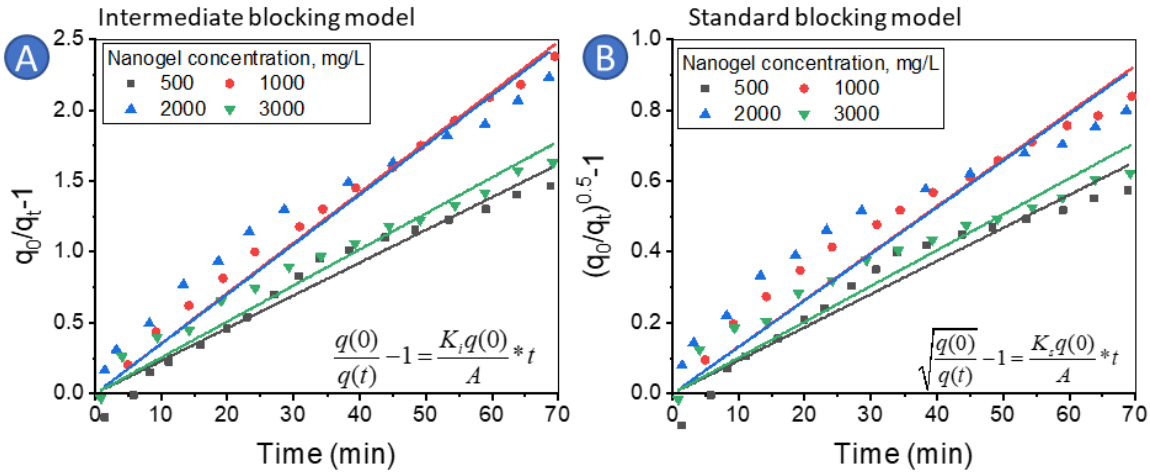

Figure 9. Filtration results fitted by intermediate blocking model (A) and Standard blocking model (B) at different nanogel concentration

Table 3. Fitting parameters of blocking models at different nanogel concentration

Nanogel Concentration, mg/L	Intermediate blocking model			Standard blocking model		
	Slope	Adj. R-Square	blocking constant, 1/cm	Slope	Adj. R-Square	blocking constant, 1/cm
500	0.0231	0.987	0.0103	0.0093	0.980	0.0042
1000	0.0354	0.997	0.0151	0.0132	0.987	0.0056
2000	0.0351	0.976	0.0183	0.0131	0.957	0.0069
3000	0.0254	0.988	0.0195	0.0101	0.977	0.0078

For the tests with different salinity and nanogel concentration, trends are clear that low salinity or high concentration would lead to lower filtration production rates and higher resistance factors. However, when the two blocking models are applied to fit the data, these trends can not be observed as the nanogel dispersion viscosity at each

circumstance is considered. The results proved that both salinity (as well as swelling ratio, which is controlled by salinity) and nanogel concentration affect the transport behavior of nanogel via the viscosity of dispersions.

3.2.2. Filtration of Nanogel in Porous Media with Different Permeability. Core chips with five different permeability were used to study the effect of porous media permeability. Permeability plays an important role in the flow transport process. Porous media with different permeability contain pore throats with different geometry, which mainly includes pore size and tortuosity.

Figure 10(A) shows the production rates during each filtration test. It is expected that the rates in low permeability porous media were lower. Resistance factors at the end of each test are demonstrated in Figure 10(B) along with the throat size of each porous media. The Pore size data was calculated using the empirical equation:

$$k = 20 \times 10^6 d^2 \phi$$

where K is permeability by Darcy, d is pore channel size by inch, and Φ is porosity. As shown in the figure, pore size increase with permeability linearly. In contrast, the resistance factor decreases with permeability logarithmically. Despite pore sizes are far larger than nanogel size, nanogel would agglomerate to form bigger particles. During transport, the nanogel agglomeration requires energy in order to deform and pass through pore throat. Hence, more energy is required in low permeability porous media and resulting in higher resistance factors. Meanwhile, at higher permeability, the difference in resistance factor between test in 141 mD and 371 mD porous media was insignificant.

Figure 11 demonstrates the results fitted by both blocking models. Parameters of the two models are shown in Table 4, which shows blocking constants and slopes are

higher with lower permeability using both models. The models are consistent with resistance factors, where the difference between the two tests conducted in porous media with higher permeability is small. This observation proves that the resistance to nanogel during transport decreases with higher permeability. However, when permeability reaches a certain value, its change does not affect nanogel transport significantly, despite the diameter of the pore throat still increases linearly with permeability.

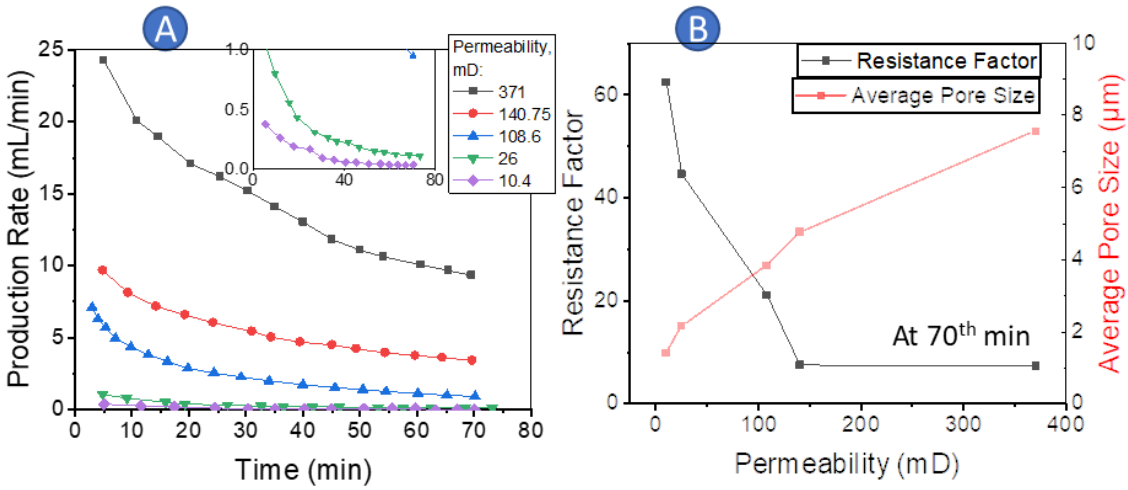

Figure 10. Production rates over time (A) and resistance factor at 70th min (B) at different permeability

3.2.3. Filtration of Nanogel at Different Driven Pressure. Driven pressure was also studied with three tests ran under different constant pressure from 10 psi to 20 psi. It is illustrated in Figure 12 that the production rate was reduced to 6.1 mL/min after 70 minutes of filtration at 20 psi. In contrast, at a driven pressure of only 10 psi, the production rate at the end of the experiment was only 3.4 mL/min. However, the difference is most likely to be caused by the different pressure, as it is not distinct anymore when comparing resistance factors among each other. The resistance factors of

each of the three tests are all between 7 and 8. Additionally, as displayed in Figure 12 and Table 5, the regressions of the three tests almost overlaid with each other, further eliminating the connection between driven pressure and nanogel injectivity.

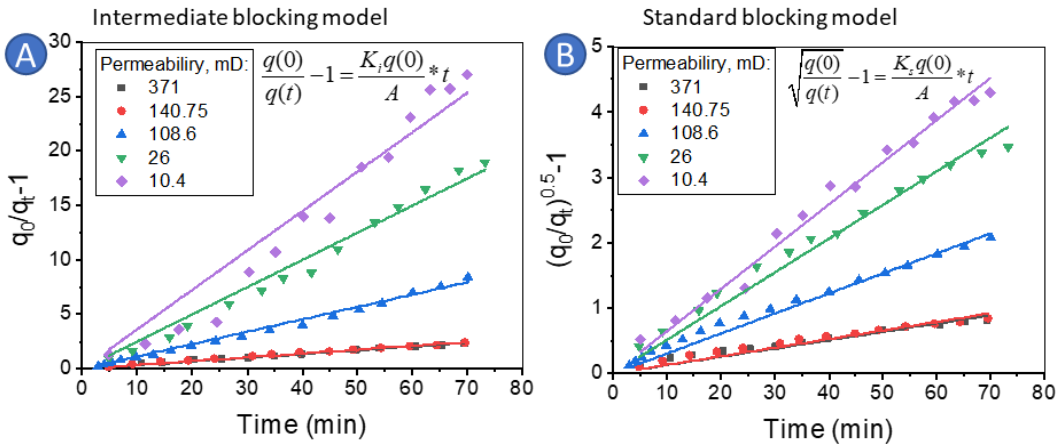

Figure 11. Filtration results fitted by intermediate blocking model (A) and Standard blocking model (B) at different permeability

4. CONCLUSIONS

In this work, HPAM-based nanogel were studied. The hydrodynamic diameter of nanogel increases with lower salinity since ions reduce the electrostatic repulsion among the polymer chain and cause particle shrinkage. Nanogel dispersion viscosity is higher at lower salinity or higher nanogel concentration, as the volumetric fraction is higher at these conditions.

Filtration tests under constant pressure in various conditions were conducted under different conditions. Furthermore, the results from all tests are fitted well by the intermediate blocking model and standard blocking model. Filtration rates are lower with

higher nanogel concentration or lower salinity, which leads to higher resistance factors. The differences are mostly caused by viscosity, which is highly affected by nanogel concentration and salinity. At a higher permeability, the resistance factor would be lower. However, once the permeability exceeded a certain value, the decrease in resistance factor became less obvious. Meanwhile, the driven pressure has little impact on the transport of nanogel as the resistance factor changes little with different driven pressures.

Table 4. Fitting parameters of blocking models at different permeability

Permeability, mD	Intermediate blocking model			Standard blocking model		
	Slope	Adj. R-Square	blocking constant, 1/cm	Slope	Adj. R-Square	blocking constant, 1/cm
371	0.034	0.997	0.0055	0.0128	0.989	0.0021
141	0.035	0.998	0.0150	0.0132	0.989	0.0056
109	0.114	0.997	0.0628	0.031	0.995	0.0169
26	0.250	0.994	0.5768	0.052	0.995	0.1190
10.4	0.362	0.983	2.0903	0.065	0.997	0.3730

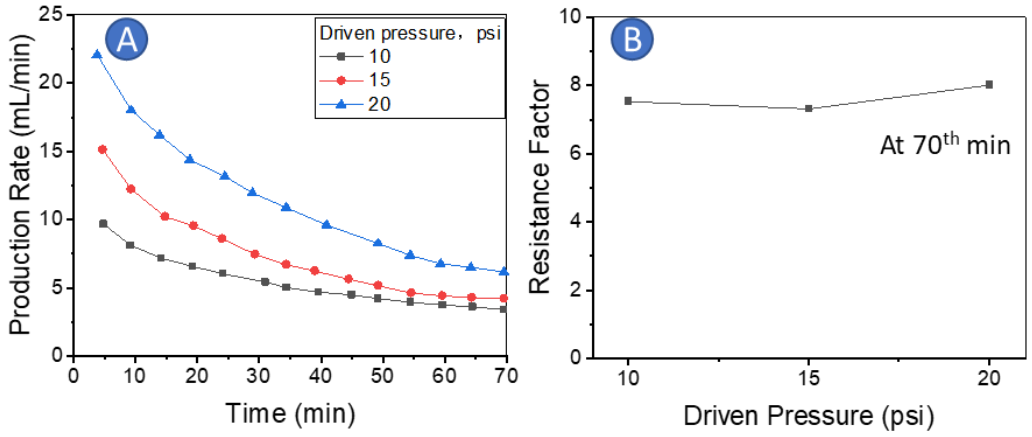

Figure 12. Production rates over time (A) and resistance factor at 70th min (B) at different driven pressure

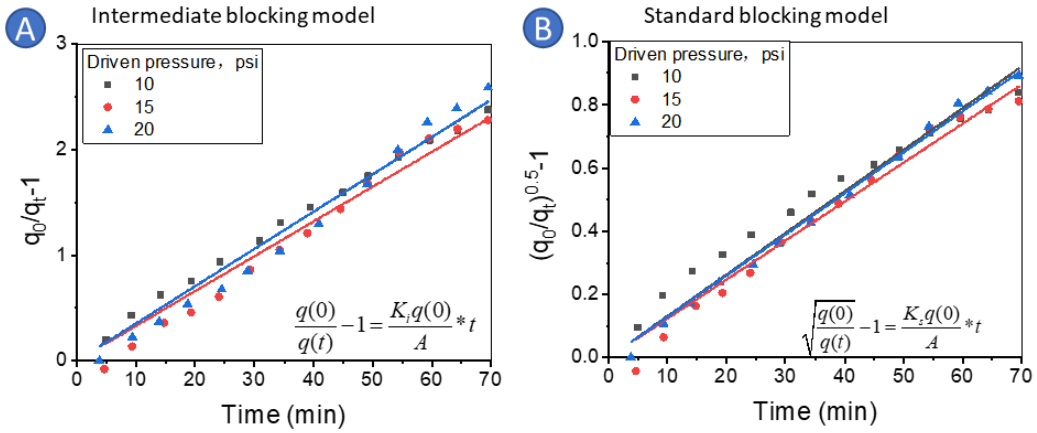

Figure 13. Filtration results fitted by intermediate blocking model (A) and Standard blocking model (B) at different driven pressure

Table 5. Fitting parameters of blocking models at different driven pressure

Driven Pressure, psi	Intermediate blocking model			Standard blocking model		
	Slope	Adj. R-Square	blocking constant, 1/cm	Slope	Adj. R-Square	blocking constant, 1/cm
10	0.0353	0.998	0.0150	0.0132	0.989	0.0056
15	0.0330	0.989	0.0118	0.0123	0.994	0.0044
20	0.0353	0.991	0.0079	0.0130	0.998	0.0029

REFERENCES

1. Bai B, Li L, Liu Y, Liu H, Wang Z, You C. Preformed Particle Gel for Conformance Control: Factors Affecting Its Properties and Applications. SPE Reserv Eval Eng [Internet]. 2007;10(04):415–22. Available from: https://doi.org/10.2118/89389-PA

2. Wang W, Liu Y, Gu Y. Application of a Novel Polymer System in Chemical Enhanced Oil Recovery (EOR). Colloid Polym Sci [Internet]. 2003;281(11):1046–54. Available from: https://doi.org/10.1007/s00396-003-0873-6

3. Wang Z, Zhao X, Bai Y, Gao Y. Study of a double cross-linked HPAM gel for in-depth profile control. J Dispers Sci Technol. 2016;37(7):1010–8.

4. Lin M, Zhang G, Hua Z, Zhao Q, Sun F. Conformation and plugging properties of crosslinked polymer microspheres for profile control. Colloids Surfaces A Physicochem Eng Asp [Internet]. 2015;477:49–54. Available from: http://www.sciencedirect.com/science/article/pii/S0927775715002794

5. Han P, Geng J, Bai B. Investigation on transport behavior of nanogel in low permeable porous medium. J Pet Sci Eng [Internet]. 2019;178:999–1005. Available from: http://www.sciencedirect.com/science/article/pii/S0920410519303560

6. Geng J, Han P, Bai B. Experimental Study on Charged Nanogels for Interfacial Tension Reduction and Emulsion Stabilization at Various Salinities and Oil Types [Internet]. SPE Asia Pacific Oil and Gas Conference and Exhibition. Brisbane, Australia: Society of Petroleum Engineers; 2018. p. 13. Available from: https://doi.org/10.2118/192118-MS

7. Geng J, Pu J, Wang L, Bai B. Surface charge effect of nanogel on emulsification of oil in water for fossil energy recovery. Fuel [Internet]. 2018;223:140–8. Available from: http://www.sciencedirect.com/science/article/pii/S0016236118304526

8. Geng J, Ding H, Han P, Wu Y, Bai B. Transportation and Potential Enhanced Oil Recovery Mechanisms of Nanogels in Sandstone. Energy & Fuels [Internet]. 2018 Aug 16;32(8):8358–65. Available from: https://doi.org/10.1021/acs.energyfuels.8b01873

9. Almohsin A, Ding H, Bai B. Experimental Study on the Transport and Improved Oil Recovery Mechanism of Submicron Particle Gel [Internet]. SPE EOR Conference at Oil and Gas West Asia. Muscat, Oman: Society of Petroleum Engineers; 2018. p. 14. Available from: https://doi.org/10.2118/190364-MS

10. Salehi M, Thomas CP, Kevwitch R, Garmeh G, Manrique EJ, Izadi M. Performance evaluation of thermally-activated polymers for conformance correction Applications. In: SPE Improved Oil Recovery Symposium. Society of Petroleum Engineers; 2012.

11. Goudarzi A, Almohsin A, Varavei A, Delshad M, Bai B, Sepehrnoori K. New experiments and models for conformance control microgels. In: SPE Improved Oil Recovery Symposium. Society of Petroleum Engineers; 2014.

12. Flory PJ. Principles of polymer chemistry. Cornell University Press; 1953.

13. Ding H, Geng J, Lu Y, Zhao Y, Bai B. Impacts of crosslinker concentration on nanogel properties and enhanced oil recovery capability. Fuel [Internet]. 2020;267:117098. Available from: http://www.sciencedirect.com/science/article/pii/S0016236120300934

14. Phenrat T, Kim H-J, Fagerlund F, Illangasekare T, Tilton RD, Lowry G V. Particle Size Distribution, Concentration, and Magnetic Attraction Affect Transport of Polymer-Modified Fe0 Nanoparticles in Sand Columns. Environ Sci Technol [Internet]. 2009 Jul 1;43(13):5079–85. Available from: https://doi.org/10.1021/es900171v

15. Jensen KH, Valente AXCN, Stone HA. Flow rate through microfilters: Influence of the pore size distribution, hydrodynamic interactions, wall slip, and inertia. Phys Fluids. 2014;26(5):52004.

16. Kim S, Marion M, Jeong B-H, Hoek EM V. Crossflow membrane filtration of interacting nanoparticle suspensions. J Memb Sci [Internet]. 2006;284(1):361–72. Available from: http://www.sciencedirect.com/science/article/pii/S0376738806005254

17. Deepak Selvakumar R, Dhinakaran S. Effective viscosity of nanofluids — A modified Krieger–Dougherty model based on particle size distribution (PSD) analysis. J Mol Liq [Internet]. 2017;225:20–7. Available from: http://www.sciencedirect.com/science/article/pii/S0167732216327350

18. Almohsin AM, Bai B, Imqam AH, Wei M, Kang W, Delshad M, et al. Transport of nanogel through porous media and its resistance to water flow. In: SPE Improved Oil Recovery Symposium. Society of Petroleum Engineers; 2014.

19. Chen L, Zhang G, Wang L, Wu W, Ge J. Zeta potential of limestone in a large range of salinity. Colloids Surfaces A Physicochem Eng Asp [Internet]. 2014;450:1–8. Available from: http://www.sciencedirect.com/science/article/pii/S0927775714002283

20. Toda K, Furuse H. Extension of Einstein's viscosity equation to that for concentrated dispersions of solutes and particles. J Biosci Bioeng [Internet]. 2006;102(6):524–8. Available from: http://www.sciencedirect.com/science/article/pii/S1389172307700063

21. Einstein A. Eine neue bestimmung der moleküldimensionen. ETH Zurich; 1905.

22. Goldrick S, Joseph A, Mollet M, Turner R, Gruber D, Farid SS, et al. Predicting performance of constant flow depth filtration using constant pressure filtration data. J Memb Sci [Internet]. 2017;531:138–47. Available from: http://www.sciencedirect.com/science/article/pii/S0376738816314223

23. Bolton GR, Boesch AW, Lazzara MJ. The effects of flow rate on membrane capacity: Development and application of adsorptive membrane fouling models. J Memb Sci [Internet]. 2006;279(1):625–34. Available from: http://www.sciencedirect.com/science/article/pii/S0376738806000226

24. Wang W, Yuan B, Su Y, Wang K, Jiang M, Moghanloo RG, et al. Nanoparticles adsorption, straining and detachment behavior and its effects on permeability of berea cores: Analytical model and lab experiments. In: SPE Annual Technical Conference and Exhibition. Society of Petroleum Engineers; 2016.

25. Li S, Hendraningrat L, Torsaeter O. Improved oil recovery by hydrophilic silica nanoparticles suspension: 2 phase flow experimental studies. In: IPTC 2013: International Petroleum Technology Conference. 2013.

III. A LABORATORY STUDY OF IMPACTS OF FLOW RATE ON NANOGEL TRANSPORT AND OIL RECOVERY IMPROVEMENT

ABSTRACT

Nanogel can be applied to increase oil recovery in low permeability reservoirs. It is proposed to achieve this goal by many mechanisms including interfacial tension reduction, wettability alteration, and improving reservoir homogeneity. Despite some promising studies on nanogels, many factors regarding nanogel flooding are still unclear to the industry and researchers. The injection velocity is one of the many factors awaiting further studies. The selection of velocity is important for most chemical floodings. It is always linked with different viscous forces, injectant retention, degradation, et cetera. Different velocities also correlate different equivalent shear rates inside porous media, which makes it more crucial for non-Newtonian injection fluids.

In this work, the impacts of injection flow rate on nanogel flooding were investigated. The partially hydrolyzed polyacrylamide based nanogel dispersion exhibited shear thinning at lower shear rates. At higher shear rates, on the other hand, its viscosity changes little. Core flooding experiments were performed in both porous media with only water phase and porous media containing residual oil. Resistance factors are higher with lower nanogel injection rates in both conditions. In cores with only water phase, nanogel were adsorbed, desorbed, and retained similarly regardless of nanogel flooding velocity. Consequently, residual resistance factors were not obviously impacted by nanogel flooding velocity. In contrast, in porous media with residual oil, a lower flow rate would result in higher residual resistance factors, possibly due to the effects of the changing

relative permeability. In addition, incremental oil recovery was higher with a lower nanogel flooding velocity.

1. INTRODUCTION

Nanogel, also known as crosslinked polymeric nanoparticle, has been proposed to improve oil recovery in low permeability reservoirs (1). It can block or reduce the permeability of pore throats, hence diverting injection fluids to unswept zones (2). By being adsorbing onto the porous media surface, it can modify rock wettability to a more favorable (water-wet) condition (3–5). It can also form emulsions with oil to decrease interfacial tension (6). As the name implies, nanogel is able to transport deep into reservoirs due to the small size and often applied as an approach to enhance oil recovery (EOR) in unfractured low permeability formations (7,8). Comparing to other EOR agents like silica and metallic nanoparticle, polymer, or in-situ gel, nanogel holds several advantages. Its viscoelasticity makes it easier to pass through channels. It is also relatively stable under some conditions like high temperature and salinity (2).

During any injection, regardless of the injected fluid, the selection of the velocity is always a factor that affects the outcome. For the secondary recovery stage, it was found that the efficiency of water flooding decreases with higher injection velocity (9), especially after it reaches a “critical velocity” (10). A lower velocity would also cause lower viscous force and result in higher oil recovery in a heavy oil reservoir (11). Laboratory studies have reported impacts of injection flow rate on improving oil recovery with solid nanoparticle (silica or metallic). Mixed results were reported with different

materials and experimental conditions. It was found that a higher injection flow rate of titanium dioxide nanoparticles can cause higher elution due to the greater hydrodynamic force (12). However, other studies also found the neglected impact of injection flow rate on the adsorption of aluminum oxide nanoparticles and the elution of silica nanoparticles (13,14). Increasing injection velocity was also found to be responsible for silica nanoparticle accumulation near the core inlet and lower incremental oil recovery (15). For a polymer flooding project, a high flow rate would result in lower thermal and chemical degradation but higher shear degradation (16). However, the more obvious impacts of injection velocity on polymer flooding is their viscosity and strength. During polymer flooding, velocity correlates an equivalent shear rate inside porous media. Since most polymers are none-Newtonian fluids, the characteristics of the polymer solution would vary with different injection velocity (17). Studies have found that mobility ratio can be affected by polymer injection velocity because of their shear-thinning or shear-thickening properties (18,19). Polymers also exhibited property change with different velocities and permeability, which both leads to different shear rates (20). Due to the likeness of the rheology between polymer and nanogel, velocity would impact nanogel flooding in a similar way.

In this study, partially hydrolyzed polyacrylamide (HPAM) based nanogel were utilized to core flooding experiments with different injection flow rate. Different porous media conditions were applied: in the porous media containing residual oil, impacts of injection flow rate on nanogel plugging and improving oil recovery were studied. However, relative permeability changes with different oil phase saturation, which affects the comparison of nanogel plugging capability among tests. Moreover, the nanogel

concentration of effluents containing oil cannot be tested. Thus, a series of experiments in a water-only condition were conducted ahead. With fewer influences, injectivity and nanogel retention were better observed and discussed.

2. EXPERIMENTAL MATERIALS

2.1. MATERIALS

The HPAM-based nanogel used in this study was prepared by suspension polyamidation following a similar procedure as our previous works (1,21). The main components to prepare the objective nanogel include AM (Acrylamide), AA (acrylic acid), and the crosslinker MBAA (N, N'-Methylenebisacrylamide). The specific weights of each component to synthesize each batch are shown in Table 1. All chemicals were purchased from Sigma-Aldrich (St. Louis, MO) and used as received.

Table 1. Components of the HPAM-based nanogel

Components	AM/g	AA/g	MBAA/mg	Water/g
Weight	13.5	1.5	2.25	15

1 wt.% NaCl solution was used in the study. Nanogel was also dispersed in the 1 wt.% NaCl brine at a concentration of 1,000 mg/L for further core flooding experiments. In addition, mineral light oil purchased from Fisher Scientific was used in core flooding experiments. At room temperature, its viscosity and density are 33.5cP and 0.83 g/ml, respectively. All cores in this study are Berea sandstone. The permeability and porosity of each core are around 110 mD and 20%.

2.2. NANOGEL CHARACTERIZATION

The nanogel at dry state was observed using a scanning electron microscope (SEM), Hitachi S-4700 FESEM. As shown in Figure 1, the nanogel at dry state are sphere-like with a diameter between 50 nm to 100 nm.

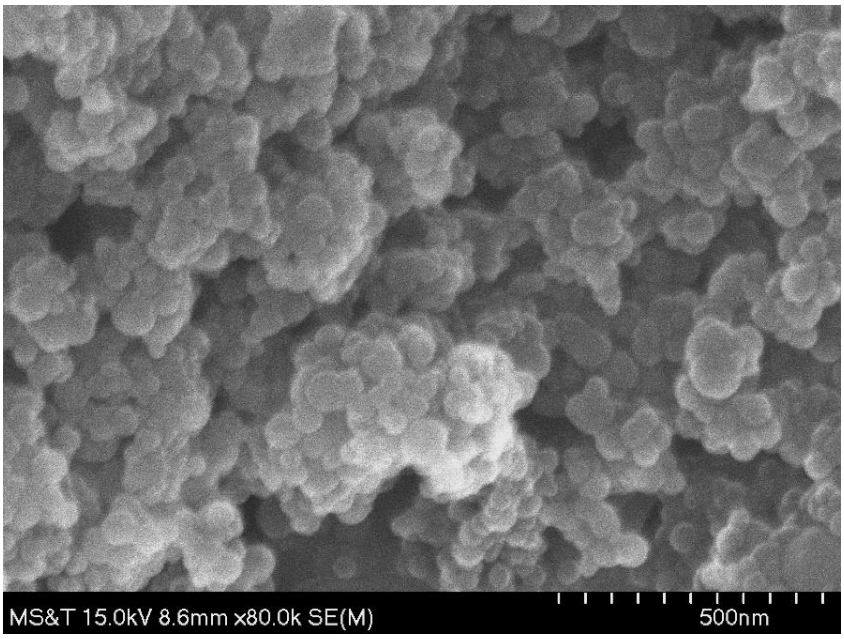

Figure 1. Dry nanogel captured by SEM

A Malvern ZS90 Nanosizer was used to measure the nanogel size and surface charge after it being dispersed in 1% NaCl brine. The hydrodynamic diameter of nanogel was measured via dynamic light scattering (DLS). Dispersion zeta potential was measured via electrophoretic light scattering (ELS). Multiple DLS and ELS tests were conducted to ensure the best results. As demonstrated in Figure 2 (A), in brine, the diameter of nanogel is between 150 nm to 250 nm for most of the DLS tests, which are multiple times larger comparing to its original size at the dry condition. This is a result of

nanogel swelling, as it tends to absorb free water and expand in the liquid phase. Compared to hydrodynamic diameter, nanogel zeta potential is in a small range between -11.25 mV to -12 mV during the majority of ELS tests (Figure 2 (B)). The nanogel is negatively charged because of the acrylic acid, which is anionic.

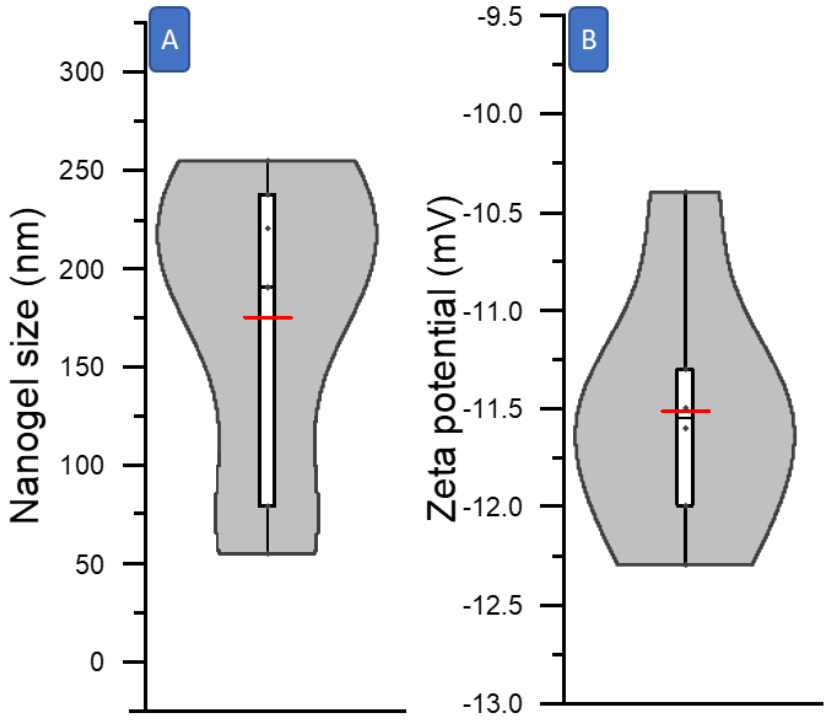

Figure 2. (A) Nanogel size measured via DLS; (B) Zeta potential measured via ELS

A Brookfield DV3T rheometer was utilized to measure the viscosity of nanogel dispersion from low to high shear rates. As illustrated in Figure 3, viscosity decreased with a faster shear rate. When the shear rate reaches 50 1/s, viscosity was decreasing at a slower speed. Eventually, when the shear rate was higher than 100 1/s, viscosity became relatively constant, which indicates that the interparticle structure might have been broken at this shear rate (1). The upper x-axis in Figure 3 shows equivalent flow rates at

the experimental condition, which match the shear rate in the lower axis. Equivalent flow rates were calculated by the equation below(22):

$$\dot{\gamma}_{eq} = 4v\left(\frac{\emptyset}{8k}\right)^{1/2} = \frac{4q}{A\sqrt{8k\phi}}$$

where A is the area, q is the flow rate (ml/sec), γ_{eq} is the shear rate(1/s), k and Φ are permeability (mD) and porosity. The calculation is based on the average properties of the cores in this study (125 mD in permeability, 20% in porosity, and 2.51 cm in diameter).

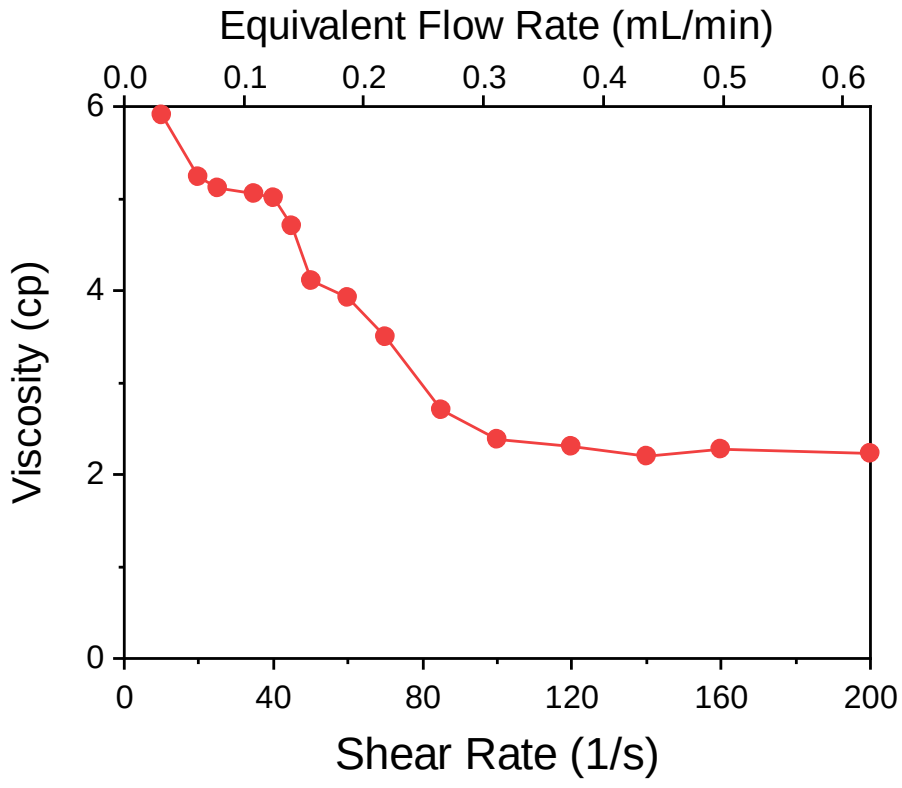

Figure 3. Viscosity of nanogel dispersion at different shear rates and their equivalent flow rates

3. EXPERIMENTAL METHOD

3.1. EXPERIMENTAL SETUP

Experiments in this study were set up similarly with our previous study(21), as shown in Figure . A syringe pump (Teledyne ISCO 500D Syringe Pump) was deployed to inject distill (DI) water into an accumulator filled with brine, oil, or nanogel dispersion. Fluids in the accumulator would be injected into the core holder. A confining pressure system was set at least 400 psi above the injection pressure to ensure injection fluid would only flow through the porous media. Test tubes were placed at the outlet to collect effluents.

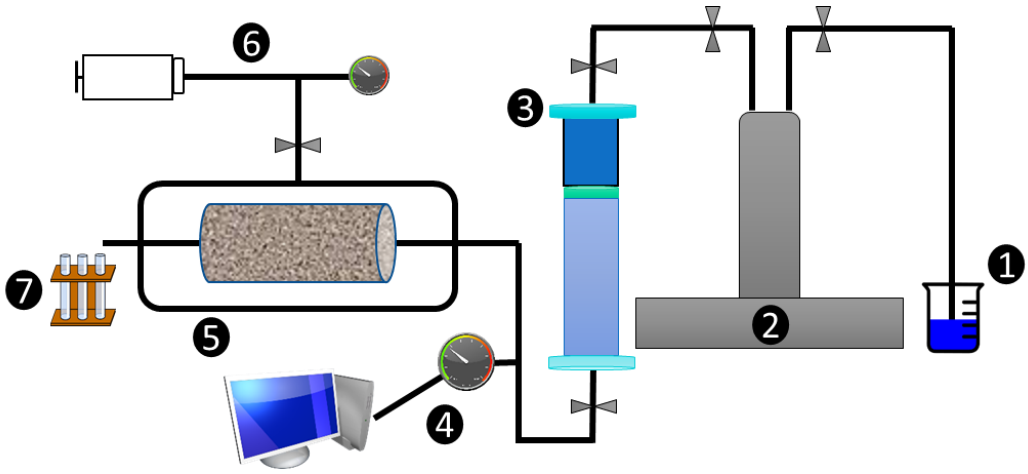

Figure 4. Schematic Diagram of the experimental setup (81)
1: DI water; 2: pump; 3: accumulator; 4: pressure sensor;
5: core holder; 6: confining pressure system; 7: tubes

Two series of core flooding experiments were conducted in this work. Experiments with only water phase inside cores were performed to study the impacts of injection rate on retention of nanogel onto rock surface and plugging efficiency during

and after nanogel flooding. When there was residual oil in place, the impacts of the injection rate on oil displacement improvement by nanogel were studied.

3.2. EXPERIMENTAL PROCEDURES

Applied nanogel flooding flow rates are shown in Table 2. Interstitial velocity is the speed injected fluids progressing in the direction of movement, which is calculated with an average porosity of 20%.

Table 2. Applied nanogel flooding injection flow rates, equivalent velocities, and equivalent shear rates

Injection flow rate, ml/min	Interstitial velocity, ft/day	Shear rate, s^{-1}
3	144.3	963
1.25	60.2	401
0.5	24.1	161
0.2	9.6	64
0.05	2.4	16

3.2.1. Nanogel Injection in One Phase Condition. During experiments with only water phase involved, nanogel dispersion with a concentration of 1,000 mg/L was injected into core samples directly after measuring their permeability. One nanogel injection flow rate was selected for each test. Effluents were collected and tested using a Shimadzu UVmini-1240 UV–vis spectrophotometer to determine their concentration. Base on the concentration of effluents, the weight of nanogel that were retained inside the porous media would be obtained. Meantime, injection pressure would be recorded to

evaluate the plugging efficiency of nanogel. Resistance factor and residual resistance factor are the main criteria. They are calculated as the following equations:

$$RF = \frac{\lambda_{water}}{\lambda_{nanogel}} = \frac{k_{water} / \mu_{water}}{k_{nanogel} / \mu_{nanogel}} = \frac{P_{nanogel}}{P_{water}}$$

$$RRF = \frac{\lambda_{first\ water\ flooding}}{\lambda_{second\ water\ flooding}} == \frac{P_{2nd}}{P_{1st}}$$

λ, k, P and μ represent mobility, effective permeability, injection pressure, and viscosity, respectively.

During nanogel floodings, injection pressures would increase continually. Hence, all tests were ended after 15 PV of nanogel injection, when the rate of adsorption between nanogel and core surface was close to constant and minimum. It will be followed by another brine injection (second water flooding) at the same injection rate. Part of the previously adsorbed nanogel would be flushed out and cause a decrease in pressure. After there is no more nanogel being flushed out and stable injection pressure, the injection rate will be changed gradually from low to high, in order to calculate the residual resistance factors at each injection rate.

3.2.2. Improving Oil Recovery with Different Nanogel Injection Rates. In addition to experiments in one phase condition, nanogel was tested to displace residual oil at different injection rates. Effluents were collected to obtain oil recovery during tests. To create a water-and-oil two-phase condition, light mineral oil was injected into each core. Brine was later being injected as water flooding and to establish a residual oil saturation. Nanogel would be injected at a selected flow rate. Different from the previous tests, nanogel flooding would not be stopped until a stable injection pressure was

observed. Another brine injection (second water flooding) would be performed following nanogel flooding to continue to improve oil recovery. During both water flooding stages, in order to obtain residual resistance factors at different injection rates, they were run at multiple flow rates. The flow rate would be switched when there is no more oil being produced and stable injection pressure. It is worth noting that during the first water flooding, an extra amount of oil would be produced when the flow rate was increased, but not vice versa.

4. RESULTS AND DISCUSSIONS

4.1. NANOGEL INJECTION IN ONE PHASE CONDITION

As shown in Table 2, nanogel dispersions were injected into five core samples at different flow rates. All injections were kept for 15 PV (pore volume) of injection, where the average PV is 5mL.

Figure 5 shows the injection pressure along with cumulative nanogel retention versus the injection volume of each test. The blue curves represent injection pressures during nanogel injections and the following brine injections. The jaggy pressure plot of the test under 0.05 mL/min flow rate is due to the large difference between injection pressure and the range of the pressure sensor. Black dot lines show the brine injection pressure prior to nanogel flooding at the same flow rate, as a reference to reflect the permeability reduction caused by the nanogel. The black scatter lines represent cumulative nanogel retentions. Because of the adsorption between nanogel and rock surface during nanogel flooding, the retention reaches to peak at the end of the stage. The

number would decrease during the following brine injection as some nanogel being flushed out.

Table 3. Properties of cores for adsorption core flooding study

Core ID	Pore Volume, mL	Permeability, mD	Length, cm	Diameter, cm	Nanogel Injection Flow Rate, mL/min
A-1	5.17	123.78	5	2.51	0.05
A-2	5.23	125.69	5	2.51	0.2
A-3	5.16	114.32	5	2.51	0.5
A-4	5.23	144.61	5	2.51	1.25
A-5	5.03	137.23	5	2.51	3

During each test, the logjam was found as nanogel injection pressure increasing constantly. This might be caused by the nanogel agglomerates, which can block pore throats by their relatively large size. Agglomerates were formed during an equilibrium state of adsorption and desorption between nanogel and rock surface (21).

As demonstrated in Figure 5, the selection of the injection rate had an obvious impact on the resistance factors of nanogel. With higher injection flow rates, nanogel injection and the following brine injection pressures were higher. As shown in Figure 6, resistance factors decreased when the flow rate was increased from 0.05 to 1.25 mL/min. The decreasing trend can be fit by power-law equations. This relationship was also consistent with the relationship between viscosity and shear rate. Moreover, since the total injection volume was the same among all experiments, tests with the lower flow rate

would cost longer injection periods. This might increase the chance of nanogel to agglomerate even more and leads to higher resistance factors.

Since the water flooding after nanogel flooding were conducted at multiple flow rates, a residual resistance factor versus flow rate plot can be displayed for each test. Residual resistance factors plots of each test were almost identical, indicating that the injection flow rate of nanogel has little effect on permeability reduction in this condition.

In addition, like resistance factors, residual resistance factors of each test decrease with a higher injection flow rate. This could be caused by the different flow patterns at different velocities. At lower velocity, the injected nanogel dispersion follows the laminar flow pattern, where the fluid flow near the core surface is flowing much slower than the flow in the middle of the pore throat. On the other hand, at higher injection velocity, the gel could “slip”, as the flow transferring from laminar to turbulence (20). These observations are consistent with the flow behaviors of millimeter-sized preformed particle gels inside open conduit fracture models (23).

Meantime, during a nanogel injection, a large amount of nanogel was adsorbed onto porous media at the earlier injection phase. After roughly 3 PV of injection, the cumulative retention increased much slower. The increase of retained nanogel weight represents the adsorption between nanogel and rock surface. It was mostly caused by the Van der Waals force between two subjects, the settlement due to the gravity and the trapping of particles. The cumulative adsorption plots (retention plots during nanogel flooding) can be fitted using the Pseudo-second-order kinetic equation (24,25):

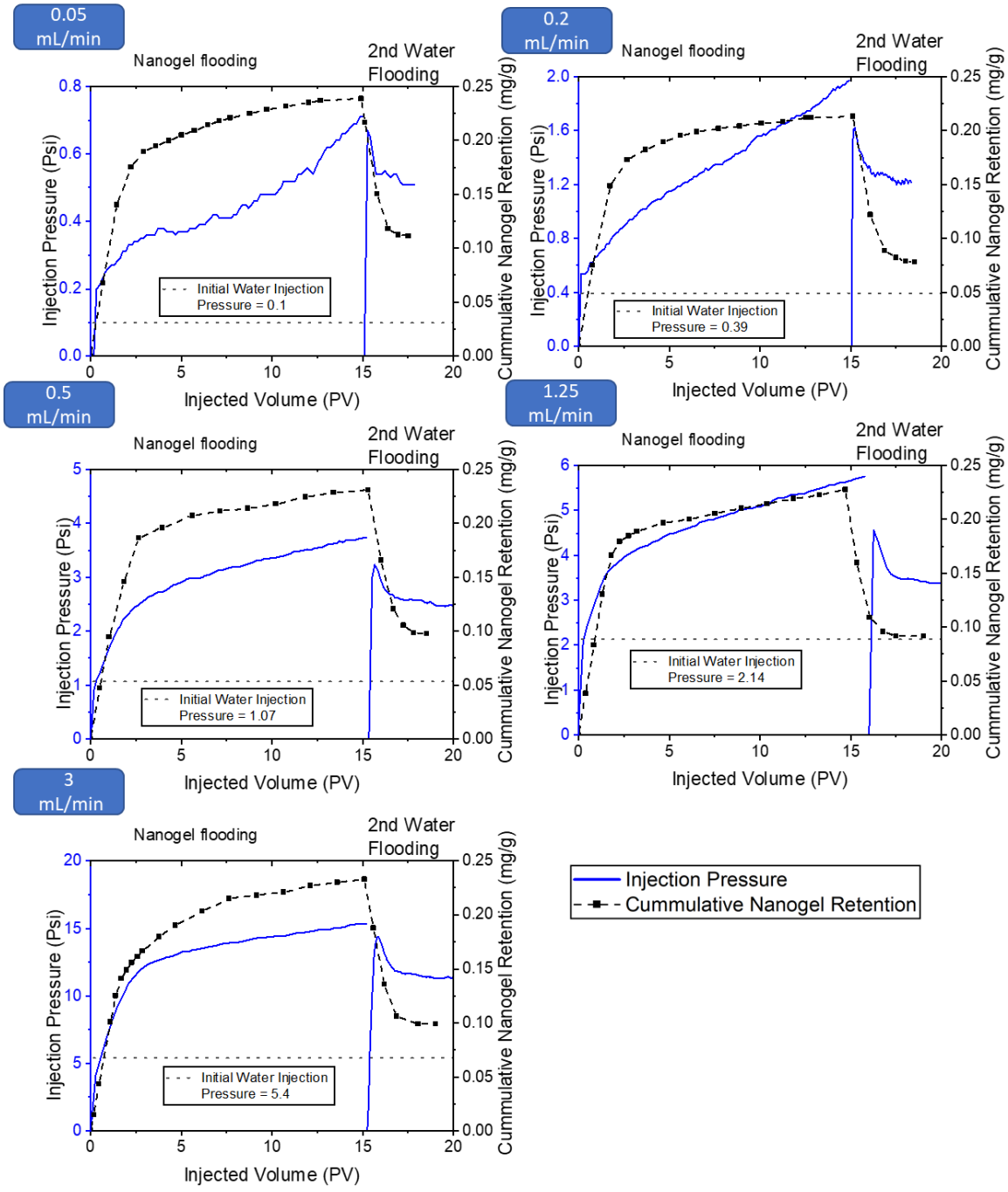

Figure 5. Injection pressure and cumulative nanogel retention during nanogel flooding and following water injection

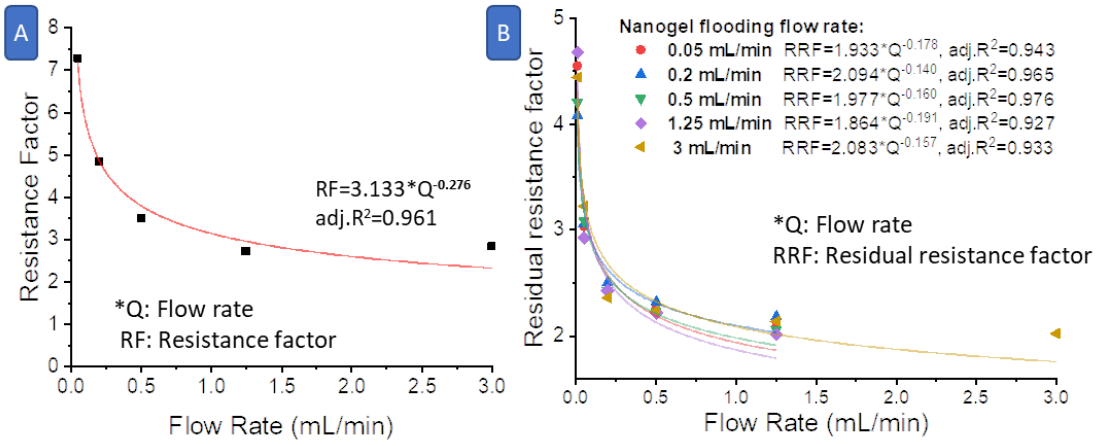

Figure 6. Resistance factors and residual resistance factors when nanogel was injected at different flow rates

$$\frac{t}{q_t} = \frac{1}{q_e}t + \frac{1}{kq_e^2}$$

where q_t represents the adsorption at any moment during tests(mg/g), q_e represents the adsorption at equilibrium (mg/g), k represents adsorption rate constant (g/mg/min), and t is time (min). The relations between t/q_t and time of each test are shown in Figure 7. The model fits the data suitably with all adjust R squares over 0.99, as demonstrated in Table 4Table 3. Furthermore, as shown in Figure 8, the adsorption rate constant increases linearly with the injection flow rate. It indicates that the differences among tests were mostly caused by the duration of injections.

During the brine injections following nanogel flooding, equal amounts of nanogel were flushed out among all tests. As summarized in Table 5, no obvious association between injection flow rate and adsorption behavior was found: the adsorption, desorption, and retention weight of nanogel were all in a small range among all tests, which further explained why residual resistance factors do not vary with different

nanogel injection velocity (Figure 6). Furthermore, trapping of nanogel would be affect by velocity but not the adsorption behavior. Hence, the adsorption between nanogel and rock surface (Van der Wall force) is the dominate reason account for the retention of nanogel.

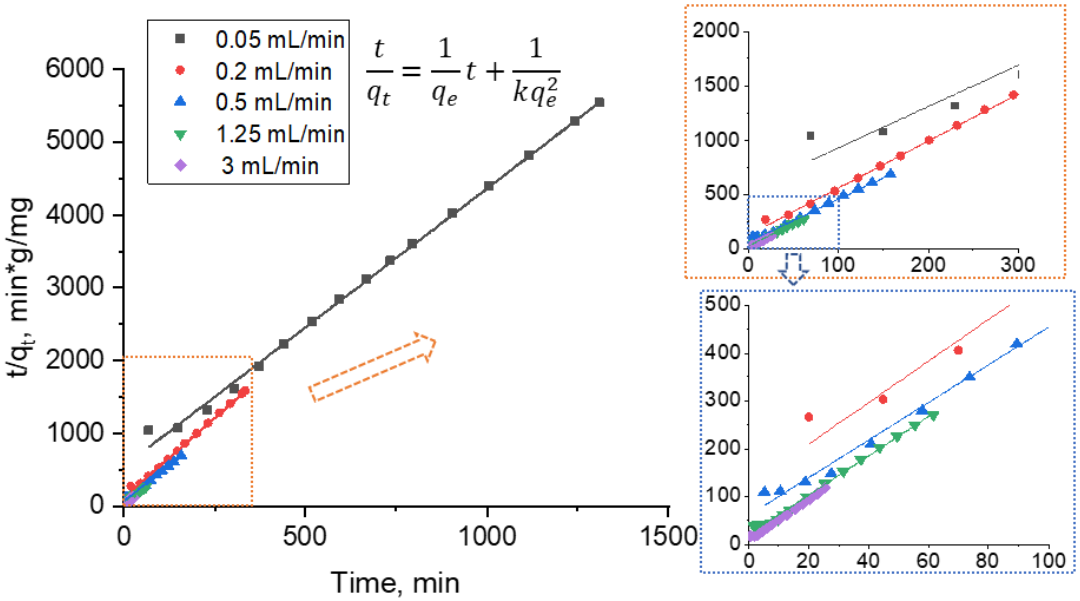

Figure 7. Adsorption of nanogel fitted by Pseudo-second-order kinetic model

Table 4. Relative parameters of the fitting model

Nanogel Injection Flow Rate, mL/min	Intercept	Slope	Adj. R-Square	K, g/mg/min	Qe, mg/g
0.05	546.09	3.82	0.997	0.027	0.262
0.2	123.04	4.34	0.998	0.153	0.230
0.5	60.95	3.93	0.996	0.254	0.254
1.25	21.22	4.10	0.995	0.794	0.244
3	11.35	3.83	0.996	1.294	0.261

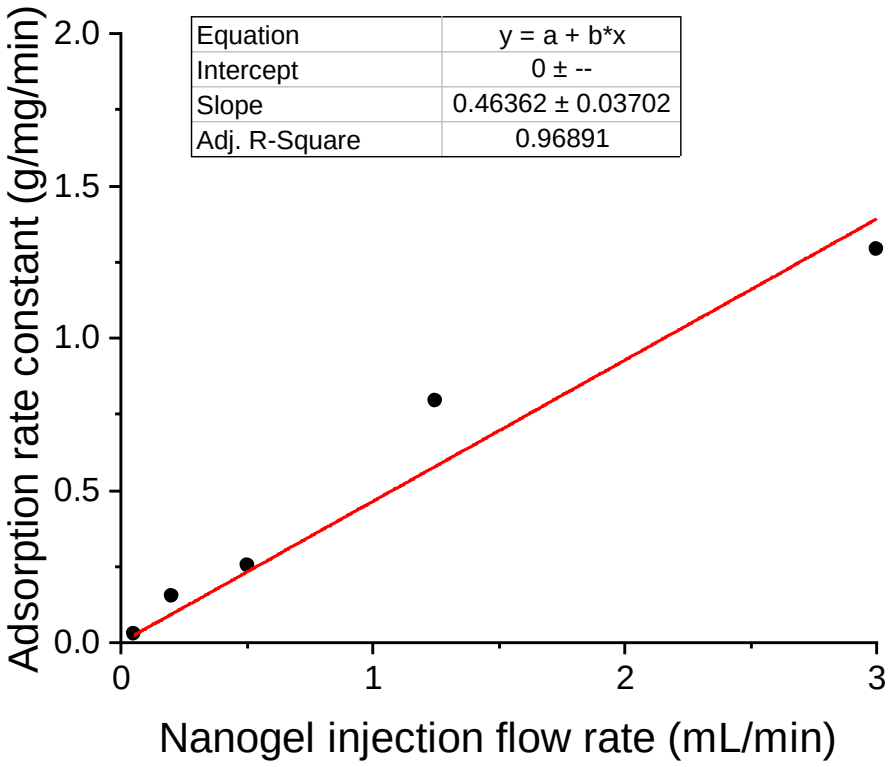

Figure 8. The relation between nanogel injection flow rates and adsorption rate constants

Table 5. Weight of nanogel adsorbed, desorbed, and retained inside porous media

Nanogel Injection Flow Rate, mL/min	Adsorption, mg/g	Final retention, mg/g	Desorption, mg/g
0.05	0.238	0.112	0.127
0.2	0.213	0.079	0.134
0.5	0.231	0.098	0.133
1.25	0.227	0.092	0.135
3	0.233	0.099	0.136

4.2. IMPROVING OIL RECOVERY IN POROUS MEDIA

Furthermore, the impacts of injection velocity in porous media with residual oil were studied. Four tests were conducted at different nanogel dispersion injection flow rates. The characteristics of porous media are shown in Table 3.

Table 6. Properties of cores for oil displacement core flooding study

Core ID	Permeability, mD	Pore Volume, mL	Length, cm	Diameter, cm	OOIP, mL	Nanogel Injection Flow Rate, mL/min
B-1	105.5	8.11	8	2.51	7.1	0.05
B-2	93.22	8.02	8	2.51	7.3	0.2
B-3	113.31	8.16	8	2.51	7	0.5
B-4	95.59	8.05	8	2.51	7.25	1.25

Prior to nanogel flooding, water flooding has been run at each of the four flow rates to ensure consistent pre-treatment oil recovery factors and injectivities across all experiments. Plugging efficiency and oil recovery improvement by nanogel were evaluated under different flow rates as displayed in Figure 9. Blue curves show the injection pressure during nanogel floodings and the following water floodings, while the dot lines represent the pre-treatment water flooding pressures at respective flow rates. Black lines represent cumulative oil recovery factors during each core flooding experiment, starting from the oil recovery at the end of the pre-treatment water flooding.

Different from the cases in single-phase saturated porous media, when residual oil existed in the porous media, nanogel injection pressures could be stabilized at the end of injections. A possible reason being accountable for this phenomenon is the hindrance

from oil on the adsorption of nanogel (2,26). The potential much lower rates of adsorption and desorption would prevent the injection pressure from increasing indefinitely.

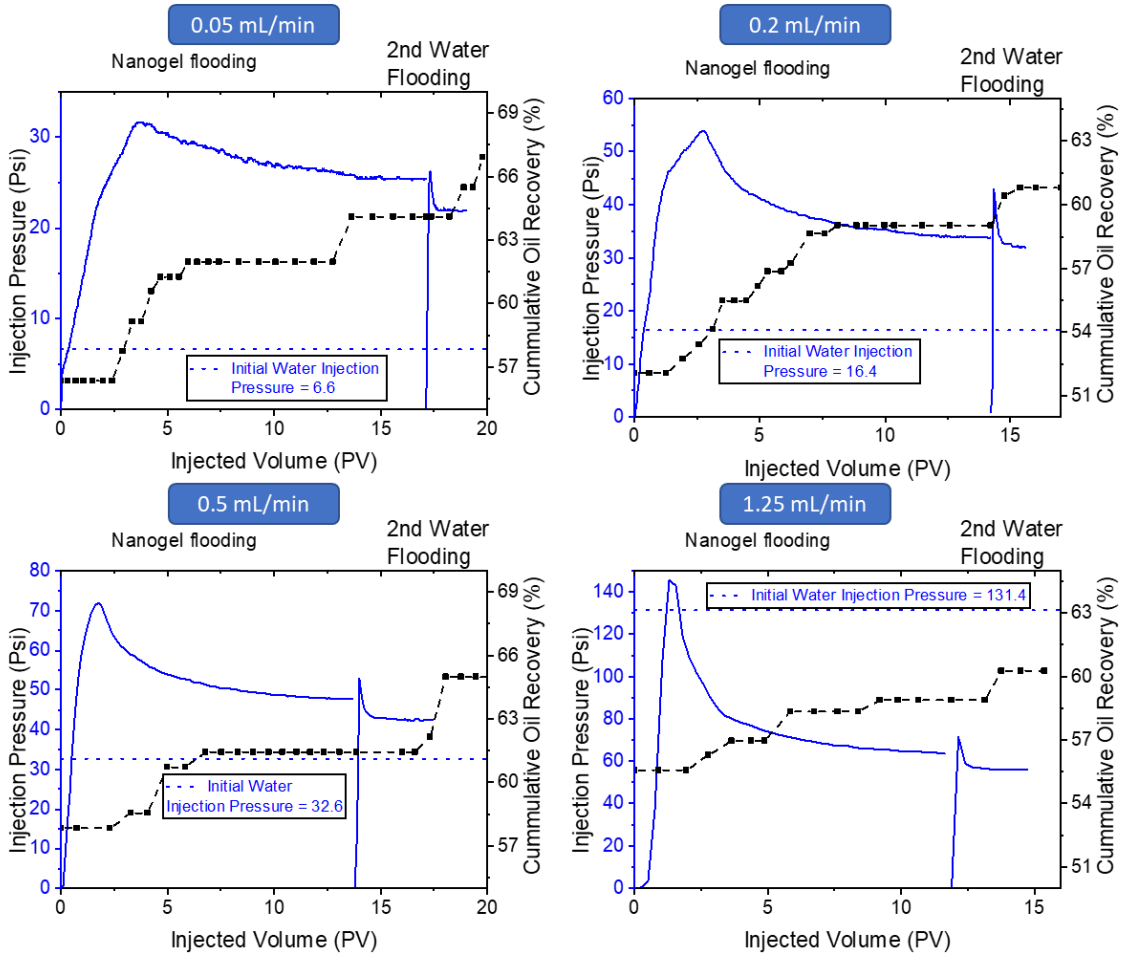

Figure 9. Injection pressure and oil recovery during nanogel flooding and second water flooding

Moreover, as shown in the plots, nanogel injection pressure decreased after a few PV of injection. This could be a result of the changing phase saturations and viscoelasticity of nanogel. During nanogel injection, as the water phase saturation

decreasing along with nanogel flooding, relative permeability to the water phase raised. Assuming nanogel stopped reducing absolute permeability after some points, effective permeability to the water would increase and result in a drop in injection pressure. At the highest selected flow rate, the nanogel flooding pressure even dropped below the initial pressure. Secondly, since the nanogel is viscoelastic and deformable, particles would be deformed to go through some pore throats, leading to higher pressure. Pressure decreases would be observed afterward as the energy from deformation being released. The previous study has found that such declines would not appear if the nanogel is rigid enough and produces little amount of oil (21).

The difference of the injection pressure increases from initial water flooding under different flow rates are similar to the previous single-phase tests: at a low flow rate, resistance factor was higher. The nanogel injection pressure at the highest point (as shown in Figure 9) also decreased with a higher injection flow rate.

In Figure 10(A), final (calculated with the stable nanogel injection pressure) and peak (calculated with the peak nanogel injection pressure) resistance factors versus different nanogel flooding flow rates were displayed. Both values decrease with a higher injection flow rate, which also corresponds to the relationship between shear rate and nanogel dispersion viscosity. Similarly to the experiments in the single-phase condition, the plots can be fit by power-law.

Brine was injected after nanogel flooding to continue improving oil recovery. All injection pressures were higher than the initial water flooding pressures, except for the test under the flow rate of 1.25 mL/min. The increases from initial pressure prove that nanogel can still be adsorbed onto rock surfaces and block porous media containing oil.

The declines of pressure at the beginning of second water flooding could be a result of both water saturation increase and flushed out nanogel.

As displayed in Figure 10(B), the difference of residual resistance factors among tests was much more noticeable compared to the results from single-phase experiments. If the nanogel flooding was performed at lower flow rates, residual resistance factors were higher. Since oil saturation affected brine injection pressure greatly, different saturations among tested porous media would result in varied residual resistance factor. Secondly, as nanogel can emulsify oil and form emulsions, different amounts of nanogel might be flushed out along with oil in different tests. Hence, different amounts of nanogel were retained inside porous media.

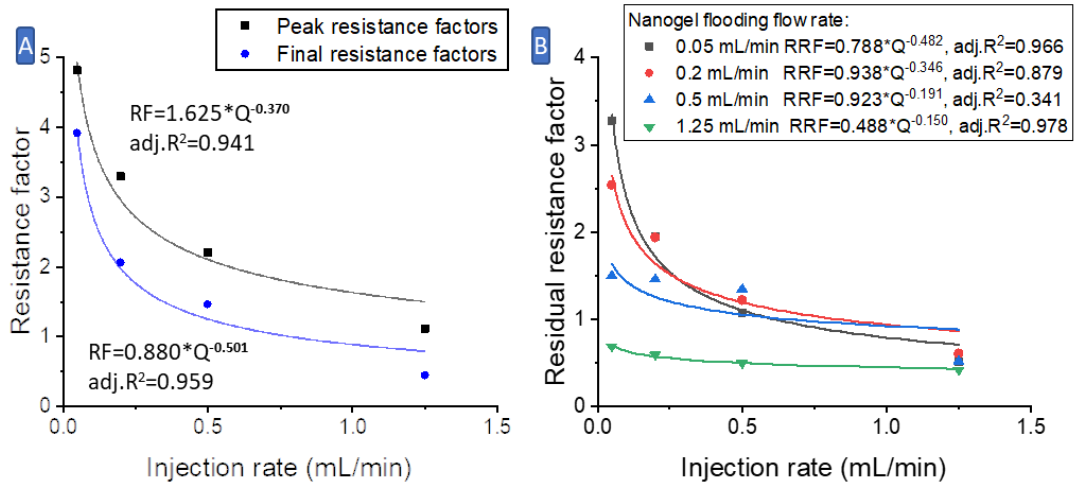

Figure 10. Resistance factors and residual resistance factors at different nanogel flooding flow rates

In each test, the oil recovery factor increased after first a few PV of nanogel injection. Nanogel can improve oil recovery by multiple mechanisms. It can reduce interfacial tension by emulsifying oil drops and modify porous media wettability (2,6). In

addition, despite hindered adsorption because of the residual oil, nanogel can still be adsorbed onto the rock surface. It led to permeability reduction of pore throats, diverting injection fluids, and eventually higher sweep efficiency.

Among all experiments, the oil recovery was improved the most with the lowest nanogel injection flow rate. The incremental oil recovery from each injection stage is summarized in Figure 11. Due to the shear thinning of the nanogel dispersion under a certain shear rate range, lower flow rates would cause lower mobility ratios. Moreover, higher resistance factors at lower flow rates indicate better capabilities to divert injection fluids for nanogel.

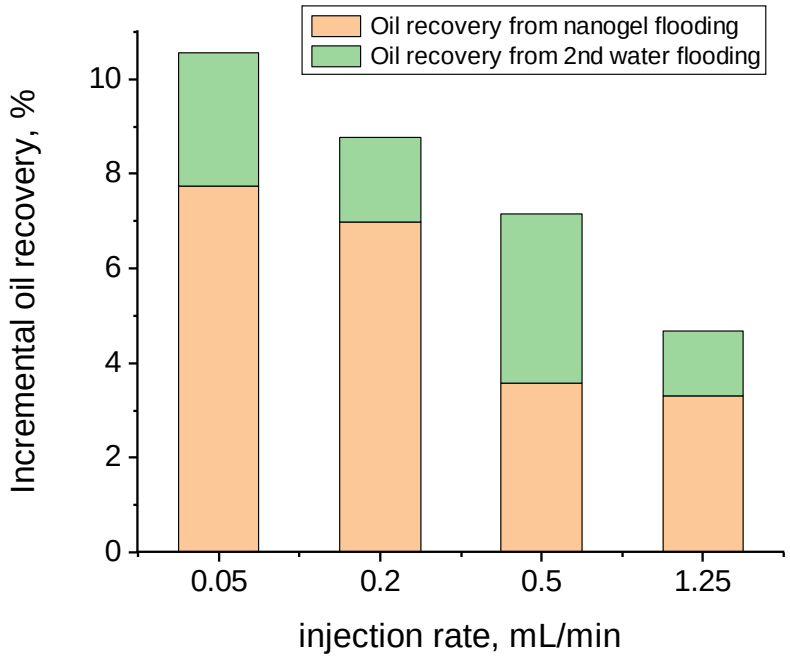

Figure 11. Incremental oil recovery at different flow rates

5. CONCLUSIONS

In this work, two series of core flooding tests were conducted in different conditions to study how flow rate affects nanogel flooding. Following conclusions were reached:

- Nanogel dispersion showed a shear thinning behavior under a shear rate of 100 1/s. Its viscosity was relatively constant above this shear rate;
- in both single-phase and two-phase conditions, resistance factors are higher with lower nanogel injection rates, indicating better plugging capability. During the water flooding following nanogel flooding, residual resistance factors decrease with an increasing flow rate in each test;
- In single-phase porous media, impacts of injection rate on nanogel retention and residual resistance factor were not evident;
- When residual oil was presented in porous media, lower flow rates would result in higher incremental oil recovery and higher residual resistance factors.

REFERENCES

1. Geng J, Pu J, Wang L, Bai B. Surface charge effect of nanogel on emulsification of oil in water for fossil energy recovery. Fuel [Internet]. 2018;223:140–8. Available from: http://www.sciencedirect.com/science/article/pii/S0016236118304526

2. Geng J, Ding H, Han P, Wu Y, Bai B. Transportation and Potential Enhanced Oil Recovery Mechanisms of Nanogels in Sandstone. Energy & Fuels [Internet]. 2018 Aug 16;32(8):8358–65. Available from: https://doi.org/10.1021/acs.energyfuels.8b01873

3. Al-Muntasheri GA, Liang F, Hull KL. Nanoparticle-Enhanced Hydraulic-Fracturing Fluids: A Review. SPE Prod Oper [Internet]. 2017;32(02):186–95. Available from: https://doi.org/10.2118/185161-PA

4. Chaudhury MK. Spread the word about nanofluids. Nature [Internet]. 2003 May 8;423:131. Available from: https://doi.org/10.1038/423131a

5. Wasan DT, Nikolov AD. Spreading of nanofluids on solids. Nature [Internet]. 2003 May 8;423:156. Available from: https://doi.org/10.1038/nature01591

6. Geng J, Han P, Bai B. Experimental Study on Charged Nanogels for Interfacial Tension Reduction and Emulsion Stabilization at Various Salinities and Oil Types [Internet]. SPE Asia Pacific Oil and Gas Conference and Exhibition. Brisbane, Australia: Society of Petroleum Engineers; 2018. p. 13. Available from: https://doi.org/10.2118/192118-MS

7. Almohsin A, Ding H, Bai B. Experimental Study on the Transport and Improved Oil Recovery Mechanism of Submicron Particle Gel [Internet]. SPE EOR Conference at Oil and Gas West Asia. Muscat, Oman: Society of Petroleum Engineers; 2018. p. 14. Available from: https://doi.org/10.2118/190364-MS

8. Ding H, Zhang N, Zhang Y, Wei M, Bai B. Experimental Data Analysis of Nanoparticles for Enhanced Oil Recovery. Ind Eng Chem Res. 2019;58(27).

9. Zhang X, Zhao L, Wang J, Chen L, Yue X. Effect of WaterFlooding Speed on Water–Oil Displacement Efficiency of Homogeneous Core BT - Proceedings of the International Field Exploration and Development Conference 2018. In: Lin J, editor. Singapore: Springer Singapore; 2020. p. 932–7.

10. Earlougher RC. Relationship between Velocity, Oil Saturation, and Flooding Efficiency. Trans AIME [Internet]. 1943;151(01):125–37. Available from: https://doi.org/10.2118/943125-G

11. Mai A, Kantzas A. Heavy Oil Waterflooding: Effects of Flow Rate and Oil Viscosity. J Can Pet Technol [Internet]. 2009;48(03):42–51. Available from: https://doi.org/10.2118/09-03-42

12. Chowdhury I, Hong Y, Honda RJ, Walker SL. Mechanisms of TiO2 nanoparticle transport in porous media: Role of solution chemistry, nanoparticle concentration, and flowrate. J Colloid Interface Sci [Internet]. 2011;360(2):548–55. Available from: http://www.sciencedirect.com/science/article/pii/S0021979711005819

13. Rahman T, George J, Shipley HJ. Transport of aluminum oxide nanoparticles in saturated sand: Effects of ionic strength, flow rate, and nanoparticle concentration. Sci Total Environ [Internet]. 2013;463–464:565–71. Available from: http://www.sciencedirect.com/science/article/pii/S0048969713007018

14. Lecoanet HF, Wiesner MR. Velocity Effects on Fullerene and Oxide Nanoparticle Deposition in Porous Media. Environ Sci Technol [Internet]. 2004 Aug 1;38(16):4377–82. Available from: https://doi.org/10.1021/es035354f

15. Hendraningrat L, Li S, Torsater O. Effect of some parameters influencing enhanced oil recovery process using silica nanoparticles: An experimental investigation. In: SPE Reservoir Characterization and Simulation Conference and Exhibition. Society of Petroleum Engineers; 2013.

16. Sheng JJ, Leonhardt B, Azri N. Status of Polymer-Flooding Technology. J Can Pet Technol [Internet]. 2015;54(02):116–26. Available from: https://doi.org/10.2118/174541-PA

17. Sun W, Li K. Experimental Evaluation of Models for Calculating Shear Rates of Polymer Solution In Porous Media [Internet]. SPE Annual Technical Conference and Exhibition. Amsterdam, The Netherlands: Society of Petroleum Engineers; 2014. p. 9. Available from: https://doi.org/10.2118/170647-MS

18. Al-Shakry B, Shiran BS, Skauge T, Skauge A. Enhanced Oil Recovery by Polymer Flooding: Optimizing Polymer Injectivity [Internet]. SPE Kingdom of Saudi Arabia Annual Technical Symposium and Exhibition. Dammam, Saudi Arabia: Society of Petroleum Engineers; 2018. p. 22. Available from: https://doi.org/10.2118/192437-MS

19. Smith FW. The Behavior of Partially Hydrolyzed Polyacrylamide Solutions in Porous Media. J Pet Technol [Internet]. 1970;22(02):148–56. Available from: https://doi.org/10.2118/2422-PA

20. Seright RS. Use of Preformed Gels for Conformance Control in Fractured Systems. SPE Prod Facil [Internet]. 1997;12(01):59–65. Available from: https://doi.org/10.2118/35351-PA

21. Ding H, Geng J, Lu Y, Zhao Y, Bai B. Impacts of crosslinker concentration on nanogel properties and enhanced oil recovery capability. Fuel [Internet]. 2020;267:117098. Available from: http://www.sciencedirect.com/science/article/pii/S0016236120300934

22. Zitha P, Chauveteau G, Zaitoun A. Permeability~Dependent Propagation of Polyacrylamides Under Near-Wellbore Flow Conditions [Internet]. SPE International Symposium on Oilfield Chemistry. San Antonio, Texas: Society of Petroleum Engineers; 1995. p. 16. Available from: https://doi.org/10.2118/28955-MS

23. Imqam A, Bai B, Al Ramadan M, Wei M, Delshad M, Sepehrnoori K. Preformed-Particle-Gel Extrusion Through Open Conduits During Conformance-Control Treatments. SPE J [Internet]. 2015;20(05):1083–93. Available from: https://doi.org/10.2118/169107-PA

24. Ho Y-S. Review of second-order models for adsorption systems. J Hazard Mater [Internet]. 2006;136(3):681–9. Available from: http://www.sciencedirect.com/science/article/pii/S0304389406000021

25. Ho YS, McKay G. Pseudo-second order model for sorption processes. Process Biochem [Internet]. 1999;34(5):451–65. Available from: http://www.sciencedirect.com/science/article/pii/S0032959298001125

26. Broseta D, Medjahed F, Lecourtier J, Robin M. Polymer Adsorption/Retention in Porous Media: Effects of Core Wettability and Residual Oil. SPE Adv Technol Ser [Internet]. 1995;3(01):103–12. Available from: https://doi.org/10.2118/24149-PA

IV. IMPACTS OF CROSSLINKER CONCENTRATION ON NANOGEL PROPERTIES AND ENHANCED OIL RECOVERY CAPABILITY

ABSTRACT

The use of nanogels, or crosslinked polymeric nanoparticles, has been proposed as a means of improving oil recovery in low permeability reservoirs. Nanogels can transport deep into reservoirs and improve homogeneity due to their small size and deformability. Typically, nanogels are polymerized using monomers and crosslinkers, which transform polymers from linear structures to 3D structures. Nanogel properties — including its swelling ratio and strength — can be fine-tuned by the crosslinker concentration. In this study, we investigated the impacts of crosslinker concentration on partially hydrolyzed polyacrylamide (HPAM)-based nanogels. The effect of the degree of crosslinking on the physicochemical properties of nanogel, the corresponding adsorbing behavior on rock surfaces, and consequently, the oil recovery improvement was studied.

The results show the nanogels maintained a lower swelling ratio and less negative charge when synthesized at a higher crosslinker concentration. Higher crosslinker concentrations also resulted in lower dispersion viscosity because of the lower volumetric fraction and weaker interparticle attraction. The relationship between viscosity and dispersion concentration is in an agreement with the Krieger-Dougherty model.

Core flooding experiments were conducted under a water-only condition and an oil-water two-phase condition. Nanogels with a lower crosslinker concentration were better able to reduce core permeability. It was discovered that nanogel injection pressure continuously increased in water-saturated porous media, whereas it reached a stable state

in a two-phase condition. Core flooding tests in water-saturated cores also indicated that nanogels with a higher degree of crosslinking adsorbed more onto rock surfaces. The adsorption over time of each test fits well with the pseudo-second order equation. In addition, despite similar interfacial reduction capability, nanogels crosslinked to a lesser degree were able to improve oil recovery to a greater extent.

1. INTRODUCTION

Nanogels, or crosslinked polymeric nanoparticles, hold promise as enhanced oil recovery (EOR) agents. They are capable of reducing interfacial tension (IFT) (1,2) and altering rock wettability (3), owing to their small size and large surface area (4–6). Moreover, nanogels have been proposed as a means of improving reservoir conformance in low permeability reservoirs (7–9).

Various types of nano and submicron-sized crosslinked polymer gels have been developed for EOR purposes and studied on a laboratory scale. Microgel, developed by the Institut Francais du Petrole (IFP), has a particle size ranging from 0.1 to 10 micrometers. Experimental studies have tested the transport and oil displacement capability of this IFP microgel. In water-saturated sandstone cores, it was found that the microgel's plugging efficiency was impacted by permeability, flow rates, concentration, and salinity (10,11). Retention tests also showed that it has a good affinity with rock surfaces (12). In the core-containing oil phase, it can increase oil recovery from 40% to 60% (13). Brightwater® is a swelling rate delayed submicro-sized polymer gel product that can expand in diameter many times when stimulated by reservoir temperature. This

feature makes it easier to inject it deep into a reservoir (14). In contrast to microgel, its injection pressure in core flooding experiments was only slightly higher than that of water flooding. After proper heating, the gel particles swell, which could significantly increase subsequent water flooding pressure due to its plugging effect (9). However, Brightwater® was not able to plug porous media when the permeability was too high (15).

Both microgel and Brightwater® are formed by monomers that include crosslinkers. Crosslinkers transfer polymer to gels with three-dimensional networks via crosslinking (16). Crosslinked polymer gel is more rigid, stable, and supportive of solid structures (17–19). It can be deformed in order to pass through pore throats. The retention of polymer gels decreases permeability and improves the homogeneity of reservoirs (20). Crosslinkers can be classified into inorganic and organic categories. Inorganic crosslinkers rely on the ionic interaction between cations and carboxylate groups. However, they are less stable in some conditions (21). In contrast, the organic crosslinker is more stable and often used in treatments for high-temperature applications (22).

When synthesizing a crosslinked polymer gel, the crosslinker concentration is crucial to the properties of the synthesized polymer gels. An obvious impact of crosslinker concentration on polymer gels is the swelling ratio. With a higher crosslinker concentration, polymer gels tend to swell less in the same solvent because of their smaller chains. Such structures make it more difficult for particles to expand. Gel strength is also affected by crosslinker concentration. Higher crosslinker concentration results in greater strength (23,24).

This study investigated the impacts of crosslinker concentration on nanogel properties, transport, and the improvement of oil recovery. Different HPAM-based nanogels were prepared by suspension polymerization for the work. Characteristics like morphology, size distribution, rheology, and surface charge were studied. Core flooding experiments in water-saturated sandstone cores were carried out to examine the adsorption between nanogels and the rock surface as well as their desorption, retention, and plugging. In addition, the EOR capabilities of each HPAM-based nanogel sample was tested in cores with original oil in place.

2. EXPERIMENTAL MATERIALS AND METHODS

2.1. MATERIALS

The HPAM-based nanogels were synthesized using acrylamide (AM, 71.08 g/mol), acrylic acid (AA, 72.06 g/mol), and the organic crosslinker N,N'-Methylenebisacrylamide (MBAA, 154.17 g/mol). Nanogel components are shown in Table 1, where the crosslinker concentration was calculated based on the molar mass.

All chemicals were purchased from Sigma-Aldrich Corp. (St. Louis, Missouri) and used as received. Four different nanogel samples were prepared using suspension polymerization (2). A typical polymerization procedure is as follows:

AA was first neutralized by NaOH to achieve a pH value of 7. Then, the proper weight of the resulting sodium acrylate along with, AM, DI water, and MBAA were mixed based on the formulation. The solution was added into a three-neck flask with n-decane, Span® 80, and Tween® 60. The flask was kept in a preheated 40 °C water bath

with stirring and nitrogen purging. After 15 minutes, a certain amount of APS (ammonium persulfate) solution was added as the reaction initiator. The reaction was kept for 2 hours. Afterward, the produced mixture was washed using acetone and oven-dried to give a white powder. To prepare the nanogel dispersion, the nanogels were dispersed in brine and would be fully dispersed after stirring and heating.

Table 1. Components of HPAM-based nanogels

Crosslinker Concentration (mol/mol)	AM/g	AA/g	MBAA/mg
0.01 %	10	5	3
0.05 %	10	5	15
0.1 %	10	5	30
1 %	10	5	300

Mineral light oil with a viscosity of 33.5 cP and a density of 0.83 g/ml at room temperature was purchased from Fisher Scientific and deployed in the study. A 1 wt.% sodium chloride (NaCl) solution was used throughout the study as brine.

2.2. NANOGEL CHARACTERIZATION

Nanogel morphology studies: The dry nanogel samples were mounted to a pin stub using carbon tape and sputter-coated with Au-Pd in order to make them conductive. A Hitachi S-4700 Field Emission Scanning Electron Microscope was then used to scan the coated nanogel surface with a focused beam of electrons. The morphology of the dry samples was captured through the scanning electron microscope (SEM) images.

After being dispersed in brine and deionized (DI) water, the hydrodynamic diameters of the swollen nanogels were measured by dynamic light scattering (DLS) with a Malvern ZS90 Nanosizer, resulting in distribution plots. The instrument determines size distributions using the different Brownian motions of particles with different sizes.

Nanogel surface charge studies: The Malvern ZS90 Nanosizer was also used to test the zeta potentials of nanogels by laser doppler micro-electrophoresis (electrophoretic light scattering). The instrument can detect the electrophoretic mobility of nanogels, which is related to their zeta potential. Nanogel zeta potentials were tested in both deionized water and 1% NaCl brine, as well.

Rheological properties: A Brookfield DV3T rheometer with a ULA spindle was used to measure the viscosity of nanogel dispersions from low to high shear rates at room temperature. The viscosities of the nanogel dispersions at different concentrations were measured and compared.

2.3. ADSORPTION BETWEEN NANOGELS AND ROCK SURFACES

Dynamic adsorption tests were conducted to study the adsorption and desorption behaviors of nanogels in sandstone cores. As shown in Table 2, four core samples within sam permeability range were utilized for the study.

The experiment setup is depicted in Figure 1: A syringe pump (No. 2 in the figure) filled with DI water (No. 1) was used to inject brine and the nanogel dispersion from an accumulator (No. 3) into core samples. The core holder (No. 5) could fit a core with a diameter of 2.54 cm and a length of 5 cm. The confining pressure system (No. 6) was set 400 psi above the injection pressure to ensure that injection fluid flowed only

through the porous media. A pressure sensor (No. 4) was connected to the inlet of the core holder to collect the injection pressure data. Test tubes (No. 7) were kept at the outlet to collect effluents. All collected effluents were tested using a Shimadzu UVmini-1240 UV–vis spectrophotometer to determine their concentrations. The measurements were based on the linear relationship between dispersion concentrations and the absorbance detected by the instrument. Based on effluent concentrations, the weight of the nanogels being adsorbed, desorbed, and retained was calculated.

Table 2. Properties of cores for adsorption core flooding study

Core ID	Length, cm	Diameter, cm	Permeability, mD	Pore Volume, mL	Crosslinker Concentration
1	5	2.51	104.02	4.91	0.01%
2			119.83	4.89	0.05%
3			124.91	5.16	0.10%
4			146.07	5.17	1%

During each test, a core was first saturated with brine. The pore volume and porosity was calculated. After measuring permeability by brine injection, the nanogel dispersion with a concentration of 1,000 mg/L was injected into the core sample at a flow rate of 0.25 ml/min. The injection was continued until the concentrations of the effluents were stable (that is, reflecting a stable rate of adsorption). Another brine injection was performed following the nanogel injection. A fraction of the adsorbed nanogels was flushed out from the porous media.

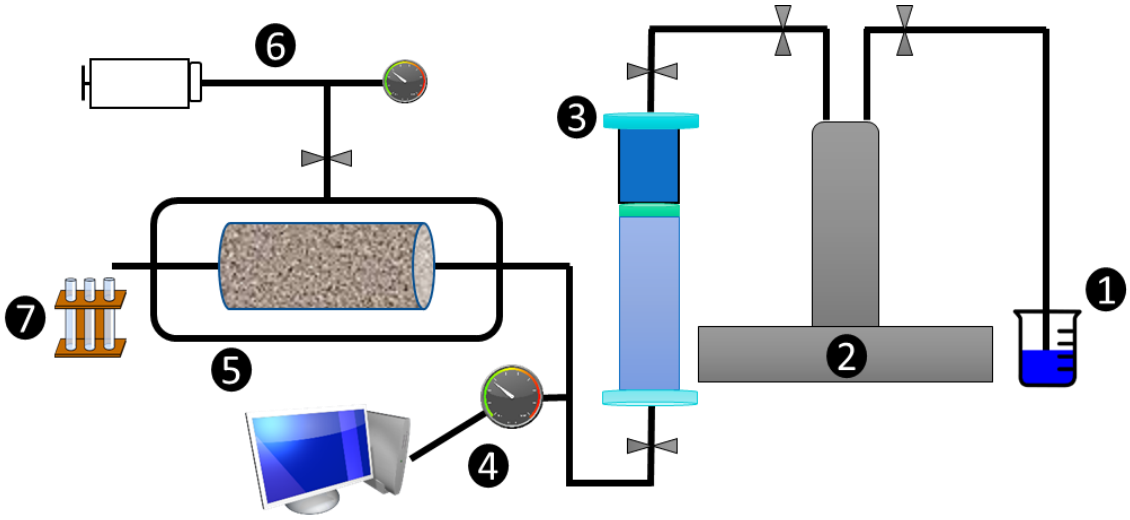

Figure 1. Schematic diagram of the experimental setup

The resistance factor (RF) and residual resistance factor (RRF) was obtained from the injection pressure. The RF reflected the transport performance of the nanogel dispersion, defined as the mobility ratio between the brine and nanogel dispersion. The RRF reflected the nanogel plugging efficiency, defined as the ratio of permeability before and after the nanogel injection. Using the same injection rate, the injection pressure ratio between the nanogel injection and water flooding and the injection pressure ratio between the post-water flooding and water flooding was calculated.

2.4. OIL RECOVERY IMPROVEMENT BY NANOGELS

The interfacial tension between oil and nanogel dispersion: The pendant drop method was deployed to observe the interfacial tension between mineral light oil and 1000 mg/L of the nanogel dispersions. An oil drop in the brine or nanogel dispersion was observed. The oil drop deformed because of the gravity and interfacial tension. The

analysis software was able to obtain the area of the oil drop and calculate the interfacial tension with the Young–Laplace equation.

Core fooding experiments in two-phase condition: Four oil displacement core flooding experiments were conducted to test the oil recovery improvement capability of each HPAM-based nanogel sample. The experimental setup was the same as in the previous adsorption tests (as depicted in Figure 1). Descriptions of the porous media are shown in Table 3.

Table 3. Properties of cores for oil displacement core flooding studies

Core ID	Length, cm	Diameter, cm	Permeability, mD	Pore Volume, mL	OOIP, mL	Crosslinker Concentration
5	8	2.51	134.18	7.84	6.2	0.01%
6			117.33	7.79	6	0.05%
7			145.13	8.11	6.55	0.10%
8			132.48	8	6.6	1%

In contrast to the single-phase core flooding tests, the mineral light oil was injected first to create an oil and water two-phase condition. Brine was injected to simulate water flooding. Afterward, 1,000 mg/L of HPAM-based nanogel dispersion in 1wt.% NaCl brine was injected to improve the homogeneity and oil recovery. Another water flooding was performed to continue improving oil recovery and obtain the residual resistance factors. The flow rate of 0.25 ml/min was set throughout the tests.

3. RESULTS AND DISCUSSIONS

3.1. NANOGEL CHARACTERIZATION

Nanogel size studies: Figure 2 shows dry nanogel samples taken by the scanning electron microscope (SEM). The SEM images show that all dry nanogels in this study are in a similar shape and size, indicating that the crosslinker concentration has little effect on the preswelling nanogel size. In general, the size of the polymer gel is determined by the polarization method, crosslinker type, and another compound during synthesization (23).

Figure 3 shows the swollen nanogels' hydrodynamic diameter measured by dynamic light scattering. The plot suggests that the nanogels swelled less when there was high crosslinker concentration and salinity, due to the pore sizes of the polymeric networks within the nanogel. High crosslinker concentration formed bridges for more polymer chains, leading to smaller pore sizes and less absorption of free water — and consequently, a lower swelling ratio. Moreover, ions in the brine reduced the electrostatic repulsion among polymer chains, also reducing the amount of swelling and resulting in nanogel shrinkage (1). These results align with the Flory-Rehner-Huggins equation, which suggests a negative correlation between the degree of swelling and ionic strength as well as between the degree of swelling and crosslinking density (7,25):

$$Q^{\frac{5}{3}} = \frac{\left(\frac{i}{2V_u S^{\frac{1}{2}}}\right)^2 + (\frac{1}{2} - x_1)/V_1}{V_E/V_0}$$

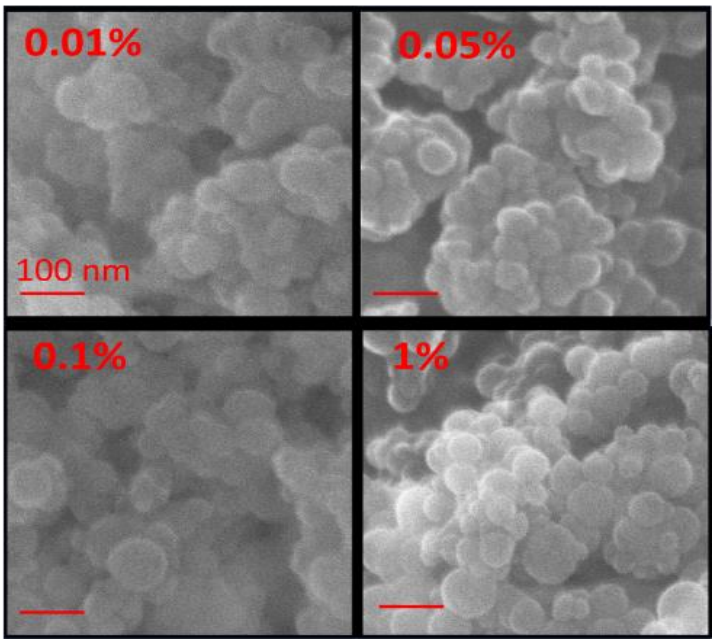

Figure 2. SEM images of dry nanogels, with scale bar 100 nm long
(1: 0.01%; 2: 0.05%; 3: 0.1%; 4: 1%)

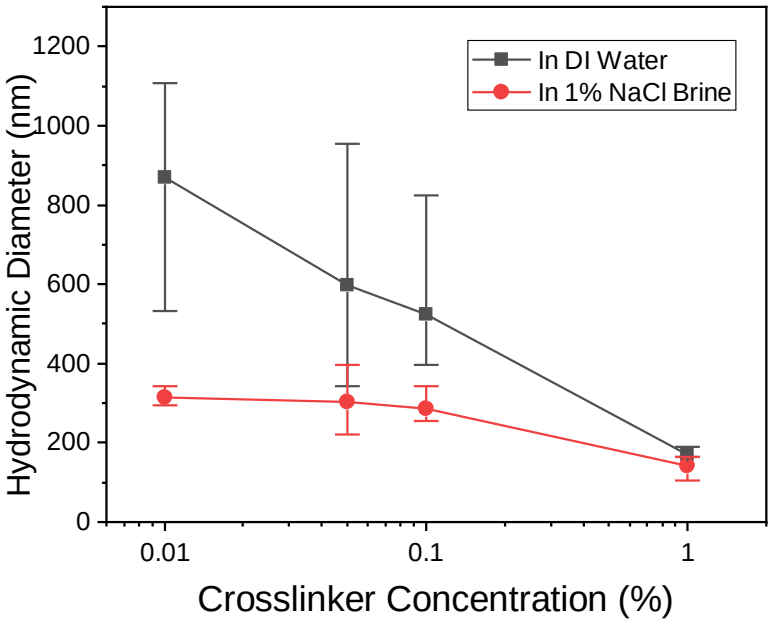

Figure 3. Hydrodynamic diameters of nanogels in DI water and brine

where Q is the degree of swelling, i/V_u is the charge density of the polymer, S is the ionic strength, $(1/2-x_1)/v_1$ is polymer-solvent affinity, and V_e/V_0 is crosslinking density.

Nanogel surface charge studies: Figure 4 shows the zeta potentials of nanogels swelled in DI water and brine. The nanogels had less negative charges in brine because ions tend to compress nanogels and reduce diffusion layer thickness (26). The plots also reveal that nanogels synthesized with a higher crosslinker concentration showed slightly less negative surface charge. Although the crosslinker is nonionic, the percentage of acrylic acid, which is anionic, would be lower with a higher crosslinker concentration. Thus, the percentage of anionic monomer content is lower in high crosslinked nanogels.

Rheological properties: The viscosities of nanogel dispersions were measured at room temperature in 1 wt% NaCl brine. As illustrated in Figure 5, each nanogel sample was tested with concentrations ranging from high to low. Some data were not recorded due to high or low torques. As the plots indicate, the viscosity changed with the shear rate when it was lower than 50 1/s. When the shear rate was higher than 50 1/s, the dispersion viscosity became relatively stable with an increasing shear rate, which indicates that the interparticle structure had been broken at this shear rate (3). The viscosity of the dispersions was clearly affected by crosslinker concentration. HPAM-based nanogel dispersions with lower crosslinker concentration were more viscous. Low crosslinker concentration led to larger swollen particles and higher volume fraction, which caused higher viscosity (27–29).

The viscosity at the shear rate of 70 1/s is summarized and displayed in Figure 6. For the 0.01% crosslinker concentration nanogel, the viscosities of the two highest dispersion concentrations were not recorded due to the high torque. Viscosities measured

at the closest shear rate were selected for the data demonstration. This shear rate was selected for comparison because viscosity varied less with the shear rate at 70 1/s. In addition, for further core flooding tests, the equivalent shear rate of the experimental condition is close to 70 1/s. The calculation is based on the following equation (30):

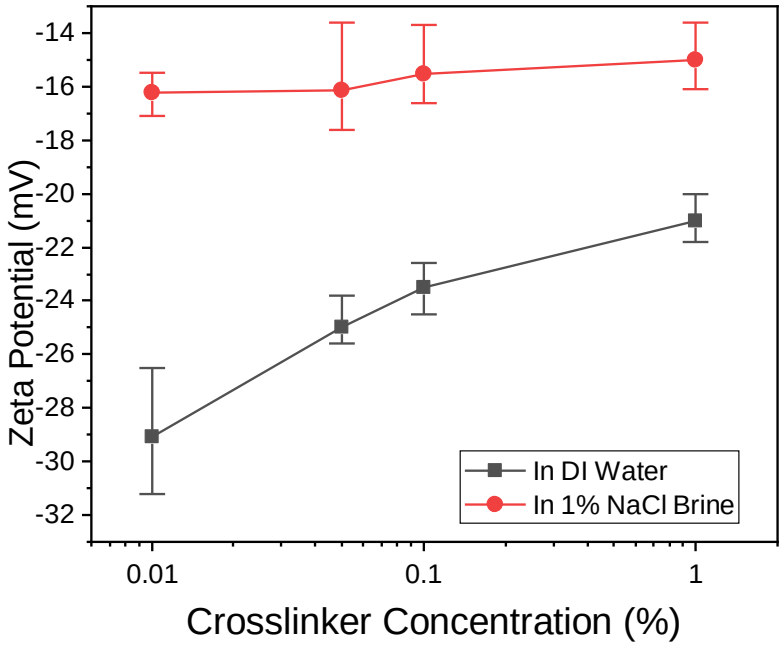

Figure 4. Zeta potential of nanogels in DI water and brine

$$\dot{\gamma}_{eq} = 4v\left(\frac{\emptyset}{8k}\right)^{1/2} = \frac{4q}{A\sqrt{8k\phi}}$$

where A is area, q is flow rate, and k and Φ are permeability and porosity. The porous media for experiments were on average 125 mD in permeability and 20% in porosity. As Figure 6(A) indicates, at lower crosslinker concentration, the relationship between viscosity and dispersion concentration is exponential. However, at higher crosslinker

concentration, the relationship is close to linear. Likewise, as shown in Figure 6 (B), the relationship between particle volume and viscosity is close to exponential and linear at high and low dispersion concentration, respectively. The Krieger-Dougherty model is often used for nanofluid viscosity prediction (29). The equation is:

$$\frac{\eta}{\eta o} = (1 - \frac{\Phi}{\Phi m})^{[\eta]\Phi m}$$

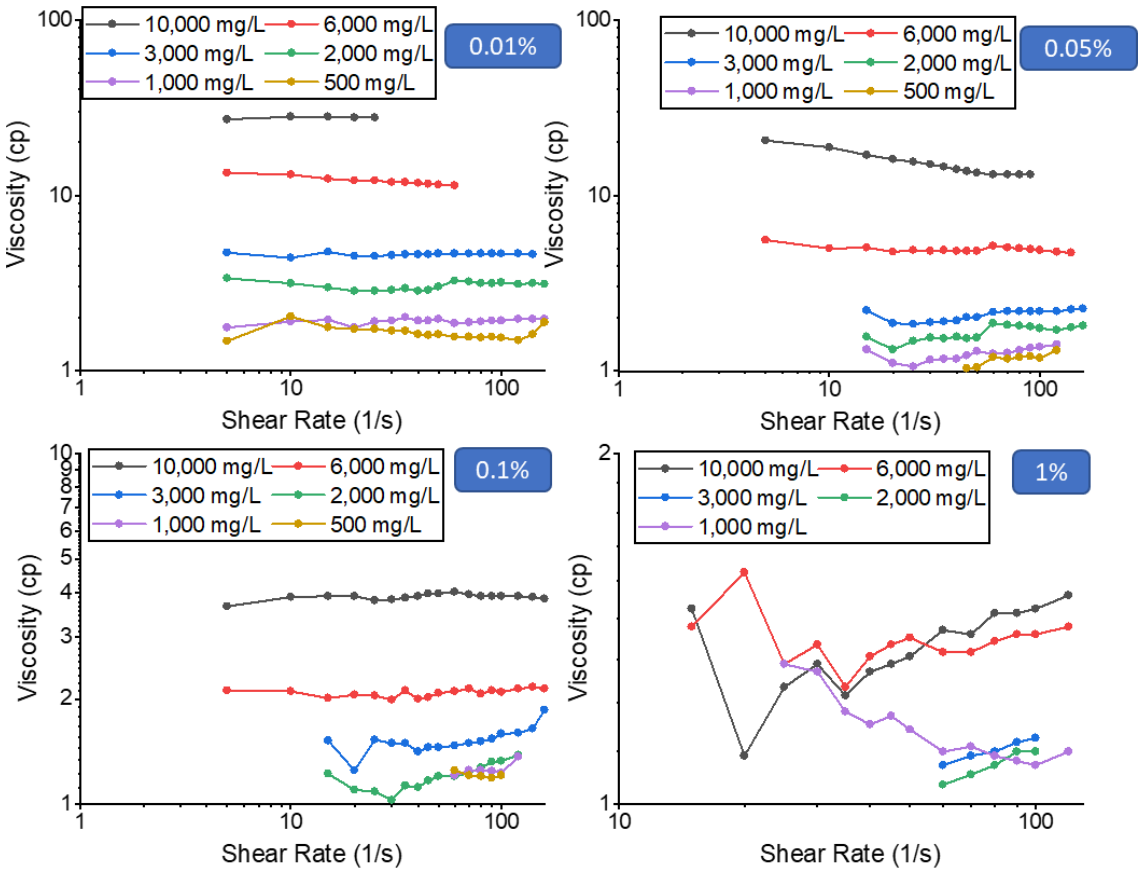

Figure 5. Nanogel dispersion at different shear rates

where [η] is the intrinsic viscosity, Φ is the volume concentration of particles, Φ_m is the maximum packing, η is the viscosity of the suspension, and η_o is the viscosity of the

medium. [η] and Φ_m of sphere dispersions are 2.5 and 0.74. The η_o is 1.077 cp for 1 wt% NaCl brine. A typical Krieger-Dougherty curve for a sphere dispersion is shown in Figure 6 (C). The plot transforms from a linear-like curve to an exponential curve with the increasing volumetric fraction. This is due to the increasing interaction among particles and multiparticle collisions at higher volumetric fraction (31).

Both the dispersion concentration and the swollen nanogel volume are proportional to the volumetric fraction. Hence, at high crosslinker concentration (low swelling ratio) or low dispersion concentration, the curves in Figure 6 (A) and (B) are close to linear because of the low volumetric fraction. In the opposite conditions, the curves appear to be exponential because of the high volumetric fraction. The relationship between viscosity and crosslinker concentration at 1,000 mg/L (the concentration for the core flooding tests) is specifically illustrated in Figure 6 (D).

3.2. ADSORPTION OF NANOGELS ON ROCK SURFACES

Each of the four nanogel dispersions was injected into cores within the same permeability range (100 – 150 mD), followed by brine flooding. During nanogel flooding, nanogels can be adsorbed onto rock surfaces with increasing injection pressure. Brine injection was performed after each nanogel flooding and the desorption process was observed. Figure 7 illustrate the injection pressure and effluent concentration of each experiment during nanogel flooding and brine re-injection, respectively. Resistance factors after 50 pore volume (PV) of injection, adsorption, desorption, and retention data are summarized in Figure 9.

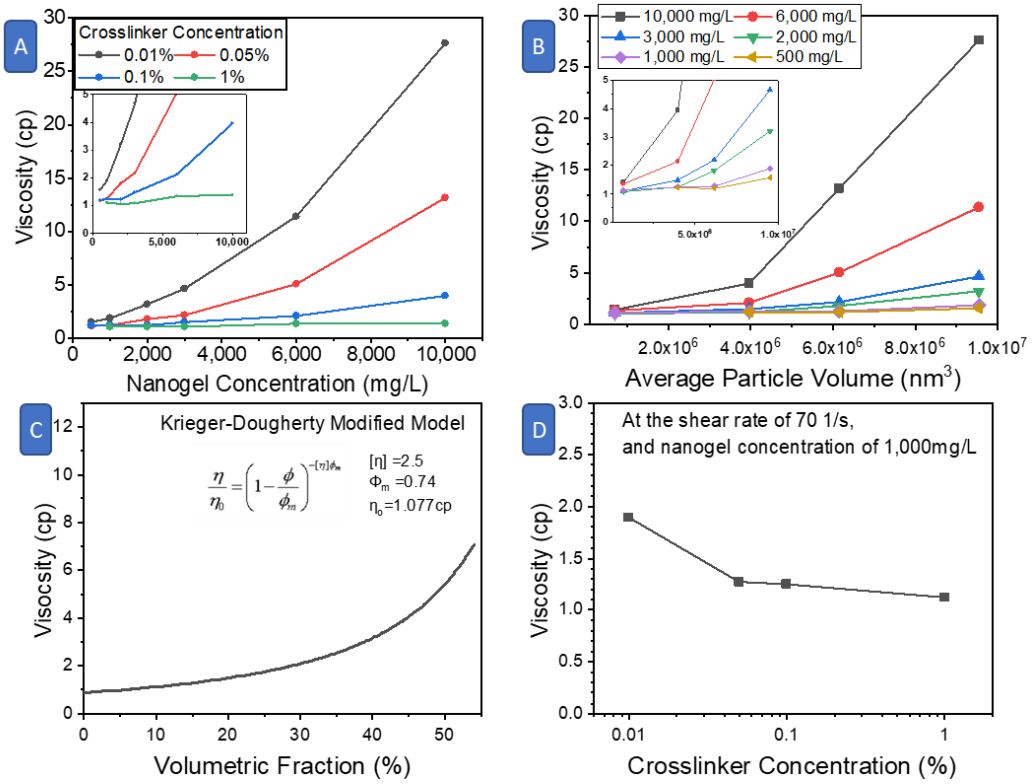

Figure 6. Dispersion viscosity at 70 1/s
a) Impacts of nanogel concentration b) Impacts of nanogel volume
c) Krieger-Dougherty model d) Impacts of crosslinker concentration at 1,000 mg/L

As shown in Figure 7, due to the complexity of the porous media structures, the logjam effect was observed as the injection pressure was continuously increased with an unsmooth pressure curve. The increasing injection pressures might be caused by desorbed nanogel agglomerates (3). At the late stage of nanogel injections, the adsorbing rate of nanogel onto the rock surface is close to their desorbing rate, which means an equilibrium state of the adsorption of nanogel onto rock surfaces. The desorbed nanogel agglomerates were associated with the interpenetrated polymer chains around nanogels and maintain their integrity when they were detached from rock surfaces. These agglomerates can block pore throats due to their large size and result in increasing injection pressure.

Meanwhile, nanogel with higher degree of crosslinking is more hard and rigid. Therefore, more noticeable fluctuation would be observed when the particles transport through pore throats.

At the same injection volume, nanogels with lower crosslinker concentration plugged the core more than the ones with higher crosslinker concentration. Since a higher crosslinker concentration leads to a lower swelling ratio of nanogel and thus the swelling nanogel has higher strength. Therefore, the pressure drop is the competition of gel strength and swelling nanogel size. With the specific nanogel recipe and rocks, the nanogels with higher degree of crosslinking have better injectivity, indicating the particle size dominants the transport behavior. The results also showed that nanogels with higher crosslinker concentration has less plugging efficiency, indicating the swollen nanogel size had more impact on the plugging efficiency compared to nanogel strength. The higher dispersion viscosity at a low crosslinker concentration also contributed to higher nanogel injection pressure as defined by Darcy's law. Meanwhile, the interaction among less crosslinked nanogels was stronger since their dispersions were more viscous. Hence, the blocking of nanogels was less possible to break.

For all four tests, the effluent concentration was below injection concentration at some points, which indicates the adsorption of nanogels on to rock surfaces. As demonstrated in Figure 7, low effluent concentration was observed during the first two PV of injection. Relatively large numbers of nanogels started being recovered at the outlet after two PVs of injection. The effluent plots reveal the fast adsorption between nanogels and porous media at the beginning of nanogel flooding and slower adsorption in the later injection stage.

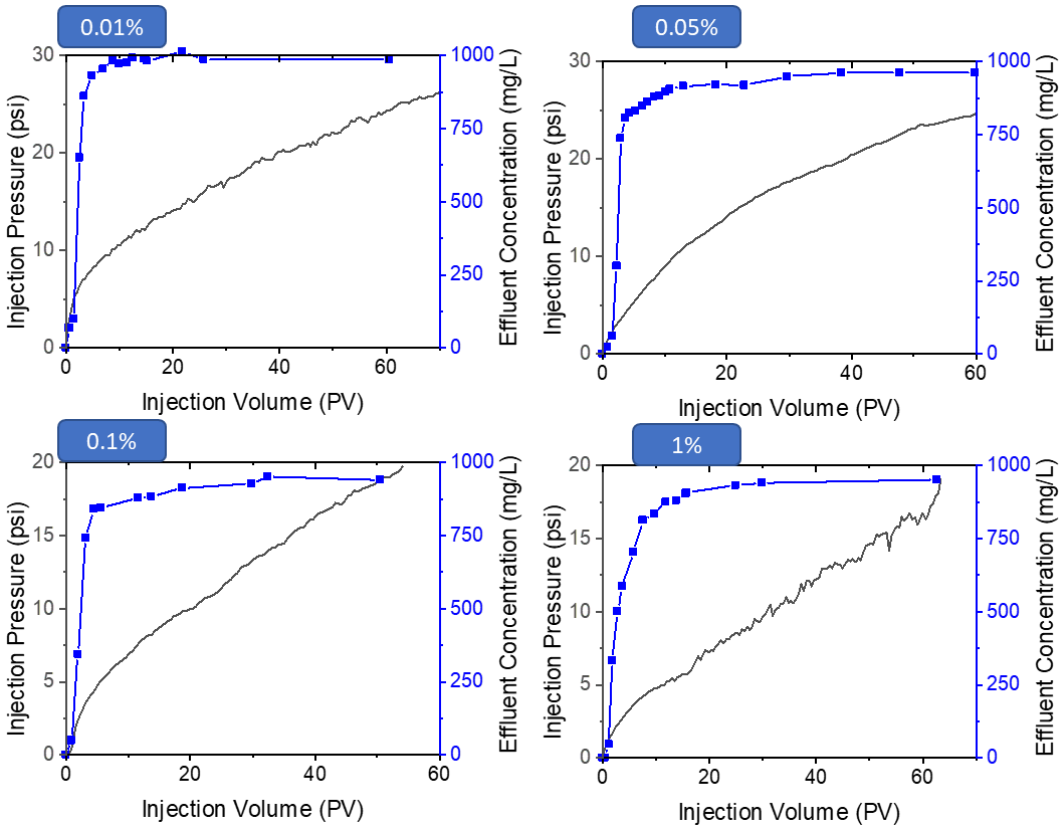

Figure 7. Injection pressure and effluent concentration during nanogel injection (adsorption)

The effluent concentrations became stable after 10 PV of injection during each test. However, the effluent concentration was closer to injection concentration when the nanogels were less crosslinked. That is, less high-crosslinked nanogels were adsorbed and vice versa.

The data can also be fitted into the pseudo-second-order kinetic equation proposed by Ho (32,33):

$$\frac{t}{q_t} = \frac{1}{q_e}t + \frac{1}{kq_e^2}$$

where q_t represents the adsorption at any moment during tests(mg/g), q_e represents the adsorption at equilibrium (mg/g), k represents adsorption rate constant (g/mg/min), and t is time (min). The plots of t/q_t versus time are displayed in Figure 8. The fitting parameters were calculated and listed in Table 4. q_e and k are calculated from the slopes and interceptions of fit lines. The equilibrize adsorption for nanogel with 0.01% crosslinker concentration was 0.26 mg/g. It rose with higher crosslinker concentrations and became 0.84 mg/g at 1%. This result is in an agreement with the experiment results. The adsorption rate constant decreased with higher crosslinker concentration. Nanogels with lower crosslinker concentrations were adsorbed onto the rock surface at a much higher rate, which further led to lower total adsorption.

Van der Waals force is one of the factors associated adsorption (3). It is calculated as the equation (34):

$$\emptyset_v = -\frac{A_H}{6}\left[\frac{a}{D} + \frac{a}{D+2a} + ln\left(\frac{D}{D+2a}\right)\right]$$

with AH representing the Hamaker constant, a representing the particle radius, and D representing the distance between the objects. In general, van der Waals force increases with higher particle sizes and smaller distances. Even though less crosslinked nanogels are larger in size and would result in greater van der Waals forces, less adsorption weight would be needed for the same thickness of the layer compared to high-crosslinked nanogels. As the layer thickness increased with adsorption, the distance between newly adsorbed nanogels and the rock increased. The larger distance weakened the van der Waals force between the rock and nanogels. Meanwhile, the thickness of the adsorbed layers during multilayer adsorption was positively correlated to the resistance factor (35).

As shown in Figure 9, resistance factors were lower with higher crosslinker concentration, showing the lower layer thickness.

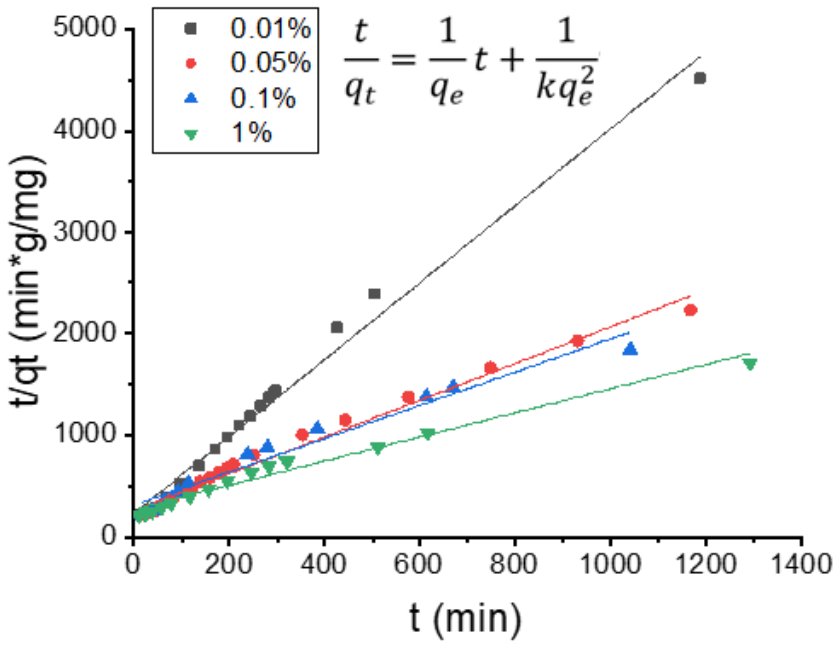

Figure 8. Pseudo-second order kinetics model for nanogel adsorption

Table 4. Parameters for the fitting of the pseudo-second order kinetics model

Crosslinker concentration	0.01%	0.05%	0.10%	1%
q_e (mg/g)	0.264	0.553	0.611	0.842
k (g/mg/min)	0.0619	0.0125	0.0085	0.0052
Slope	3.79	1.81	1.64	1.19
Interception	231.64	261.00	314.48	273.27
R-Square	0.988	0.985	0.963	0.972

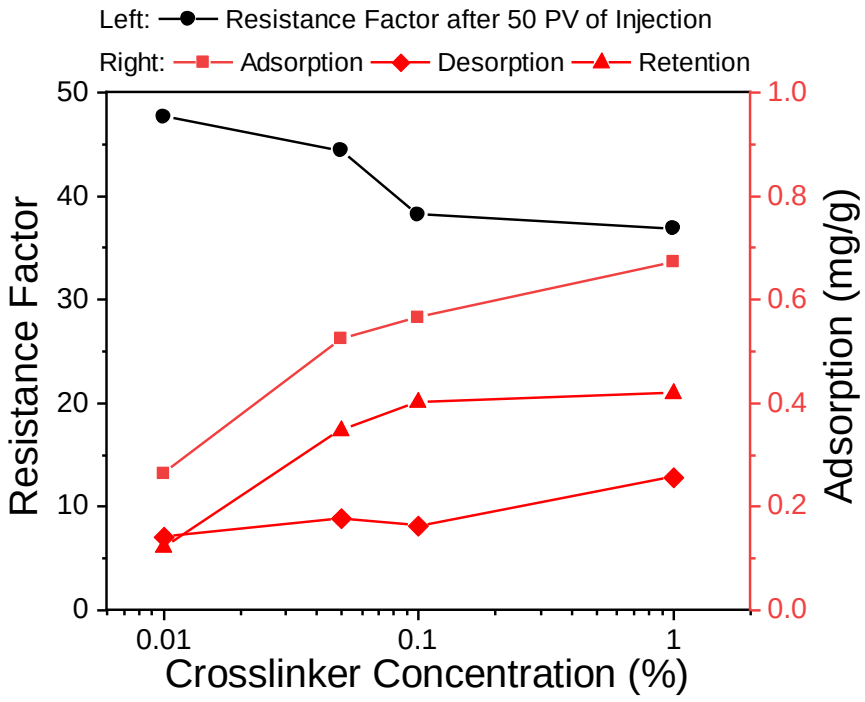

Figure 9. Impacts of crosslinker concentration on resistance factors, adsorption, desorption, and retention

Other than adsorption caused by Van der Waals force, during nanogel injection, they could also be retained due to settlement and trapping. The settlement of nanogel is also caused the gravity. However, it is unlikely to cause the difference of adsorption among all nanogels. In addition, nanogel could be trapped in pore throats, which leads to adsorption as well. Meanwhile, high-crosslinked nanogels have better injectivity as injection pressure plots indicate. Therefore, they can more easily enter more channels with lower permeability, which could contribute to higher adsorptions. As the surface charge study indicated, high-crosslinked nanogels also have less negative surface charges. Since Berea sandstone in NaCl brine has a negative zeta potential (36), nanogels with less negative charges tend to be adsorbed more on to the rock surface due to the weaker electrostatic repulsion between rock surfaces and nanogels (3,37).

At the start of the post-water flooding, as shown in Figure 10, the pressure increased immediately to the value when the nanogel flooding stopped. Then it decreased slightly before maintaining a stable pressure. The effluent concentrations were around 1000 mg/L at the start, representing the nanogels being flushed out. The concentration then decreased rapidly to negligible values. The flushed-out nanogels could have been the result of both desorption and the breakage of the blocking of nanogels. Overall, as shown in Figure 9 and Figure 10, crosslinker concentration showed a negligible impact on the desorption of nanogels.

3.3. IMPROVING OIL RECOVERY IN POROUS MEDIA

The interfacial tension between oil and nanogel dispersion: Nanogels reduce IFT because of the adsorption onto the contact surface between fluids (38). As shown in Figure 11, the interfacial tension between oil (mineral light oil) and brine was between 45 and 50 dynes/cm without any treatments. In nanogel dispersions, the IFT could be reduced to below 10 dynes/cm after one hour. The IFT was reduced similarly during each test, as shown in the figure. The results show the nanogel's ability to reduce IFT. However, it is relatively independent of the crosslinker concentration.

Oil recovery improvement in porous media: The prospect of oil recovery improvement through the use of nanogels was investigated by core flooding experiments in a two-phase condition. The injection pressure and oil recovery factor during water flooding, nanogel flooding, and post-water flooding stages are displayed in Figure 12. Blue plots represent the injection pressure. As shown in the plots, during water flooding, injection pressure at first increased before decreasing to a stable value. This is due to the

decreasing oil saturation as oil was displaced by the injected brine. Subsequently, the relative permeability to the water phase became higher. If the absolute permeability were to remain the same, the effective permeability to the water phase would accordingly be higher. Thus, the injection pressure tended to decrease.

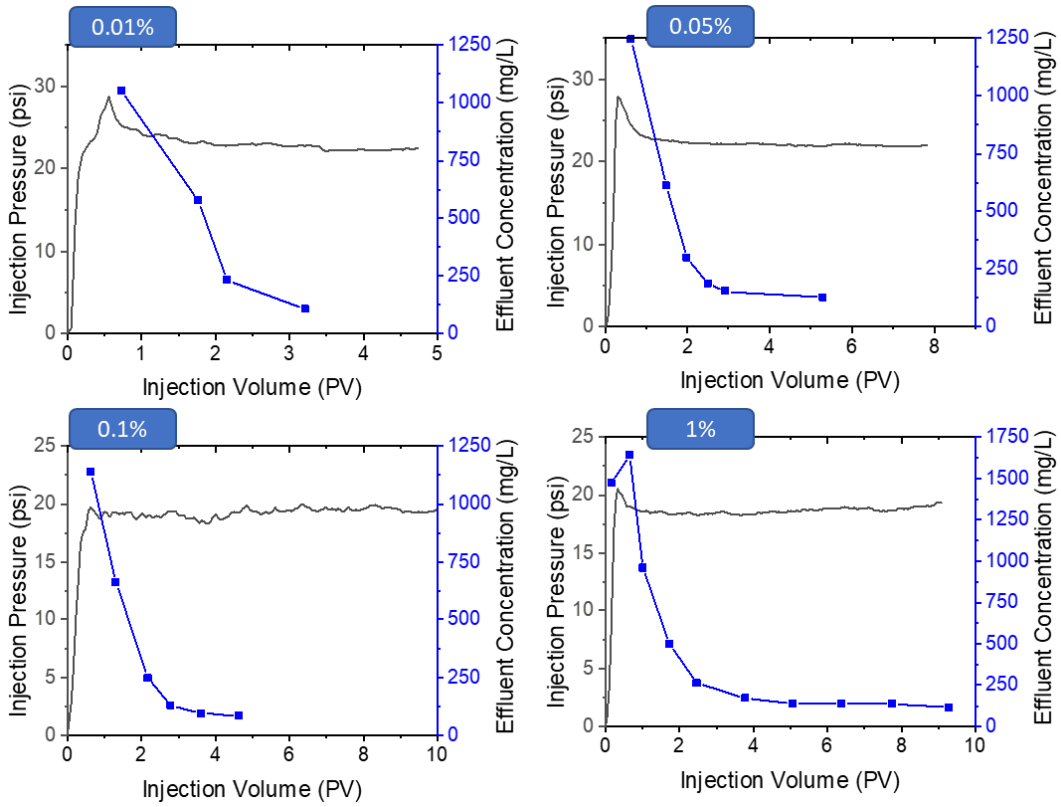

Figure 10. Injection pressure and effluent concentration during and following brine injection (desorption)

Similar trends were observed during nanogel flooding and post-water flooding, as well. Increasing water saturation and relative permeability to water were still responsible for the phenomenon, as oil was continuously being displaced. However, during nanogel flooding, the pressure drop was also caused by the viscoelasticity of nanogels. That

property allows nanogels to be deformed during transport through the porous media. As the “1%” nanogel (lowest swelling ratio) injection pressure plot reveals, with a larger difference between pore throat size and nanogel size, the injection pressure was more stable. Meanwhile, higher crosslinker concentration led to more rigid nanogels and less deformation. But for the nanogels with a higher swelling ratio, the pressure dropped greatly after reaching its highest values with the release of energy from the deformation.

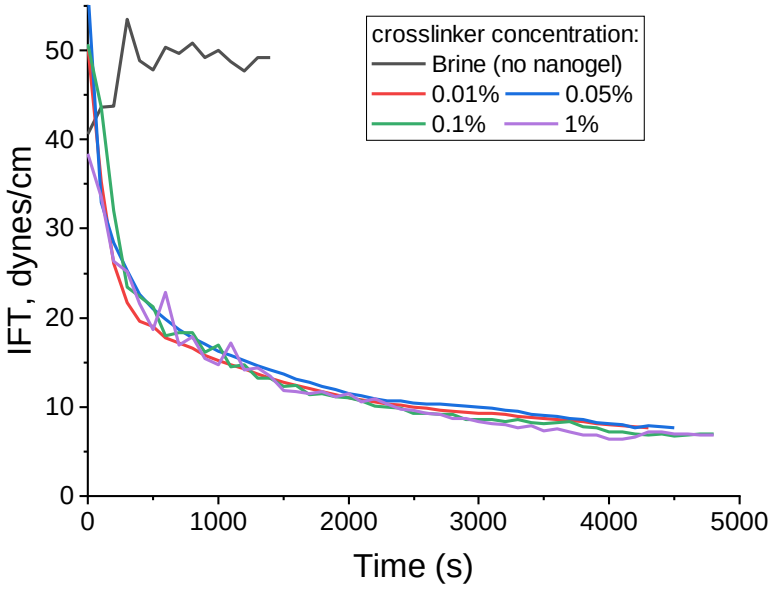

Figure 11. Interfacial tension reduction by nanogels

Compared to nanogel injection pressure in water-saturated cores, the differential pressure of nanogel flooding was stabilized at the end of the injection with much lower resistance factors. This is a very interesting result, which could have been caused by reduced adsorption between nanogels and porous media when residual oil was present. More permeability reduction could been caused by mechanical plugging (3,39).

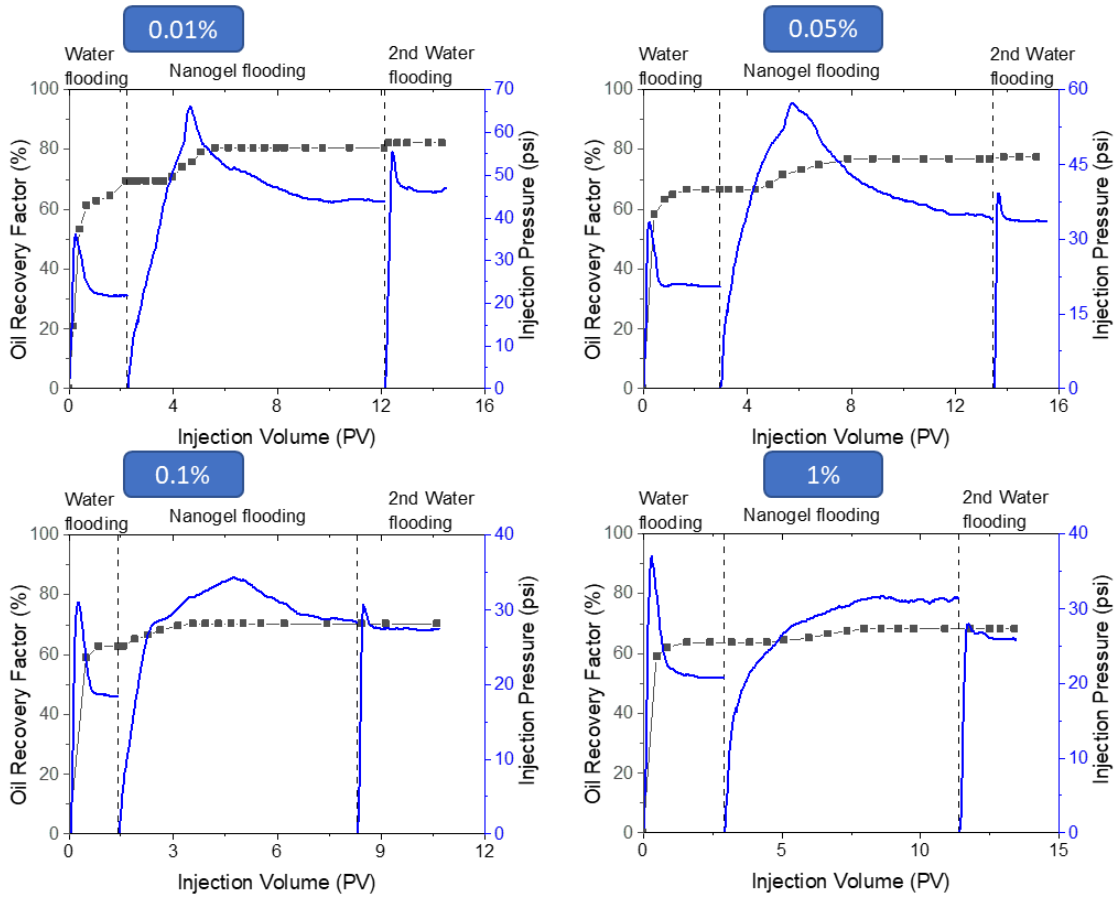

Figure 12. Injection pressure and oil recovery of each oil displacement test

The injection pressure plots reveal that low-crosslinked nanogels blocked porous media more than the highly crosslinked nanogels. The stabilized water flooding pressures were around 20 psi during all tests. When the least crosslinked nanogel sample (0.01%) was being injected, the nanogel flooding was able to increase injection pressure up to 65 psi and stabilize at 44 psi. During the subsequent water flooding, the injection pressure was still higher than 45 psi. However, when the most crosslinked sample was being injected, the pressure was only around 30 psi.

The resistance factors and residual resistance factors of each test were epitomized in Figure 13. Both RF and RRF decreased from 2 to 1.2 with an increase in crosslinker

concentration. The results are consistent with the previous adsorption study: Larger nanogel size and higher viscosity led to higher plugging efficiency.

Meanwhile, as shown in Figure 12, the initial oil recovery factors of all three tests were between 60% and 70%. Nanogel flooding and the post-water flooding successfully improved oil recovery further. Most of the incremental oil recovery was from the nanogel flooding stage; less was from the subsequent water flooding. When the crosslinker concentration was the lowest (0.01%), the nanogel flooding was able to improve oil recovery from 69.35% to 82.26%. When crosslinker concentration was 1%, the treatment only increased oil recovery from 63.64% to 68.18%.

As summarized in Figure 13, incremental oil recovery decreased with crosslinker concentration. When crosslinker concentration was low, the nanogels generated higher plugging efficiencies. Subsequently, due to the microscale heterogeneity of the cores, there was higher incremental oil recovery as a result of better conformance control. Also considering the higher dispersion viscosity of nanogels with low crosslinker concentration, the more favorable mobility ratio contributed to the change, as well. On the other hand, as previously demonstrated, each nanogel sample similarly reduced interfacial tension. The cores deployed for core flooding tests were strong water-wet with a contact angle of only 25 degrees. Even if crosslinker concentration could affect the wettability alteration caused by nanogels, the difference is unlikely to be influential. Consequently, the difference in oil recovery improvement due to nanogels was primarily caused by alterations in plugging efficiency and viscosity.

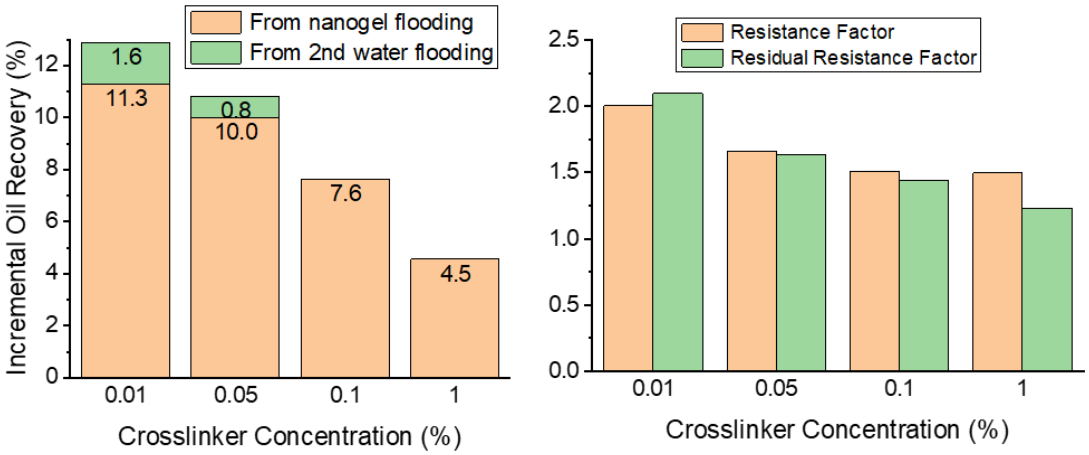

Figure 13. Incremental oil recovery and plugging capability of different nanogels

4. CONCLUSIONS

In this work, four HPAM-based nanogel samples were synthesized in order to study the impacts of crosslinker concentration. The following conclusions are drawn from the results.

- The difference among dry nanogels was not noticeable based on their SEM images. In dispersion, nanogels synthesized with a higher crosslinker concentration had a lower swelling ratio and surface charge.
- As a result of the different volumetric fraction, the viscosity of high-crosslinked nanogel dispersion was lower.
- Nanogels synthesized with a higher crosslinker concentration were found to be more adsorbed on to rock surfaces. The adsorption volume over time was in accord with the Ho pseudo-second order equation.
- Low-crosslinked nanogels were more capable of plugging porous media.

- Nanogels synthesized with a lower crosslinker concentration resulted in higher oil recovery improvement.

REFERENCES

1. Geng J, Han P, Bai B. Experimental Study on Charged Nanogels for Interfacial Tension Reduction and Emulsion Stabilization at Various Salinities and Oil Types [Internet]. SPE Asia Pacific Oil and Gas Conference and Exhibition. Brisbane, Australia: Society of Petroleum Engineers; 2018. p. 13. Available from: https://doi.org/10.2118/192118-MS

2. Geng J, Pu J, Wang L, Bai B. Surface charge effect of nanogel on emulsification of oil in water for fossil energy recovery. Fuel [Internet]. 2018;223:140–8. Available from: http://www.sciencedirect.com/science/article/pii/S0016236118304526

3. Geng J, Ding H, Han P, Wu Y, Bai B. Transportation and Potential Enhanced Oil Recovery Mechanisms of Nanogels in Sandstone. Energy & Fuels [Internet]. 2018 Aug 16;32(8):8358–65. Available from: https://doi.org/10.1021/acs.energyfuels.8b01873

4. Chaudhury MK. Spread the word about nanofluids. Nature [Internet]. 2003 May 8;423:131. Available from: https://doi.org/10.1038/423131a

5. Al-Muntasheri GA, Liang F, Hull KL. Nanoparticle-Enhanced Hydraulic-Fracturing Fluids: A Review. SPE Prod Oper [Internet]. 2017;32(02):186–95. Available from: https://doi.org/10.2118/185161-PA

6. Ding H, Zhang N, Zhang Y, Wei M, Bai B. Experimental Data Analysis of Nanoparticles for Enhanced Oil Recovery. Ind Eng Chem Res [Internet]. 2019 Jul 10;58(27):12438–50. Available from: https://doi.org/10.1021/acs.iecr.9b02132

7. Han P, Geng J, Bai B. Investigation on transport behavior of nanogel in low permeable porous medium. J Pet Sci Eng [Internet]. 2019;178:999–1005. Available from: http://www.sciencedirect.com/science/article/pii/S0920410519303560

8. Almohsin A, Ding H, Bai B. Experimental Study on the Transport and Improved Oil Recovery Mechanism of Submicron Particle Gel [Internet]. SPE EOR Conference at Oil and Gas West Asia. Muscat, Oman: Society of Petroleum Engineers; 2018. p. 14. Available from: https://doi.org/10.2118/190364-MS

9. Salehi M, Thomas CP, Kevwitch R, Garmeh G, Manrique EJ, Izadi M. Performance evaluation of thermally-activated polymers for conformance correction Applications. In: SPE Improved Oil Recovery Symposium. Society of Petroleum Engineers; 2012.

10. Almohsin AM, Bai B, Imqam AH, Wei M, Kang W, Delshad M, et al. Transport of nanogel through porous media and its resistance to water flow. In: SPE Improved Oil Recovery Symposium. Society of Petroleum Engineers; 2014.

11. Dupuis G, Bouillot J, Templier A, Zaitoun A. Successful Chemical Water Shut-Off Treatment in an Omani Field Heavy-Oil Well. In: Abu Dhabi International Petroleum Exhibition and Conference. Society of Petroleum Engineers; 2015.

12. Dupuis G, Lesuffleur T, Desbois M, Bouillot J, Zaitoun A. Water conformance treatment using SMG microgels: a successful field case. In: SPE EOR Conference at Oil and Gas West Asia. Society of Petroleum Engineers; 2016.

13. Goudarzi A, Almohsin A, Varavei A, Delshad M, Bai B, Sepehrnoori K. New experiments and models for conformance control microgels. In: SPE Improved Oil Recovery Symposium. Society of Petroleum Engineers; 2014.

14. Roussennac BD, Toschi C. Brightwater trial in Salema Field (Campos Basin, Brazil). In: SPE EUROPEC/EAGE annual conference and exhibition. Society of Petroleum Engineers; 2010.

15. Fabbri C, Klimenko A, Jouenne S, Cordelier P, Morel D. Laboratory and Simulation Investigation of the Effect of Thermally Activated Polymer on Permeability Reduction in Highly Permeable Unconsolidated Sand. In: SPE Asia Pacific Enhanced Oil Recovery Conference. Society of Petroleum Engineers; 2015.

16. Geng J. Synthesis of different sizes & functions nanoparticles. 2015;

17. Hamed GR. Materials and Compounds. In: Gent ANBT-E with R, editor. Hanser; 2012. p. 11–36. Available from: http://www.sciencedirect.com/science/article/pii/B9783446427648500235

18. Moore JW, Shorb JM, Storer D, Carter D, Smith L, Schwehm J. ChemPRIME/ChemPaths: Using an online resource for chemistry teaching. In: ABSTRACTS OF PAPERS OF THE AMERICAN CHEMICAL SOCIETY. AMER CHEMICAL SOC 1155 16TH ST, NW, WASHINGTON, DC 20036 USA; 2012.

19. Cole RC, Ali SA, Foley KA. A New Environmentally Safe Crosslinked Polymer for Fluid-Loss Control [Internet]. SPE Production Operations Symposium. Oklahoma City, Oklahoma: Society of Petroleum Engineers; 1995. p. 11. Available from: https://doi.org/10.2118/29525-MS

20. Bai B, Li L, Liu Y, Liu H, Wang Z, You C. Preformed Particle Gel for Conformance Control: Factors Affecting Its Properties and Applications. SPE Reserv Eval Eng [Internet]. 2007;10(04):415–22. Available from: https://doi.org/10.2118/89389-PA

21. Al-Muntasheri GA, Nasr-El-Din HA, Al-Noaimi K, Zitha PLJ. A Study of Polyacrylamide-Based Gels Crosslinked With Polyethyleneimine. SPE J [Internet]. 2009;14(02):245–51. Available from: https://doi.org/10.2118/105925-PA

22. Al-Muntasheri GA, Zitha PLJ, Nasr-El-Din HA. A New Organic Gel System for Water Control: a Computed Tomography Study. SPE J [Internet]. 2010;15(01):197–207. Available from: https://doi.org/10.2118/129659-PA

23. Mane S, Ponrathnam S, Chavan N. Effect of chemical cross-linking on properties of polymer microbeads: A review. Can Chem Trans. 2015;3(4):473–85.

24. Long Y, Wang Z, Ding H, Geng J, Bai B. Investigation and Characterization of a Robust Nanocomposite Preformed Particle Gel for Enhanced Oil Recovery. Energy & Fuels [Internet]. 2019 Jun 20;33(6):5055–66. Available from: https://doi.org/10.1021/acs.energyfuels.9b00778

25. Flory PJ. Principles of polymer chemistry. Cornell University Press; 1953.

26. Chen L, Zhang G, Wang L, Wu W, Ge J. Zeta potential of limestone in a large range of salinity. Colloids Surfaces A Physicochem Eng Asp [Internet]. 2014;450:1–8. Available from: http://www.sciencedirect.com/science/article/pii/S0927775714002283

27. Toda K, Furuse H. Extension of Einstein's viscosity equation to that for concentrated dispersions of solutes and particles. J Biosci Bioeng [Internet]. 2006;102(6):524–8. Available from: http://www.sciencedirect.com/science/article/pii/S1389172307700063

28. Masoumi N, Sohrabi N, Behzadmehr A. A new model for calculating the effective viscosity of nanofluids. J Phys D Appl Phys [Internet]. 2009;42(5):55501. Available from: http://dx.doi.org/10.1088/0022-3727/42/5/055501

29. Krieger IM, Dougherty TJ. A mechanism for non‐Newtonian flow in suspensions of rigid spheres. Trans Soc Rheol. 1959;3(1):137–52.

30. Zitha P, Chauveteau G, Zaitoun A. Permeability~Dependent Propagation of Polyacrylamides Under Near-Wellbore Flow Conditions [Internet]. SPE International Symposium on Oilfield Chemistry. San Antonio, Texas: Society of Petroleum Engineers; 1995. p. 16. Available from: https://doi.org/10.2118/28955-MS

31. Deepak Selvakumar R, Dhinakaran S. Effective viscosity of nanofluids — A modified Krieger–Dougherty model based on particle size distribution (PSD) analysis. J Mol Liq [Internet]. 2017;225:20–7. Available from: http://www.sciencedirect.com/science/article/pii/S0167732216327350

32. Ho Y-S. Review of second-order models for adsorption systems. J Hazard Mater [Internet]. 2006;136(3):681–9. Available from: http://www.sciencedirect.com/science/article/pii/S0304389406000021

33. Ho YS, McKay G. Pseudo-second order model for sorption processes. Process Biochem [Internet]. 1999;34(5):451–65. Available from: http://www.sciencedirect.com/science/article/pii/S0032959298001125

34. Dunphy Guzman KA, Finnegan MP, Banfield JF. Influence of Surface Potential on Aggregation and Transport of Titania Nanoparticles. Environ Sci Technol [Internet]. 2006 Dec 1;40(24):7688–93. Available from: https://doi.org/10.1021/es060847g

35. Zaitoun A, Kohler N. Two-Phase Flow Through Porous Media: Effect of an Adsorbed Polymer Layer [Internet]. SPE Annual Technical Conference and Exhibition. Houston, Texas: Society of Petroleum Engineers; 1988. p. 14. Available from: https://doi.org/10.2118/18085-MS

36. Shehata AM, Nasr-El-Din HA. Zeta Potential Measurements: Impact of Salinity on Sandstone Minerals [Internet]. SPE International Symposium on Oilfield Chemistry. The Woodlands, Texas, USA: Society of Petroleum Engineers; 2015. p. 17. Available from: https://doi.org/10.2118/173763-MS

37. Patil S, Sandberg A, Heckert E, Self W, Seal S. Protein adsorption and cellular uptake of cerium oxide nanoparticles as a function of zeta potential. Biomaterials [Internet]. 2007;28(31):4600–7. Available from: http://www.sciencedirect.com/science/article/pii/S0142961207005546

38. Agista MN, Guo K, Yu Z. A State-of-the-Art Review of Nanoparticles Application in Petroleum with a Focus on Enhanced Oil Recovery. Appl Sci [Internet]. 2018;8(6). Available from: http://www.mdpi.com/2076-3417/8/6/871

39. Broseta D, Medjahed F, Lecourtier J, Robin M. Polymer Adsorption/Retention in Porous Media: Effects of Core Wettability and Residual Oil. SPE Adv Technol Ser [Internet]. 1995;3(01):103–12. Available from: https://doi.org/10.2118/24149-PA

SECTION

3. CONCLUSIONS AND RECOMMENDATIONS

3.1. CONCLUSIONS

This research has investigated the potential of a polymeric nanogel to improve oil recovery. Firstly, the research has provided a comprehensive review of the nanoparticle researches on a laboratory scale with data analysis techniques. Then, a series of core flooding tests were run to understand the near wellbore transport of nanogel and the effect of injection rate and crosslinker density on the injectivity and EOR potential. The conclusions reached from each paper are summarized as follow:

In Paper I, a dataset consisting of core flooding tests from nanoparticles for EOR laboratory studies was built. Key parameters in six categories were collected and analyzed from a statistical aspect. Parameter distributions revealed the popular (and unpopular) selections of research topics, materials, and approaches, while grouped box plots and scatter plots discovered and proved the connection between different parameters. The analysis shows that on a laboratory scale, nanoparticles can improve oil recovery by an average of 5% of OOIP, while the highest reported oil recovery increment is 30%. IFT reduction and wettability alternation were the major EOR mechanisms investigated by most researchers. The results of IFT and contact angle tests can also indicate incremental oil recovery. Besides, several research topics such as polymeric nanoparticles have not been well investigated. It is necessary to provide an in-depth study

to understand where and how polymeric nanoparticles can be best applied in oilfields to improve oil recovery.

In Paper II, HPAM-based nanogel were studied. The hydrodynamic diameter of nanogel increases with lower salinity since ions reduce the electrostatic repulsion among the polymer chain and cause particle shrinkage. Nanogel dispersion viscosity is higher at lower salinity or higher nanogel concentration, as the volumetric fraction is higher at these conditions. Filtration tests under constant pressure in various conditions were conducted. Furthermore, the results from all tests are well fitted by the intermediate blocking model and standard blocking model. Filtration rates are lower with higher nanogel concentration or lower salinity, which leads to higher resistance factors. The differences are mostly caused by viscosity, which is highly affected by nanogel concentration and salinity. At a higher permeability, the resistance factor would be lower. However, once the permeability exceeded a certain value, the decrease in resistance factor became less obvious. Meanwhile, the driven pressure has little impact on the transport of nanogel as the resistance factor changes little with different driven pressures.

In Paper III, core flooding tests were conducted to study how flow rate affects nanogel flooding. First and foremost, nanogel dispersion showed shear-thinning behavior under a shear rate of 100 1/s. Different flow rates would correspond to different equivalent shear rates during the transport of nanogel in porous media. In both single-phase and two-phase conditions, resistance factors are higher with lower nanogel injection rate. In single-phase porous media, impacts of injection rate on nanogel retention and residual resistance factor were not obvious. When residual oil was

presented in porous media, a lower flow rate would result in higher incremental oil recovery and higher residual resistance factors.

The work in Paper IV displays the impacts of crosslinker concentration on nanogel properties, transport behavior, and EOR potential. The difference among dry nanogels was not noticeable based on their SEM images. In dispersion, nanogels synthesized with a higher crosslinker concentration had a lower swelling ratio and surface charge. As a result of the different volumetric fraction, the viscosity of high-crosslinked nanogel dispersion was lower. Nanogels synthesized with a higher crosslinker concentration were found to be more adsorbed onto sandstone surfaces. The adsorption volume over time was in accord with Ho's pseudo-second-order equation. Low-crosslinked nanogels were more capable of plugging porous media and resulted in higher oil recovery improvement.

3.2. RECOMMENDATIONS

Since nanoparticles, including nanogel, are small subjects, to fully understand the mechanism of their transport behavior and the oil displacement process, experiments should be observed at a much smaller scale. Micromodels shall be used to display the geometric flow of nanoparticle inside porous media to study this subject more comprehensively.

As shown in Paper III and Paper IV, nanogel injection pressure would keep increasing in a single-phase condition while it is easy to reach a stabilized condition in a water/oil two-phase condition. In mature oilfields, the high permeability channels/streaks are often flushed out by water while unswept zones or areas have a lot of oil are

remained. This pressure response in one-phase and two-phase conditions could lead to nanogel selective propagation through oil-rich zones/areas while it forms a good plugging in water-swept zone/areas. Further researches can be conducted to know whether we can take advantage of this feature to significantly improve nanogel EOR potential.

BIBLIOGRAPHY

1. Terry RE. Enhanced oil recovery. Encyclopedia of Physical Science and Technology. Academic press; 2001.

2. Alvarado V, Manrique E. Enhanced Oil Recovery: An Update Review. Vol. 3, Energies . 2010.

3. Green DW, Willhite GP. Enhanced oil recovery. Vol. 6. Henry L. Doherty Memorial Fund of AIME, Society of Petroleum Engineers …; 1998.

4. Ding H, Zhang N, Zhang Y, Wei M, Bai B. Experimental Data Analysis of Nanoparticles for Enhanced Oil Recovery. Ind Eng Chem Res [Internet]. 2019 Jul 10;58(27):12438–50. Available from: https://doi.org/10.1021/acs.iecr.9b02132

5. Bailey B, Crabtree M, Tyrie J, Elphick J, Kuchuk F, Romano C, et al. Water control. Oilf Rev. 2000;12(1):30–51.

6. Anderson WG. Wettability Literature Survey-Part 6: The Effects of Wettability on Waterflooding. J Pet Technol [Internet]. 1987;39(12):1605–22. Available from: https://doi.org/10.2118/16471-PA

7. Chaudhury MK. Spread the word about nanofluids. Nature [Internet]. 2003 May 8;423:131. Available from: https://doi.org/10.1038/423131a

8. Wasan DT, Nikolov AD. Spreading of nanofluids on solids. Nature [Internet]. 2003 May 8;423:156. Available from: https://doi.org/10.1038/nature01591

9. Mohammed MA, Babadagli T. Experimental Investigation of Wettability Alteration in Oil-Wet Reservoirs Containing Heavy Oil. SPE Reserv Eval Eng [Internet]. 2016;19(04):633–44. Available from: https://doi.org/10.2118/170034-PA

10. Roustaei A. An Evaluation of Spontaneous Imbibition of Water into Oil-Wet Carbonate Reservoir Cores Using Nanofluid. Petrophysics [Internet]. 2014;55(01):31–7. Available from: https://doi.org/

11. Cao N, Mohammed MA, Babadagli T. Wettability Alteration of Heavy-Oil-Bitumen-Containing Carbonates by Use of Solvents, High-pH Solutions, and Nano/Ionic Liquids. SPE Reserv Eval Eng [Internet]. 2017;20(02):363–71. Available from: https://doi.org/10.2118/183646-PA

12. Cheraghian G, Hendraningrat L. A review on applications of nanotechnology in the enhanced oil recovery part A: effects of nanoparticles on interfacial tension. Int Nano Lett [Internet]. 2016;6(2):129–38. Available from: https://doi.org/10.1007/s40089-015-0173-4

13. Wagner OR, Leach RO. Effect of Interfacial Tension on Displacement Efficiency. Soc Pet Eng J [Internet]. 1966;6(04):335–44. Available from: https://doi.org/10.2118/1564-PA

14. Agista MN, Guo K, Yu Z. A State-of-the-Art Review of Nanoparticles Application in Petroleum with a Focus on Enhanced Oil Recovery. Appl Sci [Internet]. 2018;8(6). Available from: http://www.mdpi.com/2076-3417/8/6/871

15. Alomair OA, Matar KM, Alsaeed YH. Nanofluids application for heavy oil recovery. In: SPE Asia Pacific Oil & Gas Conference and Exhibition. Society of Petroleum Engineers; 2014.

16. Hendraningrat L, Shidong L, Torsaeter O. A glass micromodel experimental study of hydrophilic nanoparticles retention for EOR project. In: SPE Russian Oil and Gas Exploration and Production Technical Conference and Exhibition. Society of Petroleum Engineers; 2012.

17. Li S, Genys M, Wang K, Torsæter O. Experimental study of wettability alteration during nanofluid enhanced oil recovery process and its effect on oil recovery. In: SPE Reservoir Characterisation and Simulation Conference and Exhibition. Society of Petroleum Engineers; 2015.

18. Li S, Hendraningrat L, Torsaeter O. Improved oil recovery by hydrophilic silica nanoparticles suspension: 2 phase flow experimental studies. In: IPTC 2013: International Petroleum Technology Conference. 2013.

19. Li S, Torsæter O. Experimental Investigation of the Influence of Nanoparticles Adsorption and Transport on Wettability Alteration for Oil Wet Berea Sandstone [Internet]. SPE Middle East Oil & Gas Show and Conference. Manama, Bahrain: Society of Petroleum Engineers; 2015. p. 16. Available from: https://doi.org/10.2118/172539-MS

20. Shahrabadi A, Bagherzadeh H, Roostaie A, Golghanddashti H. Experimental investigation of HLP nanofluid potential to enhance oil recovery: A mechanistic approach. In: SPE International Oilfield Nanotechnology Conference and Exhibition. Society of Petroleum Engineers; 2012.

21. Han P, Geng J, Bai B. Investigation on transport behavior of nanogel in low permeable porous medium. J Pet Sci Eng [Internet]. 2019;178:999–1005. Available from: http://www.sciencedirect.com/science/article/pii/S0920410519303560

22. Jensen KH, Valente AXCN, Stone HA. Flow rate through microfilters: Influence of the pore size distribution, hydrodynamic interactions, wall slip, and inertia. Phys Fluids. 2014;26(5):52004.

23. Geng J. Synthesis of different sizes & functions nanoparticles. 2015;

24. Mane S, Ponrathnam S, Chavan N. Effect of chemical cross-linking on properties of polymer microbeads: A review. Can Chem Trans. 2015;3(4):473–85.

25. Long Y, Wang Z, Ding H, Geng J, Bai B. Investigation and Characterization of a Robust Nanocomposite Preformed Particle Gel for Enhanced Oil Recovery. Energy & Fuels [Internet]. 2019 Jun 20;33(6):5055–66. Available from: https://doi.org/10.1021/acs.energyfuels.9b00778

26. Sun X, Zhang Y, Chen G, Gai Z. Application of nanoparticles in enhanced oil recovery: a critical review of recent progress. Energies. 2017;10(3):345.

27. Olayiwola SO, Dejam M. A comprehensive review on interaction of nanoparticles with low salinity water and surfactant for enhanced oil recovery in sandstone and carbonate reservoirs. Fuel [Internet]. 2019;241:1045–57. Available from: http://www.sciencedirect.com/science/article/pii/S0016236118321914

28. Bera A, Belhaj H. Application of nanotechnology by means of nanoparticles and nanodispersions in oil recovery - A comprehensive review. J Nat Gas Sci Eng [Internet]. 2016;34:1284–309. Available from: http://www.sciencedirect.com/science/article/pii/S1875510016305704

29. Li K, Wang D, Jiang S. Review on enhanced oil recovery by nanofluids. Oil Gas Sci Technol d'IFP Energies Nouv. 2018;73:37.

30. Cheraghian G, Hendraningrat L. A review on applications of nanotechnology in the enhanced oil recovery part B: effects of nanoparticles on flooding. Int Nano Lett [Internet]. 2016;6(1):1–10. Available from: https://doi.org/10.1007/s40089-015-0170-7

31. Sheng JJ. Status of surfactant EOR technology. Petroleum [Internet]. 2015;1(2):97–105. Available from: http://www.sciencedirect.com/science/article/pii/S2405656115000334

32. Sheng JJ, Leonhardt B, Azri N. Status of Polymer-Flooding Technology. J Can Pet Technol [Internet]. 2015;54(02):116–26. Available from: https://doi.org/10.2118/174541-PA

33. Bai B, Liu Y, Coste J-P, Li L. Preformed Particle Gel for Conformance Control: Transport Mechanism Through Porous Media. SPE Reserv Eval Eng [Internet]. 2007;10(02):176–84. Available from: https://doi.org/10.2118/89468-PA

34. Geng J, Ding H, Han P, Wu Y, Bai B. Transportation and Potential Enhanced Oil Recovery Mechanisms of Nanogels in Sandstone. Energy and Fuels. 2018;32(8).

35. Sorbie KS, Seright RS. Gel Placement in Heterogeneous Systems With Crossflow [Internet]. SPE/DOE Enhanced Oil Recovery Symposium. Tulsa, Oklahoma: Society of Petroleum Engineers; 1992. p. 18. Available from: https://doi.org/10.2118/24192-MS

36. McLaughlin HC, Diller J, Ayres HJ. Treatment of Injection and Producing Wells with Monomer Solution [Internet]. SPE Oklahoma City Regional Meeting. Oklahoma City, Oklahoma: Society of Petroleum Engineers; 1975. p. 8. Available from: https://doi.org/10.2118/5364-MS

37. Norman CA, Smith JE, Thompson RS. Economics of In-Depth Polymer Gel Processes [Internet]. SPE Rocky Mountain Regional Meeting. Gillette, Wyoming: Society of Petroleum Engineers; 1999. p. 8. Available from: https://doi.org/10.2118/55632-MS

38. Lantz M, Muniz G. Conformance Improvement Using Polymer Gels: A Case Study Approach [Internet]. SPE Improved Oil Recovery Symposium. Tulsa, Oklahoma, USA: Society of Petroleum Engineers; 2014. p. 16. Available from: https://doi.org/10.2118/169072-MS

39. Bai B, Huang F, Liu Y, Seright RS, Wang Y. Case study on prefromed particle gel for in-depth fluid diversion. In: SPE symposium on improved oil recovery. Society of Petroleum Engineers; 2008.

40. Bai B, Wei M, Liu Y. Field and Lab Experience With a Successful Preformed Particle Gel Conformance Control Technology [Internet]. SPE Production and Operations Symposium. Oklahoma City, Oklahoma, USA: Society of Petroleum Engineers; 2013. p. 17. Available from: https://doi.org/10.2118/164511-MS

41. National Nanotechnology Initiative (NNI). What It Is and How It Works | Nano [Internet]. Available from: https://www.nano.gov/nanotech-101/what

42. Dowling A, Clift R, Grobert N, Hutton D, Oliver R, O'Neill O, et al. Nanoscience and nanotechnologies : opportunities and uncertainties. London R Soc R Acad Eng Rep. 2004;

43. Al-Muntasheri GA, Liang F, Hull KL. Nanoparticle-Enhanced Hydraulic-Fracturing Fluids: A Review. SPE Prod Oper [Internet]. 2017;32(02):186–95. Available from: https://doi.org/10.2118/185161-PA

44. Ganesh VK. Nanotechnology in civil engineering. Eur Sci Journal, ESJ. 2012;8(27).

45. Kubik T, Bogunia-Kubik K, Sugisaka M. Nanotechnology on duty in medical applications. Curr Pharm Biotechnol. 2005;6(1):17–33.

46. Duncan T V. Applications of nanotechnology in food packaging and food safety: barrier materials, antimicrobials and sensors. J Colloid Interface Sci. 2011;363(1):1–24.

47. Alaskar MN, Ames MF, Connor ST, Liu C, Cui Y, Li K, et al. Nanoparticle and Microparticle Flow in Porous and Fractured Media--An Experimental Study. SPE J [Internet]. 2012;17(04):1160–71. Available from: https://doi.org/10.2118/146752-PA

48. Rahmani AR, Bryant SL, Huh C, Ahmadian M, Zhang W, Liu QH. Characterizing Reservoir Heterogeneities Using Magnetic Nanoparticles [Internet]. SPE Reservoir Simulation Symposium. Houston, Texas, USA: Society of Petroleum Engineers; 2015. p. 29. Available from: https://doi.org/10.2118/173195-MS

49. Aftab A, Ismail AR, Ibupoto ZH, Akeiber H, Malghani MGK. Nanoparticles based drilling muds a solution to drill elevated temperature wells: A review. Renew Sustain Energy Rev [Internet]. 2017 Sep 1 [cited 2019 Feb 11];76:1301–13. Available from: https://www.sciencedirect.com/science/article/pii/S1364032117303623

50. Cai J, Chenevert ME, Sharma MM, Friedheim JE. Decreasing Water Invasion Into Atoka Shale Using Nonmodified Silica Nanoparticles. SPE Drill Complet [Internet]. 2012;27(01):103–12. Available from: https://doi.org/10.2118/146979-PA

51. Vryzas Z, Mahmoud O, Nasr-El-Din HA, Kelessidis VC. Development and testing of novel drilling fluids using Fe 2 O 3 and SiO 2 nanoparticles for enhanced drilling operations. In: International Petroleum Technology Conference. International Petroleum Technology Conference; 2015.

52. Miranda CR, Lara LS de, Tonetto BC. Stability and Mobility of Functionalized Silica Nanoparticles for Enhanced Oil Recovery Applications [Internet]. SPE International Oilfield Nanotechnology Conference and Exhibition. Noordwijk, The Netherlands: Society of Petroleum Engineers; 2012. p. 11. Available from: https://doi.org/10.2118/157033-MS

53. Ragab AMS, Hannora AE. An experimental investigation of silica nano particles for enhanced oil recovery applications. In: SPE North Africa Technical Conference and Exhibition. Society of Petroleum Engineers; 2015.

54. Hendraningrat L, Li S, Torsaeter O. Enhancing oil recovery of low-permeability berea sandstone through optimised nanofluids concentration. In: SPE Enhanced Oil Recovery Conference. Society of Petroleum Engineers; 2013.

55. Roustaei A, Saffarzadeh S, Mohammadi M. An evaluation of modified silica nanoparticles' efficiency in enhancing oil recovery of light and intermediate oil reservoirs. Egypt J Pet. 2013;22(3):427–33.

56. El-Diasty AI. The potential of nanoparticles to improve oil recovery in bahariya formation, Egypt: An experimental study. In: SPE Asia Pacific Enhanced Oil Recovery Conference. Society of Petroleum Engineers; 2015.

57. Zargartalebi M, Kharrat R, Barati N. Enhancement of surfactant flooding performance by the use of silica nanoparticles. Fuel. 2015;143:21–7.

58. Roustaei A, Moghadasi J, Bagherzadeh H, Shahrabadi A. An experimental investigation of polysilicon nanoparticles' recovery efficiencies through changes in interfacial tension and wettability alteration. In: SPE International Oilfield Nanotechnology Conference and Exhibition. Society of Petroleum Engineers; 2012.

59. Tarek M. Investigating nano-fluid mixture effects to enhance oil recovery. In: SPE Annual Technical Conference and Exhibition. Society of Petroleum Engineers; 2015.

60. Ogolo NA, Olafuyi OA, Onyekonwu MO. Enhanced oil recovery using nanoparticles. In: SPE Saudi Arabia section technical symposium and exhibition. Society of Petroleum Engineers; 2012.

61. Hendraningrat L, Torsaeter O. Unlocking the potential of metal oxides nanoparticles to enhance the oil recovery. In: offshore technology conference-Asia. Offshore Technology Conference; 2014.

62. Esfandyari Bayat A, Junin R, Samsuri A, Piroozian A, Hokmabadi M. Impact of metal oxide nanoparticles on enhanced oil recovery from limestone media at several temperatures. Energy & Fuels. 2014;28(10):6255–66.

63. Wang L, Zhang G, Li G, Zhang J, Ding B. Preparation of microgel nanospheres and their application in EOR. In: International Oil and Gas Conference and Exhibition in China. Society of Petroleum Engineers; 2010.

64. Almohsin A, Ding H, Bai B. Experimental Study on the Transport and Improved Oil Recovery Mechanism of Submicron Particle Gel [Internet]. SPE EOR Conference at Oil and Gas West Asia. Muscat, Oman: Society of Petroleum Engineers; 2018. p. 14. Available from: https://doi.org/10.2118/190364-MS

65. Geng J, Ding H, Han P, Wu Y, Bai B. Transportation and Potential Enhanced Oil Recovery Mechanisms of Nanogels in Sandstone. Energy & Fuels [Internet]. 2018 Aug 16;32(8):8358–65. Available from: https://doi.org/10.1021/acs.energyfuels.8b01873

66. Chauveteau G, Omari A, Tabary R, Renard M, Veerapen J, Rose J. New size-controlled microgels for oil production. In: SPE international symposium on oilfield chemistry. Society of Petroleum Engineers; 2001.

67. Feng Y, Tabary R, Renard M, Le Bon C, Omari A, Chauveteau G. Characteristics of microgels designed for water shutoff and profile control. In: International Symposium on Oilfield Chemistry. Society of Petroleum Engineers; 2003.

68. Almohsin AM, Bai B, Imqam AH, Wei M, Kang W, Delshad M, et al. Transport of nanogel through porous media and its resistance to water flow. In: SPE Improved Oil Recovery Symposium. Society of Petroleum Engineers; 2014.

69. Goudarzi A, Almohsin A, Varavei A, Delshad M, Bai B, Sepehrnoori K. New experiments and models for conformance control microgels. In: SPE Improved Oil Recovery Symposium. Society of Petroleum Engineers; 2014.

70. Dupuis G, Lesuffleur T, Desbois M, Bouillot J, Zaitoun A. Water conformance treatment using SMG microgels: a successful field case. In: SPE EOR Conference at Oil and Gas West Asia. Society of Petroleum Engineers; 2016.

71. Roussennac BD, Toschi C. Brightwater trial in Salema Field (Campos Basin, Brazil). In: SPE EUROPEC/EAGE annual conference and exhibition. Society of Petroleum Engineers; 2010.

72. Salehi M, Thomas CP, Kevwitch R, Garmeh G, Manrique EJ, Izadi M. Performance evaluation of thermally-activated polymers for conformance correction Applications. In: SPE Improved Oil Recovery Symposium. Society of Petroleum Engineers; 2012.

73. Fabbri C, Klimenko A, Jouenne S, Cordelier P, Morel D. Laboratory and Simulation Investigation of the Effect of Thermally Activated Polymer on Permeability Reduction in Highly Permeable Unconsolidated Sand. In: SPE Asia Pacific Enhanced Oil Recovery Conference. Society of Petroleum Engineers; 2015.

74. Al-Muntasheri GA, Nasr-El-Din HA, Al-Noaimi K, Zitha PLJ. A Study of Polyacrylamide-Based Gels Crosslinked With Polyethyleneimine. SPE J [Internet]. 2009;14(02):245–51. Available from: https://doi.org/10.2118/105925-PA

75. Hendraningrat L, Zhang J. Polymeric nanospheres as a displacement fluid in enhanced oil recovery. Appl Nanosci. 2015;5(8):1009–16.

76. Lenchenkov NS, Slob M, van Dalen E, Glasbergen G, van Kruijsdijk C. Oil Recovery from Outcrop Cores with Polymeric Nano-Spheres. In: SPE Improved Oil Recovery Conference. Society of Petroleum Engineers; 2016.

77. Geng J, Han P, Bai B. Experimental Study on Charged Nanogels for Interfacial Tension Reduction and Emulsion Stabilization at Various Salinities and Oil Types [Internet]. SPE Asia Pacific Oil and Gas Conference and Exhibition. Brisbane, Australia: Society of Petroleum Engineers; 2018. p. 13. Available from: https://doi.org/10.2118/192118-MS

78. Geng J, Pu J, Wang L, Bai B. Surface charge effect of nanogel on emulsification of oil in water for fossil energy recovery. Fuel [Internet]. 2018;223:140–8. Available from: http://www.sciencedirect.com/science/article/pii/S0016236118304526

79. Wang W, Yuan B, Su Y, Wang K, Jiang M, Moghanloo RG, et al. Nanoparticles adsorption, straining and detachment behavior and its effects on permeability of berea cores: Analytical model and lab experiments. In: SPE Annual Technical Conference and Exhibition. Society of Petroleum Engineers; 2016.

80. Phenrat T, Kim H-J, Fagerlund F, Illangasekare T, Tilton RD, Lowry G V. Particle Size Distribution, Concentration, and Magnetic Attraction Affect Transport of Polymer-Modified Fe0 Nanoparticles in Sand Columns. Environ Sci Technol [Internet]. 2009 Jul 1;43(13):5079–85. Available from: https://doi.org/10.1021/es900171v

81. Ding H, Geng J, Lu Y, Zhao Y, Bai B. Impacts of crosslinker concentration on nanogel properties and enhanced oil recovery capability. Fuel [Internet]. 2020;267:117098. Available from: http://www.sciencedirect.com/science/article/pii/S0016236120300934

VITA

Haifeng Ding (丁海峰) was born in Heilongjiang Province, China. He was admitted to the China University of Petroleum - Beijing (CUPB), Beijing, China in 2010 and received his bachelor's degree in Petroleum Engineering in 2014. He later joined Dr. Baojun Bai's research group in 2014 and received his Master of Science in Petroleum Engineering from Missouri University of Science and Technology, U.S. in December 2016. He continued to pursue a Ph.D. degree in the same research group and received his Doctor of Philosophy in Petroleum Engineering from Missouri University of Science and Technology in May 2020.